

DETERMINATION OF
OPTICAL CONSTANTS BY ELLIPSOMETRY

DETERMINATION OF
OPTICAL CONSTANTS BY ELLIPSOMETRY

by

ERNEST COLIN ROWE, B.Sc.

A Thesis

Submitted to the Faculty of Graduate Studies

in Partial Fulfilment of the Requirements

for the Degree

Master of Science

McMaster University

August 1969

MASTER OF SCIENCE (1969)
(Physics)

McMASTER UNIVERSITY
Hamilton, Ontario

TITLE: Optical Constants by Ellipsometry

AUTHOR: Ernest Colin Rowe, B.Sc. (British Columbia)

SUPERVISOR: Professor J. Shewchun

NUMBER OF PAGES: viii, 99

SCOPE AND CONTENTS:

The standard technique of ellipsometry allows the determination of the optical constants of a substrate material provided either the surface is free of an oxide film or the oxide film thickness and optical constants of this oxide film are known. The majority of ellipsometric measurements performed on materials known to grow natural oxides is done by removing the natural oxide (either by cleaving or etching) and performing the measurements at one angle of incidence *in vacuo*. These processes perturb the surface and the reported values of optical constants may be questionable.

The technique to be presented here assumes the material to be studied has a naturally-occurring oxide. Measurements are performed at several angles of incidence and the optical equations are solved for a self-consistent oxide film thickness until the best fit substrate optical constants have been found. The optical constants of the oxide film are then determined.

ACKNOWLEDGEMENTS

The author wishes to express his gratitude to his research supervisor, Dr. J. Shewchun, for his guidance throughout the course of this work. Thanks are also due Dr. F. L. McCrackin of the United States National Bureau of Standards for supplying a copy of his computer program. Dr. R. Kelly and Mr. M. Arora are thanked for supplying several films of molybdenum for study. The assistance of Dr. B. K. Garside in proof-reading several manuscripts is gratefully acknowledged.

The National Research Council of Canada and the Ontario Government are thanked for their financial assistance in the form of fellowships.

TABLE OF CONTENTS

	Page
CHAPTER I INTRODUCTION AND HISTORY	1
CHAPTER II THEORY	6
CHAPTER III ANALYSIS OF THE EQUATIONS	26
CHAPTER IV EXPERIMENTAL	53
CHAPTER V COMPUTER PROGRAM	65
CHAPTER VI DISCUSSION	72
APPENDIX I DERIVATION OF THE WAVE EQUATIONS	90
APPENDIX II INVERSION OF THE FILM-FREE TRANSCENDENTAL ELLIPSOMETRY EQUATIONS	93
BIBLIOGRAPHY	98

LIST OF ILLUSTRATIONS

		Page
Figure 2-1	Reflection and refraction of light at a boundary between two optically different media.	9
Figure 2-2	Reflection and refraction of light at a boundary between a transparent medium n_1 and an absorbing substrate of complex refractive index $n_3 - j k_3$.	12
Figure 2-3	Reflection model for elliptical polarization.	17
Figure 3-1	Plot of phase change $\bar{\Delta}$ versus angle of incidence for bare substrates.	32
Figure 3-2	Plot of azimuth $\bar{\psi}$ versus angle of incidence for bare substrates.	33
Figure 3-3	Plot of phase change $\Delta - \bar{\Delta}$ for oxide films on a silicon substrate.	35
Figure 3-4	Plot of phase change $\Delta - \bar{\Delta}$ for oxide films on an aluminum substrate.	36
Figure 3-5	Plot of phase change $\Delta - \bar{\Delta}$ for oxide films on an iron substrate.	37
Figure 3-6	Plot of phase change $\Delta - \bar{\Delta}$ for oxide films on a gold substrate.	38
Figure 3-7	Plot of change of azimuth $\psi - \bar{\psi}$ for oxide films on a silicon substrate.	40
Figure 3-8	Plot of change of azimuth $\psi - \bar{\psi}$ for oxide films on an aluminum substrate.	41
Figure 3-9	Plot of change of azimuth $\psi - \bar{\psi}$ for oxide films on an iron substrate.	42
Figure 3-10	Plot of change of azimuth $\psi - \bar{\psi}$ for oxide films on a gold substrate.	43
Figure 3-11	Effect of an oxide extinction coefficient on the phase change $\Delta - \bar{\Delta}$ for oxide films on silicon.	45
Figure 3-12	Effect of an oxide extinction coefficient on the phase change $\Delta - \bar{\Delta}$ for oxide films on aluminum.	46

LIST OF ILLUSTRATIONS (Cont'd)

		Page
Figure 3-13	Effect of an oxide extinction coefficient on the phase change $\Delta - \bar{\Delta}$ for oxide films on iron.	47
Figure 3-14	Effect of an oxide extinction coefficient on the phase change $\Delta - \bar{\Delta}$ for oxide films on gold.	48
Figure 3-15	Effect of an oxide extinction coefficient on the change in azimuth $\psi - \bar{\psi}$ for oxide films on silicon.	49
Figure 3-16	Effect of an oxide extinction coefficient on the change in azimuth $\psi - \bar{\psi}$ for oxide films on aluminum.	50
Figure 3-17	Effect of an oxide extinction coefficient on the change in azimuth $\psi - \bar{\psi}$ for oxide films on iron.	51
Figure 3-18	Effect of an oxide extinction coefficient on the change in azimuth $\psi - \bar{\psi}$ for oxide films on gold.	52
Figure 4-1	Graphical representation of the ellipsometer angles Δ and ψ for reflection greater than the principal angle.	54
Figure 4-2	Representation of Rothen's early ellipsometer.	55
Figure 4-3	Symbolic representation of present ellipsometer for quarter-wave plate mounted before sample holder.	58
Figure 4-4	Photograph of present ellipsometer for quarter-wave plate mounted before sample holder.	58
Figure 4-5	Symbolic representation of present ellipsometer for quarter-wave plate mounted after sample holder.	60
Figure 4-6	Photograph of present ellipsometer for quarter-wave plate mounted after sample holder.	60

LIST OF ILLUSTRATIONS (Cont'd)

		Page
Figure 4-7	Graphical representation of ellipsometric parameters.	61
Figure 5-1	Flow-chart of computer program used to determine substrate optical constants.	66
Figure 6-1	Plot of substrate refractive index versus oxide film thickness for aluminum determined by this ellipsometric technique.	74
Figure 6-2	Plot of substrate extinction coefficient versus oxide film thickness for aluminum determined by this ellipsometric technique.	75
Figure 6-3	Plot of oxide extinction coefficient versus oxide film thickness for aluminum substrate.	77
Figure 6-4	Plot of substrate refractive index for silicon versus oxide film thickness determined by this ellipsometric technique.	81
Figure 6-5	Plot of substrate extinction coefficient for silicon versus oxide film thickness determined by this ellipsometric technique.	82

LIST OF TABLES

	Page
Table 5-1. McCrackin's Zone Scheme.	68
Table 6-1 Optical Constants of Aluminum determined by ellipsometry in air.	73
Table 6-2 Optical constants of Molybdenum determined by ellipsometry in air.	78
Table 6-3 Optical constants of silicon determined by ellipsometry in air.	80
Table 6-4 Variation of "pseudo-optical constants" and normal reflectivity with oxide film thickness for silicon.	85
Table 6-5 Variation of "pseudo-optical constants" and normal reflectivity with oxide film thickness for aluminum.	86
Table 6-6 Variation of "pseudo-optical constants" and normal reflectivity with oxide film thickness for tungsten.	87
Table 6-7 Calculated maximum oxide thickness for several materials for a 0.1 percent deviation in normal reflectivity from the true substrate values.	88

CHAPTER I

INTRODUCTION AND HISTORY

Ellipsometry has been called the art of measuring and analyzing the elliptical polarization of light. In this general sense, no restriction has been placed upon the method in which the elliptical polarization is obtained. For the work to be discussed here, ellipsometry will be referred to as elliptical polarization caused by reflection of plane polarized light from an absorbing medium (substrate) or an absorbing medium (substrate) with an adhering oxide film. The majority of the work here consists of calculating the optical constants of the absorbing medium (substrate) and the optical constants of the adhering oxide film along with its thickness.

Fundamental studies of reflection from optical media were performed by Augustin Fresnel in the nineteenth century. At the boundary of two non-absorbing dielectric media, Fresnel's formulae indicate that the two reflected components of light, one vibrating parallel to plane of incidence and the other perpendicular to the plane of incidence (denoted as the p and s components respectively) undergo a phase shift of either 0 or 180 degrees at the interface of a non-absorbing medium. At a certain angle of incidence, the parallel component becomes zero---this critical angle being called the Brewster angle. It was found experimentally that the parallel component did not vanish completely when the angle of incidence was equal to the Brewster angle. Rayleigh¹ explained this fact in terms of the ellipticity of the reflected light --- if the incident light is plane polarized at 45 degrees to the principal planes, the ratio of the reflected amplitudes in the plane of incidence and perpendicular to the plane of incidence is called the

ellipticity of the reflected light. Lord Rayleigh concluded that the ellipticity of the light reflected by clean liquids was much less than that of contaminated surface; i.e. it depends upon the absorption coefficient.

At about the same time, Drude² was examining the properties of light reflected from solids rather than liquids. He was able to correlate quantitatively the optical thickness of a film and the optical constants of the material (substrate) upon which the film was evaporated. Two parameters were used to characterize the ellipse representing the reflected light:

1) the ratio $\tan \psi = \frac{\rho^p}{\rho^s}$

(eq. 1-1)

where the angle ψ is called the azimuth and ρ^p and ρ^s are the reflection coefficients of the components in the plane and perpendicular to the plane of incidence after reflection.

2) the differential phase change for the two polarization

$$\Delta = \delta^p - \delta^s$$

(eq. 1-2)

where δ^p and δ^s are the absolute phase shifts of these same components brought about by reflection.

Starting from Maxwell's equations and the appropriate boundary conditions, Drude obtained a general expression relating the Fresnel reflection coefficients (for the p and s polarizations) and the film thickness d to the ellipticity ($\tan \psi$) and the change in phase (Δ) namely:

$$\tan \psi \exp j\Delta = \frac{r_{12}^p + r_{23}^p \cdot \exp -j \cdot x}{1 + r_{12}^p \cdot r_{23}^p \cdot \exp -j \cdot x} \frac{1 + r_{12}^s \cdot r_{23}^s \cdot \exp -j \cdot x}{r_{12}^s + r_{23}^s \cdot \exp -j \cdot x}$$

where the variable x denotes $4\pi n_2 \cos \phi d / \lambda$, an additional change in phase upon traversing the film

n_2 = index of refraction for this film,
 ϕ = angle of incidence,
 d = film thickness,
 and λ = wavelength of the incident light.

The values of Δ and ψ can be obtained experimentally by measuring the orientation of the elliptically polarized light. For thin films, Drude³ expanded $\exp(-j \cdot x)$ as $(1 - j \cdot x)$ and determined two linear equations for the angles Δ and ψ , viz.;

$$\Delta - \bar{\Delta} = - \alpha d \quad (\text{eq. 1-4})$$

$$\psi - \bar{\psi} = \beta d \quad (\text{eq. 1-5})$$

where the barred quantities $\bar{\Delta}$ and $\bar{\psi}$ denote the measurements that would be obtained for Δ and ψ in the absence of an oxide film; the quantities $\bar{\Delta}$ and $\bar{\psi}$ are functions of the substrate optical constants and angle of the incidence only. These linear equations were tested by Tronstad⁴ by measuring monomolecular films of fatty acids adsorbed on a mercury surface. He found good agreement between measured values and theoretical ones.

In 1944, Rothen⁵ developed the ellipsometer in much the same form as it is today. More recent changes involve the substitution of photomultiplier tubes for half-shade detection devices thus greatly en-

hancing the sensitivity to detect oxide film thickness. Shortly after the development of the ellipsometer, Vasicek⁶ published a series of articles on the optical properties of thin films. He managed to show that the Drude general equation could be developed in a useable form without approximation.

R. J. Archer⁷, in 1957, developed better expansion coefficients α and β than those of Drude as used in expressions 1-4 and 1-5. With these new coefficients, he was able to determine the rate of growth of oxide films on silicon and germanium. McCrackin, Passaglia, Stromberg, and Steinberg⁸, in 1963, developed the exact equations for determining film thicknesses once the optical constants were known and produced a computer program for their calculation.⁹ An added feature they presented was a method to account for a non-exact quarter-wave plate and an averaging technique for determining Δ and ψ from the polarizer and analyzer readings. In 1964 Burge and Bennett¹⁰ showed Archer's linear relations to be more exact than the Drude linear relations, both being inadequate for oxide films greater than about 50 Angstroms. They maintained that the variation in the ellipsometric parameters Δ and ψ with angle of incidence could not be used to determine the presence of a surface oxide film; their reason being that variation of these parameters with angle of incidence for a film-covered surface was practically identical with that for a fictitious film-free surface with slightly different optical constants. It is this claim that is to be refuted here. In 1965 Saxena¹¹

extended the range of the Archer linear equation to certain ranges in the thick film region since plots of Δ versus ψ are periodic in film thickness.

A recent paper by Vedam et al²⁸ shows a method of determining substrate optical constants using the fact that the normal reflectivity of a substrate remains constant to within 0.1% with increasing oxide film thickness up to about 200 Angstroms. They chose silicon, a material for which this is true. Other materials show larger deviation in normal reflectivity with oxide film thickness.²⁹

CHAPTER II

THEORY

The propagation of electromagnetic waves in an homogeneous isotropic medium can be expressed by Maxwell's equations (see appendix I) yielding the wave equation for the electric field

$$\nabla^2 \vec{E} - \frac{\mu\epsilon}{c^2} \frac{\partial^2 \vec{E}}{\partial t^2} - \frac{4\pi\mu\sigma}{c^2} \frac{\partial \vec{E}}{\partial t} = 0. \quad (\text{eq. 2-1})$$

For a plane-wave solution of the form

$$\vec{E} = \vec{E}_0 \exp j(\omega t - \vec{\Gamma} \cdot \vec{r}), \quad (j = \sqrt{-1}) \quad (\text{eq. 2-2})$$

the propagation vector $\vec{\Gamma}$ is a complex number whose magnitude is

$$\Gamma = \frac{\omega}{c} \sqrt{\mu\epsilon - j \frac{4\pi\mu\sigma}{\omega}}. \quad (\text{eq. 2-3})$$

In free space, the wave propagates with the velocity of light, c , and the magnitude of the propagation vector is simply

$$\Gamma = \frac{\omega}{c}.$$

In the medium, the velocity of propagation is slower. In fact, we say the phase velocity is divided by a complex refractive index

$$\tilde{n} = \sqrt{\mu\epsilon - j \frac{4\pi\mu\sigma}{\omega}} = n - j k, \quad (\text{eq. 2-4})$$

so that the propagation vector is

$$\vec{\Gamma} = \frac{n\omega}{c} - j \frac{k\omega}{c} \quad (\text{eq. 2-5})$$

Eq. 2-4 serves to define the index of refraction n for the medium and the extinction coefficient k . To see the effect of this extinction coefficient, consider a plane wave propagating in the z direction. Applying eq. 2-5 to eq. 2-2 shows that

$$E_z = E_{0z} \exp j\omega(t - \frac{nz}{c}) \exp -(\frac{k\omega z}{c}) \quad (\text{eq. 2-6})$$

This result shows that the velocity of the wave in the medium is reduced to c/n and that the wave is damped as it propagates. Several terms are used to describe the damping. These terms will be included here for completeness and because there appears to be a great deal of confusion in the literature as to their meaning. An absorption coefficient η is defined by the condition that the energy of the wave decrease by a factor $1/e$ in a distance $1/\eta$. The current density associated with the wave (eq. 2-6) can be calculated by applying Ampere's law giving the result

$$\vec{J} = \frac{4\pi\mu\sigma}{c} - \frac{j\omega\mu\epsilon}{c} \vec{E} = -j \frac{\omega}{c} \tilde{n}^2 \vec{E} \quad (\text{eq. 2-7})$$

The rate of production of Joule heat is the real part of $(\vec{J} \cdot \vec{E})$. Thus the fraction of energy lost due to Joule heating per unit thickness of the

material is given by

$$\begin{aligned} \eta &= \frac{\operatorname{Re} (\vec{J} \cdot \vec{E})}{|\vec{E}|^2} = \operatorname{Re} \left(-j \frac{\omega}{c} \tilde{n}^2 \right) \\ &= \frac{2 n k \omega}{c} = \frac{4 \pi n k}{\lambda} . \end{aligned} \quad (\text{eq. 2-8})$$

An absorption index χ is defined as simply the nk product in the above expression. An attenuation constant α is defined in terms of the amplitude of the electric vector decreasing by a factor $1/e$ in a distance $1/\alpha$, so that

$$\alpha = 1/2\eta = \frac{nk\omega}{c} = \frac{2\pi nk}{\lambda} = \frac{2\pi\chi}{\lambda} . \quad (\text{eq. 2-9})$$

In order to describe the state of polarization of the propagating waves, it is convenient to treat waves with electric vectors vibrating parallel (p) to the plane of incidence separately from those with vectors vibrating normal (s) to the plane of incidence.

Consider a light wave propagating in the z direction of a right-handed co-ordinate system (see fig. 2-1). We specify the amplitude of the electric vector travelling in the positive direction in the q^{th} medium and polarized with the electric vector parallel to the plane of incidence by $E_q^+(p)$; similarly $E_q^+(s)$ denotes the component of the electric vector perpendicular to the plane of incidence travelling in the positive direction. A negative sign on the superscript denotes a wave travelling in the negative direction. Applying Maxwell's equations at the interface of the two media leads to the following results:

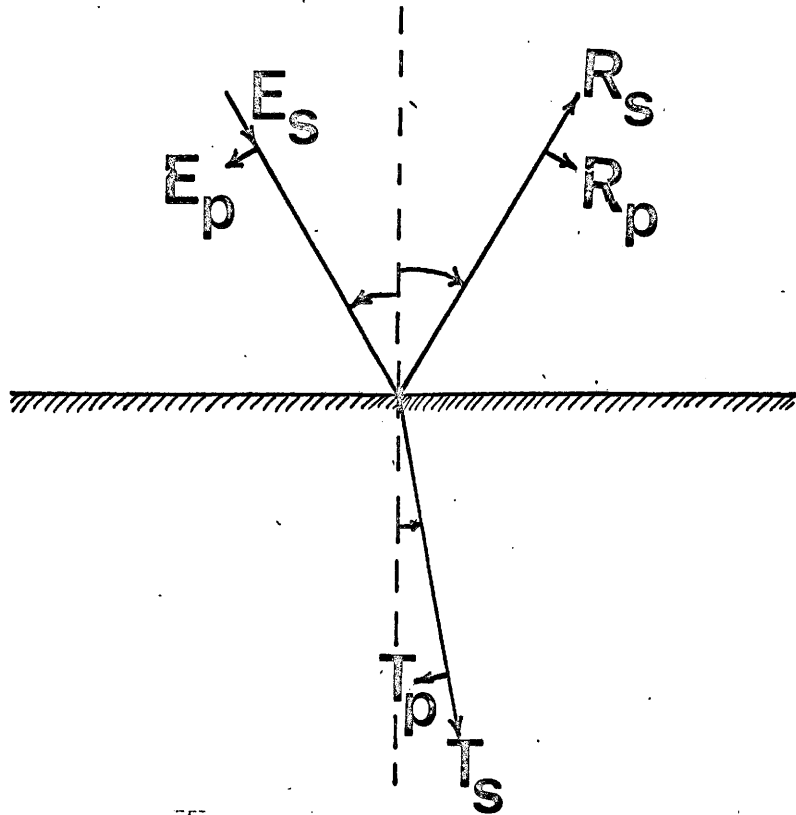


Figure 2-1 Reflection and refraction of light at a boundary between two optically different media.

a) Law of Reflection

$$\phi_1 = \phi_1^r \quad (\text{eq. 2-10})$$

i.e. the angle of incidence equals the angle of reflection.

b) Snell's Law of Refraction

$$n_1 \cdot \sin \phi_1 = n_2 \cdot \sin \phi_2 \quad (\text{eq. 2-11})$$

c) Fresnel Reflection and Transmission Coefficients^{20,21}

$$r_{12}^p = \frac{E_1^-(p)}{E_1^+(p)} = \frac{n_2 \cdot \cos \phi_1 - n_1 \cdot \cos \phi_2}{n_2 \cdot \cos \phi_1 + n_1 \cdot \cos \phi_2} \quad (\text{eq. 2-12})$$

$$t_{12}^p = \frac{E_2^+(p)}{E_1^+(p)} = \frac{2 \cdot n_1 \cos \phi_1}{n_2 \cdot \cos \phi_1 + n_1 \cdot \cos \phi_2} \quad (\text{eq. 2-13})$$

$$r_{12}^s = \frac{E_1^-(s)}{E_1^+(s)} = \frac{n_1 \cdot \cos \phi_1 - n_2 \cdot \cos \phi_2}{n_1 \cdot \cos \phi_1 + n_2 \cdot \cos \phi_2} \quad (\text{eq. 2-14})$$

and

$$t_{12}^s = \frac{E_2^+(s)}{E_1^+(s)} = \frac{2 \cdot n_1 \cos \phi_1}{n_1 \cdot \cos \phi_1 + n_2 \cdot \cos \phi_2} \quad (\text{eq. 2-15})$$

Here n_1 and n_2 are the optical constants for the two media and ϕ_1 and ϕ_2 are the angles of propagation in these same two media. When both media are transparent, the optical constants are their respective refractive indices. In this case they are real numbers given by:

$$n_i = \sqrt{\frac{\mu_i \epsilon_i}{\mu_0 \epsilon_0}} \quad (\text{eq. 2-16})$$

where the zero subscript indicates the "free space" value of the particular variable. For the particular case of two transparent dielectric media, all of the terms in Snell's law and the Fresnel coefficients are real.

For an absorptive medium the Fresnel equations are still valid, along with the Snell's law expressions, provided a "complex index of refraction" defined by $\tilde{n} = n - j.k$ ($j = \sqrt{-1}$) is used to characterize these materials. Complex Fresnel coefficients indicate that the reflected and refracted rays suffer a phase shift at the interface which is neither 0 or 180 degrees.

Film-Free Reflection

Consider a light wave resolved into parallel and perpendicular components of the electric vector. This wave is travelling through a transparent dielectric medium of refractive index n_1 and striking the interface between the dielectric medium and an absorbing substrate of refractive index $\tilde{n}_3 = n_3 - j.k_3$. This configuration is shown in fig. 2-2. The basic equations describing the reflection remain as in eqs. 2-10 through 2-15 with n_2 replaced with \tilde{n}_3 and ϕ_2 replaced with the complex angle ϕ . Application of Snell's law yields the result

$$\begin{aligned} \cos \phi &= \sqrt{1 - \sin^2 \phi} \\ &= \frac{1}{n_3 - j k_3} \sqrt{(n_3 - j k_3)^2 - n_1^2 \sin^2 \phi_1} \quad (\text{eq. 2-17}) \end{aligned}$$

The Fresnel reflection coefficients can then be expressed in terms of the angle of incidence ϕ_1 and the substrate optical constants by substitution into eqs. 2-12 and 2-14 giving

REFLECTION FROM AN ABSORBING SUBSTRATE

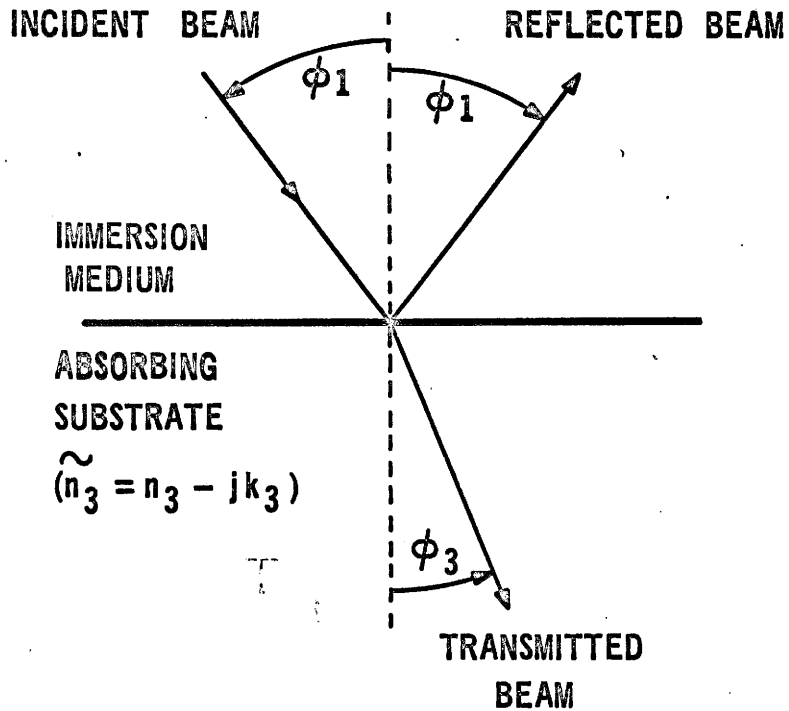


Figure 2-2 Reflection and refraction of light at a boundary between a transparent medium n_1 and an absorbing substrate of complex refractive index $n_3 - j k_3$.

$$r_{13}^p = \frac{(n_3 - j k_3)^2 \cos \phi_1 - (n_3 - j k_3)^2 - n_1^2 \sin^2 \phi_1}{(n_3 - j k_3)^2 \cos \phi_1 + (n_3 - j k_3)^2 - n_1^2 \sin^2 \phi_1} \quad (\text{eq. 2-18})$$

and

$$r_{13}^s = \frac{n_1 \cos \phi_1 - (n_3 - j k_3)^2 - n_1^2 \sin^2 \phi_1}{n_1 \cos \phi_1 + (n_3 - j k_3)^2 - n_1^2 \sin^2 \phi_1} \quad (\text{eq. 2-19})$$

For simplicity, it is convenient to define

$$w = (n_3 - j k_3)^2 - n_1^2 \sin^2 \phi_1 \quad (\text{eq. 2-20})$$

With this definition,

$$\begin{aligned} r_{13}^p &= \frac{(w^2 + n_1^2 \sin^2 \phi_1) \cos \phi_1 - n_1 w}{(w^2 + n_1^2 \sin^2 \phi_1) \cos \phi_1 + n_1 w} \\ &= \frac{(n_1 \sin \phi_1 \tan \phi_1 - w) (n_1 \cos \phi_1 - w)}{(n_1 \sin \phi_1 \tan \phi_1 + w) (n_1 \cos \phi_1 + w)}, \end{aligned} \quad (\text{eq. 2-21})$$

and

$$r_{13}^s = \frac{n_1 \cos \phi_1 - w}{n_1 \cos \phi_1 + w} \quad (\text{eq. 2-22})$$

The ratio of these two reflection coefficients serves to characterize the change in the state of polarization of the reflected light beam, in fact

$$\begin{aligned}
 \frac{r_{13}^p}{r_{13}^s} &= \frac{|r_{13}^p| \exp j\delta p}{|r_{13}^s| \exp j\delta s} = \tan \psi \exp j \Delta \\
 &= \frac{n_1 \sin \phi_1 \tan \phi_1 - w}{n_1 \sin \phi_1 \tan \phi_1 + w} \\
 &= \frac{1 - \frac{w}{n_1 \sin \phi_1 \tan \phi_1}}{1 + \frac{w}{n_1 \sin \phi_1 \tan \phi_1}} \quad . \quad (\text{eq. 2-23})
 \end{aligned}$$

Because we are dealing with reflection from a substrate devoid of any oxide film, we will denote the phase change Δ and the ellipticity ψ by $\bar{\Delta}$ and $\bar{\psi}$ respectively. Eq. 2-23 is of the form

$$y = \frac{1 - x}{1 + x} \quad \text{whose inverse is} \quad x = \frac{1 - y}{1 + y} \quad .$$

Inversion of eq. 2-23 allows one to calculate the substrate optical constants from the experimentally measureable angles $\bar{\Delta}$ and $\bar{\psi}$. Inverting eq. 2-23, rationalizing, and factoring yields the result

$$\frac{w}{n_1 \sin \phi_1 \tan \phi_1} = \frac{\cos 2\bar{\psi} - j \sin 2\bar{\psi} \sin \bar{\Delta}}{1 + \sin 2\bar{\psi} \cos \bar{\Delta}} \quad . \quad (\text{eq. 2-24})$$

The substrate optical constants n_3 and k_3 are "hidden" in the term w . Application of definition eq. 2-20 to eq. 2-24 and squaring both sides of the resultant expression yields, after some algebraic manipulation,

$$\frac{n_3^2 - k_3^2 - n_1^2 \sin^2 \phi_1 - 2 j n_3 k_3}{n_1^2 \sin^2 \phi_1 \tan^2 \phi_1} = \frac{\cos^2 2\bar{\psi} - \sin^2 2\bar{\psi} \sin^2 \bar{\Delta} - 2 j \sin 2\bar{\psi} \cos 2\bar{\psi} \sin \bar{\Delta}}{(1 + \sin 2\bar{\psi} \cos \bar{\Delta})^2}$$

(eq. 2-25)

Finally, by separating this expression into real and complex components, we obtain two equations in n_3 and k_3 .

Real part:

$$n_3^2 - k_3^2 = n_1^2 \sin^2 \phi_1 \left[1 + \tan^2 \phi_1 \frac{\cos^2 2\bar{\psi} - \sin^2 2\bar{\psi} \sin^2 \bar{\Delta}}{(1 + \sin 2\bar{\psi} \cos \bar{\Delta})^2} \right]$$

(eq. 2-26)

Complex part:

$$2 n_3 k_3 = \frac{n_1^2 \sin^2 \phi_1 \tan^2 \phi_1 \sin 4\bar{\psi} \sin \bar{\Delta}}{(1 + \sin 2\bar{\psi} \cos \bar{\Delta})^2}$$

(eq. 2-27)

For calculation purposes on substrates containing oxide films, the inverse of eqs. 2-26 and 2-27 is necessary, i.e. solve for $\bar{\Delta}$ and $\bar{\psi}$ in terms of the substrate optical constants n_3 and k_3 . This calculation is done in appendix II. The result of such a calculation is

$$\tan \bar{\Delta} = \sin Q \tan 2P, \quad (\text{eq. 2-28})$$

$$\text{and} \quad \cos 2\bar{\psi} = \sin 2P \cos Q. \quad (\text{eq. 2-29})$$

$$\text{where} \quad \tan P = \frac{(n_3^4 + k_3^4 + n_1^4 \sin^4 \phi_1 + 2n_3^2 k_3^2 - 2(n_3^2 - k_3^2)n_1^2 \sin^2 \phi_1)^{1/4}}{n_1 \sin \phi_1 \tan \phi_1} \quad (\text{eq. 2-30})$$

and
$$\tan 2Q = \frac{2 n_3 k_3}{n_3^2 - k_3^2 - n_1^2 \sin^2 \phi_1} . \quad (\text{eq. 2-31})$$

Reflection from a substrate with adhering surface film.¹²

Consider a plane electromagnetic wave striking the surface of an optical system as shown in figure 2-3. The system of reflected waves is replaced by an equivalent wave R leaving the film; D is the equivalent of all waves entering the substrate; A and B are the equivalent waves striking and reflecting from the film-substrate interface respectively. Applying Maxwell's equations of tangential electric field components and normal magnetic field components being continuous across the boundaries at $z = 0$ and $z = d$, yields the following:

At the surface $z = 0$:

parallel components:

$$(E_p - R_p) \cos \phi_1 = (A_p - B_p) \cos \phi_2 \quad (\text{eq. 2-32})$$

$$(E_p + R_p) n_1 = (A_p + B_p) \tilde{n}_2 \quad (\text{eq. 2-33})$$

perpendicular components:

$$E_s + R_s = A_s + B_s \quad (\text{eq. 2-34})$$

$$(E_s - R_s) n_1 \cos \phi_1 = (A_s - B_s) \tilde{n}_2 \cos^* \phi \quad (\text{eq. 2-35})$$

At the surface $z = d$:

parallel components:

$$(A_p e^{-j\tau} - B_p e^{-j\tau}) \cos^* \phi_2 = D_p e^{-j\tau} \cos^* \phi_3 \quad (\text{eq. 2-36})$$

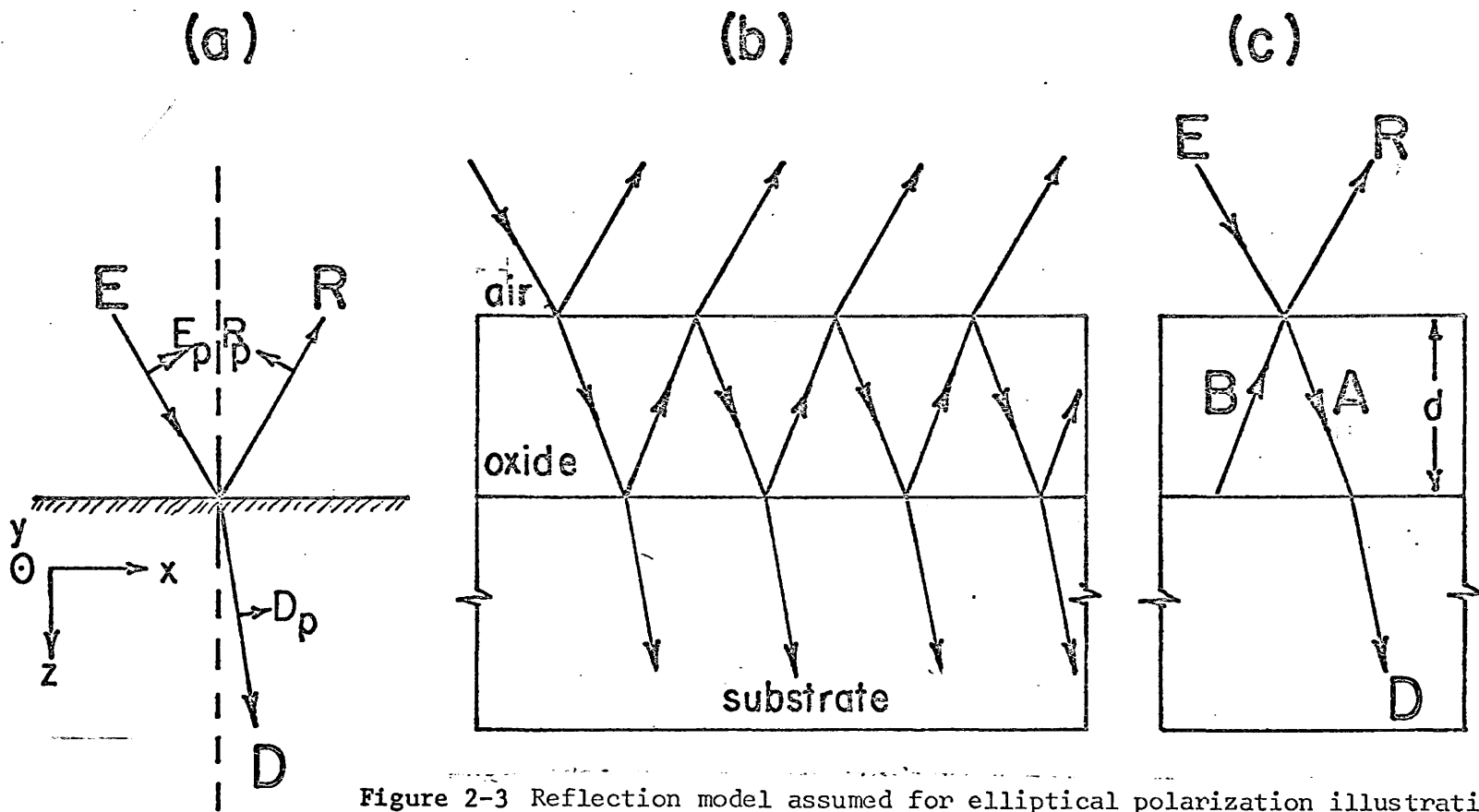


Figure 2-3 Reflection model assumed for elliptical polarization illustrating
 (a) Sign convention,
 (b) Multiple reflections assumed to occur in oxide,
 and (c) Reflection system assumed equivalent to (b).
 (Reproduced from Leberknight and Lustman.)

$$(A_p e^{-j\tau_A} + B_p e^{-j\tau_B}) \bar{n}_2 = D_p e^{-j\tau_D} \bar{n}_3 \quad (\text{eq. 2-37})$$

perpendicular components:

$$A_s e^{-j\tau_A} + B_s e^{-j\tau_B} = D_s e^{-j\tau_D} \quad (\text{eq. 2-38})$$

$$(A_s e^{-j\tau_A} - B_s e^{-j\tau_B}) \bar{n}_2 \cos^* \phi_2 = D_s e^{-j\tau_D} \bar{n}_3 \cos^* \phi_3 \quad (\text{eq. 2-39})$$

where $\tau_A = (2\pi/\lambda) \bar{n}_2 (x \sin^* \phi_2 + d \cos^* \phi_2)$,
 $\tau_B = (2\pi/\lambda) \bar{n}_2 (x \sin^* \phi_2 - d \cos^* \phi_2)$,
and $\tau_D = (2\pi/\lambda) \bar{n}_3 (x \sin^* \phi_3 + d \cos^* \phi_3)$.

Now if eq. 2-36 is multiplied by $e^{+j\tau_A} \bar{n}_3$ and eq. 2-37 multiplied by $\cos^* \phi_3 e^{+j\tau_A}$ their right hand sides become identical so that D_p is eliminated giving

$$(A_p - B_p e^{j(\tau_A - \tau_B)}) \bar{n}_3 \cos^* \phi_2 = (A_p + B_p e^{j(\tau_A - \tau_B)}) \bar{n}_2 \cos^* \phi_3.$$

Solving this expression for A_p and calling $\delta = \tau_A - \tau_B$ we find

$$A_p = B_p e^{j\delta} \frac{(\bar{n}_3 \cos^* \phi_2 + \bar{n}_2 \cos^* \phi_3)}{(\bar{n}_3 \cos^* \phi_2 - \bar{n}_2 \cos^* \phi_3)} \quad (\text{eq. 2-40})$$

Substituting this result into eqs. 2-32 and 2-33 and dividing the resulting expression eliminates B_p giving

$$\frac{(E_p - R_p) \cos \phi_1}{(E_p + R_p) n_1} = \frac{\cos \phi_2}{\bar{n}_2} \frac{e^{j\delta} (\bar{n}_3 \cos^* \phi_2 + \bar{n}_2 \cos^* \phi_3) - (\bar{n}_3 \cos^* \phi_2 - \bar{n}_2 \cos^* \phi_3)}{e^{j\delta} (\bar{n}_3 \cos^* \phi_2 + \bar{n}_2 \cos^* \phi_3) + (\bar{n}_3 \cos^* \phi_2 - \bar{n}_2 \cos^* \phi_3)}$$

After some tedious algebraic manipulation, this expression reduces to

$$\begin{aligned}
 \frac{R_p}{E_p} &= \frac{(\tilde{n}_2 \tilde{n}_3 \cos \phi_1 \cos^* \phi_2 - n_1 \tilde{n}_2 \cos^* \phi_2 \cos^* \phi_3) + (\tilde{n}_2^2 \cos \phi_1 \cos^* \phi_3 - n_1 \tilde{n}_3 \cos^* \phi_2) P}{(\tilde{n}_2 \tilde{n}_3 \cos \phi_1 \cos^* \phi_2 + n_1 \tilde{n}_2 \cos^* \phi_2 \cos^* \phi_3) + (\tilde{n}_2^2 \cos \phi_1 \cos^* \phi_3 + n_1 \tilde{n}_3 \cos^* \phi_2) P} \\
 &= \frac{\tilde{n}_3 \cos \phi_1 - n_1 \cos^* \phi_3}{\tilde{n}_3 \cos \phi_1 + n_1 \cos^* \phi_3} \frac{1 + aP}{1 + bP} \\
 &= r_{13}^p \frac{1 + aP}{1 + bP} \quad . \quad (\text{eq. 2-41})
 \end{aligned}$$

where
$$P = \frac{e^{j\delta} - 1}{e^{j\delta} + 1} = \tanh j\delta/2 \quad , \quad (\text{eq. 2-42})$$

$$a = \frac{n_1 \cos \phi_1}{(\tilde{n}_3 \cos \phi_1 - n_1 \cos^* \phi_3)} \frac{\tilde{n}_2 \cos^* \phi_3}{n_1 \cos^* \phi_2} - \frac{\tilde{n}_3 \cos^* \phi_2}{\tilde{n}_2 \cos \phi_1} \quad , \quad (\text{eq. 2-43})$$

and
$$b = \frac{n_1 \cos \phi_1}{(\tilde{n}_3 \cos \phi_1 + n_1 \cos^* \phi_3)} \frac{\tilde{n}_2 \cos^* \phi_3}{n_1 \cos^* \phi_2} + \frac{\tilde{n}_3 \cos^* \phi_2}{\tilde{n}_2 \cos \phi_1} \quad . \quad (\text{eq. 2-44})$$

In a similar way, we can obtain an expression for the reflectivity of the perpendicular components (R_s/E_s). If we multiply eq. 2-39 by $e^{j\tau}A$ and eq. 2-38 by $e^{j\tau}A \tilde{n}_3 \cos^* \phi_3$, their right hand sides become equal, so that D_s is eliminated, giving

$$A_s = B_s e^{j\delta} \frac{(\tilde{n}_2 \cos^* \phi_2 + \tilde{n}_3 \cos^* \phi_3)}{(\tilde{n}_2 \cos^* \phi_2 - \tilde{n}_3 \cos^* \phi_3)} \quad . \quad (\text{eq. 2-45})$$

Substituting this result into eqs. 2-34 and 2-35 and dividing the resulting expressions eliminates B_s , so that

$$\frac{(E_s - R_s)n_1 \cos \phi_1}{(E_s + R_s)} = n_2 \cos^* \phi_2 \frac{e^{j\delta} (\bar{n}_2 \cos^* \phi_2 + \bar{n}_3 \cos^* \phi_3) - (\bar{n}_2 \cos^* \phi_2 - \bar{n}_3 \cos^* \phi_3)}{e^{j\delta} (\bar{n}_2 \cos^* \phi_2 + \bar{n}_3 \cos^* \phi_3) + (\bar{n}_2 \cos^* \phi_2 - \bar{n}_3 \cos^* \phi_3)}$$

Further algebraic manipulation along with definition eq. 2-42 reduces this expression to

$$\begin{aligned} \frac{R_s}{E_s} &= \frac{(n_1 \cos \phi_1 - \bar{n}_3 \cos^* \phi_3)}{(n_1 \cos \phi_1 + \bar{n}_3 \cos^* \phi_3)} \frac{1 + c P}{1 + e P} \\ &= r_{13}^s \frac{1 + c P}{1 + b P} \end{aligned} \quad (\text{eq. 2-46})$$

where

$$c = \frac{n_1 \cos \phi_1}{(n_1 \cos \phi_1 - \bar{n}_3 \cos^* \phi_3)} \frac{\bar{n}_3 \cos^* \phi_3}{\bar{n}_2 \cos^* \phi_2} - \frac{\bar{n}_2 \cos^* \phi_2}{n_1 \cos \phi_1} \quad , \quad (\text{eq. 2-47})$$

and

$$e = \frac{n_1 \cos \phi_1}{(n_1 \cos \phi_1 + \bar{n}_3 \cos^* \phi_3)} \frac{\bar{n}_3 \cos^* \phi_3}{\bar{n}_2 \cos^* \phi_2} + \frac{\bar{n}_2 \cos^* \phi_2}{n_1 \cos \phi_1} \quad , \quad (\text{eq. 2-48})$$

Dividing eq. 2-41 by 2-46 gives

$$\frac{R_p}{R_s} \cdot \frac{E_s}{E_p} = \frac{r_{13}^p}{r_{13}^s} \cdot \frac{1 + a P}{1 + b P} \cdot \frac{1 + e P}{1 + c P} \quad (\text{eq. 2-49})$$

Noting that the left hand side of eq. 2-49 is simply the ratio of the two reflection coefficients for the whole system resolved in and normal to the plane of incidence, we may re-write the expression in terms of the parameters describing the elliptical polarization, $\tan \psi$ and $\exp j\Delta$. In addition, the ratio (r_{13}^P/r_{13}^S) is the analogous expression for a substrate devoid of any surface film and can be described in terms of the "free-surface" angles $\bar{\Delta}$ and $\bar{\psi}$. Making these changes, eq. 2-49 becomes

$$Z^* = \frac{\tan \psi}{\tan \bar{\psi}} \cdot \exp j(\Delta - \bar{\Delta}) = \frac{(1+a P) \cdot (1+e P)}{(1+b P) \cdot (1+c P)} \quad (\text{eq. 2-50})$$

This expression is the generalized ellipsometry equation 1-3 re-cast in a slightly different form. It can be solved exactly for Δ and ψ ; in fact

$$\Delta = \bar{\Delta} + \tan^{-1} \left\{ \frac{\text{Im} (Z^*)}{\text{Re} (Z^*)} \right\}, \quad (\text{eq. 2-51})$$

and
$$\psi = \tan^{-1} \left[\tan \bar{\psi} \sqrt{\text{Re}^2 (Z^*) + \text{Im}^2 (Z^*)} \right]. \quad (\text{eq. 2-52})$$

The generalized ellipsometry equation is useful in the form of eq. 2-50 since this allows us to see, quite readily, how the thin-film expansions used by several authors^{7,10,11} come about.

Approximate Solutions

For thin films, the phase change δ undergone in traversing the oxide film is small so that the phase term, P , reduces to a simpler form

$$P = \tanh j\delta/2 \approx j\delta/2 = j \frac{2\pi}{\lambda} \tilde{n}_2 \cos^* \phi_2 d \quad (\text{eq. 2-53})$$

If the terms in P are taken to be very small, eq. 2-50 can be approximated as

$$Z^* = \frac{\tan \psi}{\tan \bar{\psi}} \exp j(\Delta - \bar{\Delta}) \approx 1 + (a+e-b-c) P, \quad (\text{eq. 2-54})$$

From the expressions for a, b, c, and e, the bracketed quantity, after applying Snell's law to eliminate ϕ_2 and ϕ_3 , becomes

$$(a+e-b-c) = \frac{2n_1 \cos \phi_1 \sin^2 \phi_1 (\bar{n}_2^2 - n_1^2) \left[\frac{1}{\bar{n}_3^2} - \frac{1}{\bar{n}_2^2} \right]}{\bar{n}_2 \cos^* \phi_2 \left[1 - \frac{n_1^2}{\bar{n}_3^2} \cos^2 \phi_1 - \frac{n_1^2 \sin^2 \phi_1}{\bar{n}_3^2} \right]}. \quad (\text{eq. 2-55})$$

Substitution of this expression along with eq. 2-53 into eq. 2-54 yields

$$Z^* = \frac{\tan \psi}{\tan \bar{\psi}} \exp j(\Delta - \bar{\Delta}) \approx 1 - j \frac{4\pi n_1 \cos \phi_1 \sin^2 \phi_1 (\bar{n}_2^2 - n_1^2) \left(\frac{1}{\bar{n}_2^2} - \frac{1}{\bar{n}_3^2} \right)}{\lambda \left[1 - \frac{n_1^2}{\bar{n}_3^2} \cos^2 \phi_1 - \frac{n_1^2 \sin^2 \phi_1}{\bar{n}_3^2} \right]}. \quad (\text{eq. 2-56})$$

If we now explicitly introduce the complex refractive indices for the substrate and the oxide, and note that, in general,

$$\begin{aligned} 1/\bar{n}^2 &= 1/(n - j k)^2 = \frac{n^2 - k^2}{(n^2 + k^2)^2} + j \frac{2nk}{(n^2 + k^2)^2} \\ &= a + j a' \end{aligned} \quad (\text{eq. 2-57})$$

the bracketed quantities in the denominator of eq. 2-56 become

$$\begin{aligned}
 & (1 - n_1^2(a_3 + ja_3'))(\cos^2\phi_1 - n_1^2(a_3 + ja_3')\sin^2\phi_1) \\
 & = \cos^2\phi_1 - n_1^2 a_3 + n_1^4 (a_3^2 - a_3'^2) \sin^2\phi_1 - j n_1^2 a_3' (1 - 2n_1^2 a_3 \sin^2\phi_1) \\
 & = \quad \quad \quad x \quad \quad - \quad j y. \quad \quad \quad (\text{eq. 2-58})
 \end{aligned}$$

Rationalizing eq. 2-56 by multiplying the numerator and denominator by the complex conjugate of eq. 2-58, and expanding the bracketed quantities in the numerator of eq. 2-56 with the aid of eq. 2-57, gives the result

$$Z^* = \frac{\tan\psi}{\tan\bar{\psi}} \exp j(\Delta - \bar{\Delta}) \approx 1 - j \frac{4\pi n_1 \cos\phi_1 \sin^2\phi_1}{\lambda(x^2 + y^2)} (\mu + j\nu)d.$$

(eq. 2-59)

where

$$\begin{aligned}
 \mu = & (n_2^2 - k_2^2 - n_1^2) [(a_2' - a_3')x + (a_2' - a_3')y] + (2n_2 k_2) \\
 & [(a_2' - a_3')x + (a_2 - a_3)y]
 \end{aligned}$$

(eq. 2-60)

and

$$\nu = (n_2^2 - k_2^2 - n_1^2) [(a_2 - a_3)y + (a_2' - a_3')x] + (2n_2 k_2) [(a_2' - a_3')y - (a_2 - a_3)x].$$

(eq. 2-61)

For convenience, we define the thin film expansion coefficients α and β' as

$$\alpha = \frac{4\pi n_1 \cos \phi_1 \sin^2 \phi_1 \mu}{\lambda (x^2 + y^2)} \quad , \quad (\text{eq. 2-62})$$

and

$$\beta' = \frac{2\pi n_1 \cos \phi_1 \sin^2 \phi_1 \nu}{\lambda (x^2 + y^2)} \quad . \quad (\text{eq. 2-63})$$

With these definitions, eq. 2-59 becomes

$$Z^* = \frac{\tan \psi}{\tan \bar{\psi}} \exp j(\Delta - \bar{\Delta}) \approx (1 + 2\beta'd) - j\alpha d \quad . \quad (\text{eq. 2-64})$$

By performing different expansions on the left-hand side of this expression, the various thin film approximations reported in the literature can be obtained. Separating eq. 2-64 into real and complex components and dividing gives

$$\Delta - \bar{\Delta} = \tan^{-1} \frac{-\alpha d}{1 + 2\beta'd} \quad (\text{eq. 2-64})$$

Also by separating eq. 2-64 into real and complex components, squaring, and adding gives

$$\begin{aligned} \frac{\tan \psi}{\tan \bar{\psi}}^2 &= (1 + 2\beta'd)^2 + \alpha^2 d^2 \\ &= 1 + 4\beta'd + (4\beta'^2 + \alpha^2)d^2 \quad . \end{aligned}$$

Expanding $\tan^2 \psi$ as a truncated power series about the point $\bar{\psi}$, the previous expression becomes

$$\begin{aligned} \frac{\tan^2 \bar{\psi} + 2(\psi - \bar{\psi}) \sec^2 \bar{\psi} \tan \bar{\psi}}{\tan^2 \bar{\psi}} &= 1 + \frac{4(\psi - \bar{\psi})}{\sin 2\bar{\psi}} \\ &= 1 + 4\beta'd + (4\beta'^2 + \alpha^2)d^2, \end{aligned}$$

Hence,

$$\psi - \bar{\psi} = \beta' \sin 2\bar{\psi} d + (\beta'^2 + 1/4\alpha^2) \sin 2\bar{\psi} d^2. \quad (\text{eq. 2-65})$$

These two approximate expressions 2-64 and 2-65 can be reduced to those reported by Saxena¹¹ by neglecting the term $2\beta'd$ with respect to unity and αd . However, they differ from those of Saxena in two respects:²³

(1) the coefficient α contains the oxide extinction coefficient k_2 , not necessarily zero. Neglect of this extinction coefficient can lead to erroneous thickness calculations for very thin films (less than 50 angstroms) --- the only regime where the thin film expansions are valid.

(2) the term y contains a factor $2n_1^2 a_3 \sin^2 \phi_1$ which is not always small compared to unity and thus should not be neglected.

The expansions used by Archer⁷ can be obtained from the above expressions by neglecting the term $2\beta'd$ with respect to unity and by approximating the \tan^{-1} function by the first order term in its power series expansion in the phase change equation 2-64: The parabolic term in film thickness in eq. 2-65 is neglected by Archer.

The thin film approximations are unfortunately valid only for very thin films -- of order 50 angstroms and less. Since they are sufficiently complicated to require a computer for their calculation, it is of better advantage to solve the exact equations 2-51 and 2-52.

CHAPTER III

AN ANALYSIS OF THE EQUATIONS

The Inversion Angles:

Initially the inversion angles P and Q used in solving for $\bar{\Delta}$ and $\bar{\psi}$ were analyzed for various combinations of n_3 and k_3 .

Case 1: $n_3 \gg k_3$; $n_3 \neq 0$ and $k_3 \neq 0$.

Here $\tan 2Q = \frac{2 \cdot n_3 \cdot k_3}{n_3^2 - k_3^2 - n_1^2 \cdot \sin^2 \phi_1}$ is always positive provided

$n_3^2 > k_3^2 + n_1^2 \cdot \sin^2 \phi_1$ --so that the angle 2Q always lies in the first or third quadrant, i.e.

$$\begin{array}{lll} 90^\circ > 2Q > 0^\circ & \text{or} & -90^\circ > 2Q > -180^\circ & \text{or} & 270^\circ > 2Q > 180^\circ \\ 45^\circ > Q > 0^\circ & & -45^\circ > Q > -90^\circ & & 135^\circ > Q > 90^\circ \end{array}$$

$$\begin{array}{lll} 1/2 > \sin Q > 0 & -1 > \sin Q > -1 & 1 > \sin Q > 1/2 \\ 1 > \cos Q > 1/2 & 1/2 > \cos Q > 0 & 0 > \cos Q > -1/2 \end{array}$$

We see that there are three possible regions where the angle Q may lie for this case, with sinQ and cosQ possibly taking on both positive and negative signs. Now looking at the expression for the angle P:

$$\tan P = \frac{[n_3^4 + k_3^4 + n_1^4 \cdot \sin^4 \phi_1 + 2 \cdot n_3^2 \cdot k_3^2 - 2 \cdot n_1^2 \cdot (n_3^2 - k_3^2) \cdot \sin^2 \phi_1]^{1/4}}{n_1 \cdot \sin \phi_1 \cdot \tan \phi_1}$$

This expression is always positive so that the angle P always lies in the first or third quadrants. As a result the angle 2P always lies in the first two quadrants, so that tan 2P can take on either sign and sin 2P is always positive. Now since $\bar{\psi}$ is determined by $\cos 2\bar{\psi} = \cos Q \cdot \sin 2P$, the angle $2\bar{\psi}$ takes on the same sign as the angle Q. For the cases where cos Q is positive, lying between 0 and 1, the angle $2\bar{\psi}$ lies between 0° and 90° or $\bar{\psi}$ lies between 0° and 45° . When cos Q is negative, cos $2\bar{\psi}$ can assume values between zero and $-1/2$ so that $\bar{\psi}$ can assume values between 67.5° and 45° , 112.5° and 135° , -67.5° and -45° , and -112.5° and -135° . A similar situation occurs for the angle $\bar{\Delta}$ since tan 2P takes on both signs and a variety of magnitudes since tan P can vary between infinity and zero. As a result $\bar{\Delta}$ must lie between 0° and 180° . The two regions $135^\circ > \bar{\psi} > 112.5^\circ$ and $-45^\circ > \bar{\psi} > -67.5^\circ$ can be rejected on physical grounds since the ellipticity tan ψ is negative in these two ranges --- an impossibility since $\tan\psi = \frac{|E(p)|}{|E(s)|} > 0$.

Case 2: $n_3 \geq k_3$; $n_3 \neq 0$ and $k_3 \neq 0$.

If n_3 is such that $k_3^2 + \sin^2\phi_1 \cdot n_1^2 > n_3^2 > k_3^2$ then tan 2Q lies between infinity and $(-2 \cdot n_3 \cdot k_3 / n_1^2 \cdot \sin^2\phi_1)$.

Consequently:

$$\begin{array}{llll}
 360^\circ > 2Q > 270^\circ & \text{or} & 270^\circ > 2Q > 90^\circ & \text{or} & 0^\circ > 2Q > -90^\circ \\
 180^\circ > Q > 135^\circ & & 135^\circ > Q > 45^\circ & & 0^\circ > Q > -45^\circ
 \end{array}$$

$$\begin{array}{lll}
 1/2 > \sin Q > 0 & 1 > \sin Q > 1/2 & 0 > \sin Q > -1/2 \\
 -1/2 > \cos Q > -1 & +1/2 > \cos Q > -1/2 & -1/2 > \cos Q > -1
 \end{array}$$

The expression for $\tan P$ is always positive so that the angle P always lies in the first or third quadrants. As a result the angle $2P$ always lies in the first two quadrants and $\tan 2P$ can take on either sign and $\sin 2P$ is always positive, and less than or equal to unity. Again $2\bar{\psi}$ lies in the same quadrants as Q , i.e.

$$180^\circ > 2\bar{\psi} > 135^\circ \quad \text{or} \quad 135^\circ > 2\bar{\psi} > 45^\circ \quad \text{or} \quad 0^\circ > 2\bar{\psi} > -45^\circ$$

$$90^\circ > \bar{\psi} > 67.5^\circ \quad 67.5^\circ > \bar{\psi} > 22.5^\circ \quad 0 > \bar{\psi} > -22.5^\circ$$

The third region for negative angles is, as before, physically inconsistent with the positive ellipticity since the tangent of the negative angles in this range are negative. Since $\tan 2P$ can take either sign and a wide range of magnitudes -- a result of the variation in ϕ_1 , $\tan \bar{\Delta}$ can take on all magnitudes and either sign so that $\bar{\Delta}$ lies between 0° and 180° .

Case 3: $n_3 = k_3 \neq 0$

$$\text{For this case, } \tan 2Q = \frac{2.n_3^2}{n_1^2 \cdot \sin^2 \phi_1} = \frac{2.k_3^2}{n_1^2 \cdot \sin^2 \phi_1}$$

which can take on values between minus infinity and $-2.n_3^2/n_1^2$. Hence:

$$360^\circ > 2Q > 270^\circ \quad \text{or} \quad 180^\circ > 2Q > 90^\circ \quad \text{or} \quad 0^\circ > 2Q > -90^\circ$$

$$180^\circ > Q > 135^\circ \quad 90^\circ > Q > 45^\circ \quad 0^\circ > Q > -45^\circ$$

$$1/2 > \sin Q > 0 \quad 1 > \sin Q > 1/2 \quad 0 > \sin Q > -1/2$$

$$-1/2 > \cos Q > -1 \quad 1/2 > \cos Q > 0 \quad 1 > \cos Q > 1/2$$

As in the other cases $\tan P$ is always positive; $\tan 2P$ can take all magnitudes and either sign; $\sin 2P$ is always positive. This results in $2\bar{\psi}$ located in the regions:

$$\begin{array}{lll} 180^\circ > 2\bar{\psi} > 135^\circ & 90^\circ > 2\bar{\psi} > 45^\circ & 0 > 2\bar{\psi} > -45^\circ \\ 90^\circ > \bar{\psi} > 67.5^\circ & 45^\circ > \bar{\psi} > 22.5^\circ & 0 > \bar{\psi} > -22.5^\circ \end{array}$$

The last region is eliminated on account of negative ellipticity. Again because of the wide variation in $\tan 2P$, $\bar{\Delta}$ can lie between 0° and 180° .

Case 4: $n_3 \neq 0$ and $k_3 = 0$

For this case $\tan 2Q = 0$, so that $2Q$ is a multiple of 180 degrees.

Thus Q is a multiple of 90° . Also for this case

$$\tan P = \frac{n_3^2 - n_1^2 \cdot \sin^2 \phi_1}{n_1 \cdot \sin \phi_1 \cdot \tan \phi_1}$$

Here $n_3 > n_1$ since the substrate is a more optically dense medium. Then $\tan P$ is positive (not complex), and P lies between 0° and 90° or between 180° and 270° . As a result, $2P$ lies between 0° and 180° and $\tan 2P$ can take on all magnitudes and both signs while $\sin 2P$ is always positive. For the even multiples of 180° for $2Q$, $\sin Q = 1$ and $\bar{\Delta}$ takes on values between 0° and 180° ; $\cos Q = 0$ so $\cos 2\bar{\psi} = 0$, i.e. $2\bar{\psi} = -90^\circ, +90^\circ, \text{ or } +270^\circ$ or $\bar{\psi} = -45^\circ, 45^\circ, \text{ or } 135^\circ$. The only physically meaningful solution is $\bar{\psi} = 45^\circ$ since the tangent of the other two values is negative implying a negative ellipticity. For the odd multiples of 180° for $2Q$, $\sin Q = 0$ and $\cos Q = \pm 1$ resulting in $\tan \bar{\Delta} = 0$, i.e. $\bar{\Delta}$ is a multiple of 180° ; $\cos 2\bar{\psi} = \pm \sin 2P$ for this case so that $2\bar{\psi}$ takes on all values and so does $\bar{\psi}$. However physically this represents

reflection from a dielectric medium so that the reflected E vectors in both p and s polarizations have the same magnitude or $\tan \bar{\psi} = 1$. This has solution $\bar{\psi}$ equal to a multiple of 45 degrees. Consequently the odd multiples of 180° for $2Q$ have no physical meaning, but are extraneous solutions implicit in the inversion.

Case 5: $n_3 \ll k_3$: $n_3 \neq 0$ and $k_3 \neq 0$

Here $\tan 2Q$ is negative since it is dominated by the term in the denominator. As a result the angle $2Q$ either lies between -90° and 0° or 90° and 180° or 270° and 360° .

$$\begin{array}{lll} 0^\circ > 2Q > -90^\circ & 180^\circ > 2Q > 90^\circ & 360^\circ > 2Q > 270^\circ \\ 0^\circ > Q > -45^\circ & 90^\circ > Q > 45^\circ & 180^\circ > Q > 135^\circ \end{array}$$

$$\begin{array}{lll} 0 > \sin Q > -1/2 & 1 > \sin Q > 1/2 & 1/2 > \sin Q > 0 \\ 1 > \cos Q > 1/2 & 1/2 > \cos Q > 0 & -1/2 > \cos Q > -1 \end{array}$$

Tan P is always positive so that $2P$ lies between 0° and 180° with $\sin 2P$ being positive. For $\cos Q$ positive, $\cos 2\bar{\psi}$ lies between 0 and 1 so that $\bar{\psi}$ lies between 0° and 45° . When $\cos Q$ is negative, $\cos 2\bar{\psi}$ values between 0 and -1. Consequently $2\bar{\psi}$ lies between -270° and -90° or between 90° and 270° so that $\bar{\psi}$ can lie between -135° and -45° ; and -45° ; 45° and 135° ; 225° and 315° . However the regions between -90° and -45° ; 90° and 135° and 270° and 315° have negative tangents-hence a negative ellipticity and are not

physically acceptable solutions. So for $\cos Q$ negative, the allowed regions for $\bar{\psi}$ are between -135° and -90° ; 45° and 90° ; 225° and 270° . For the phase change $\bar{\Delta}$ acceptable solutions are between 0° and 180° since $\tan 2P$ can take on all values.

Case 6: $n_3 = 0$ and $k_3 \neq 0$

This case is impossible physically since it represents a purely absorbing medium having zero conductivity.

Plotting the free-surface angles $\bar{\Delta}$ and $\bar{\psi}$ as a function of angle of incidence ϕ_1 shows that the azimuth angle $\bar{\psi}$ goes through a minimum at the Brewster angle. In addition, the phase change $\bar{\Delta}$ varies from 180° to 0° --- the change occurring rapidly about the Brewster angle (at the Brewster angle, $\bar{\Delta} = 90^\circ$). The rate of change is a function of the magnitude of the extinction coefficient k_3 . For small k_3 , the change is very abrupt; for large k_3 the change is gradual. Figures 3-1 and 3-2 show $\bar{\Delta}$ and $\bar{\psi}$ plotted as functions of the angle of incidence ϕ_1 . The following materials were chosen since they have a wide range of optical constants:

Silicon ¹⁴	$n_3 = 4.05$	and	$k_3 = 0.028,$
Aluminum ¹⁷	$n_3 = 0.82$	and	$k_3 = 5.99,$
Iron ¹⁸	$n_3 = 3.35$	and	$k_3 = 3.84,$
Gold ¹⁹	$n_3 = 0.382$	and	$k_3 = 2.295.$

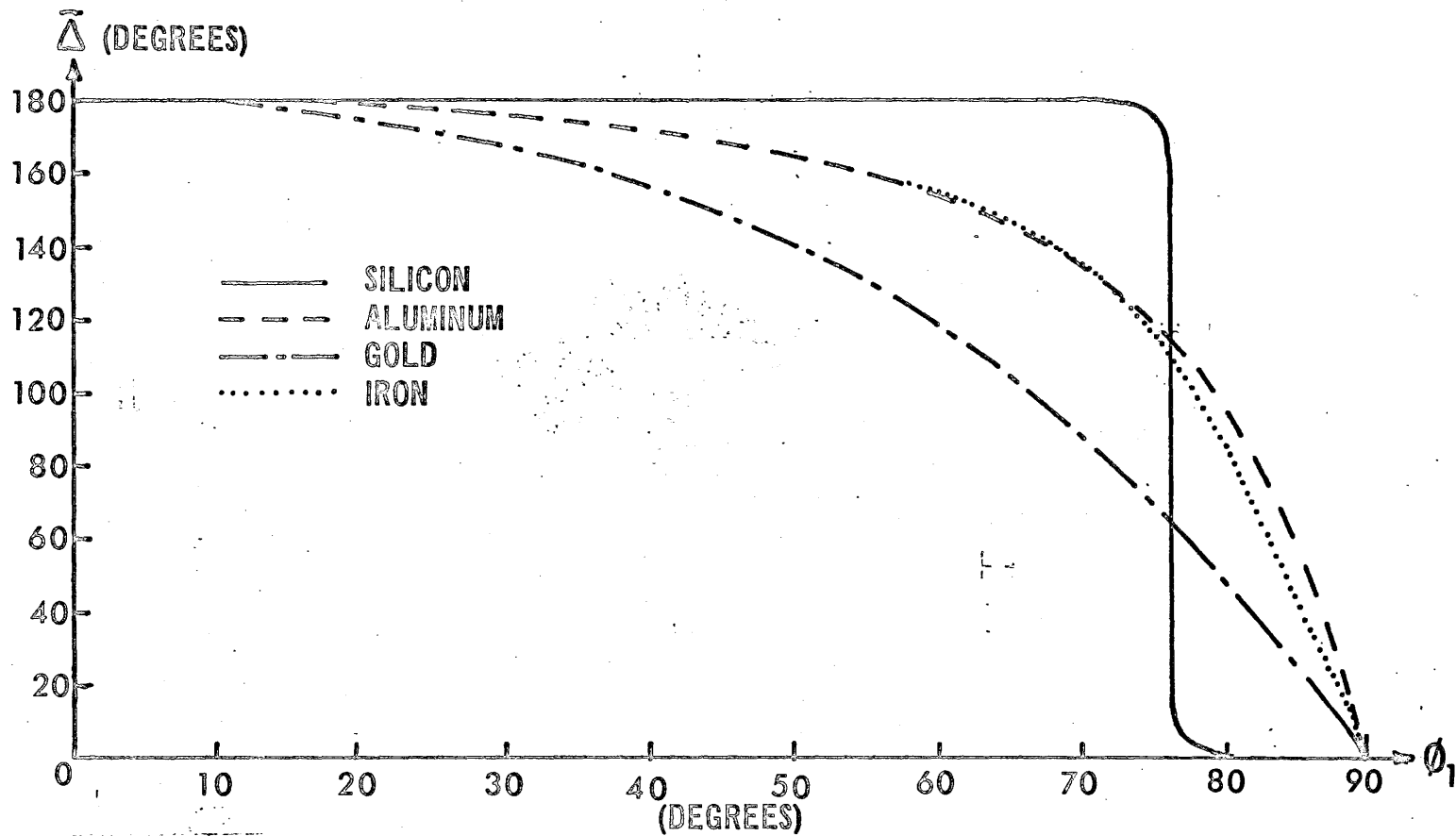


Figure 3-1

VARIATION OF FREE SURFACE ANGLE $\bar{\Delta}$ WITH ANGLE OF INCIDENCE ϕ_1

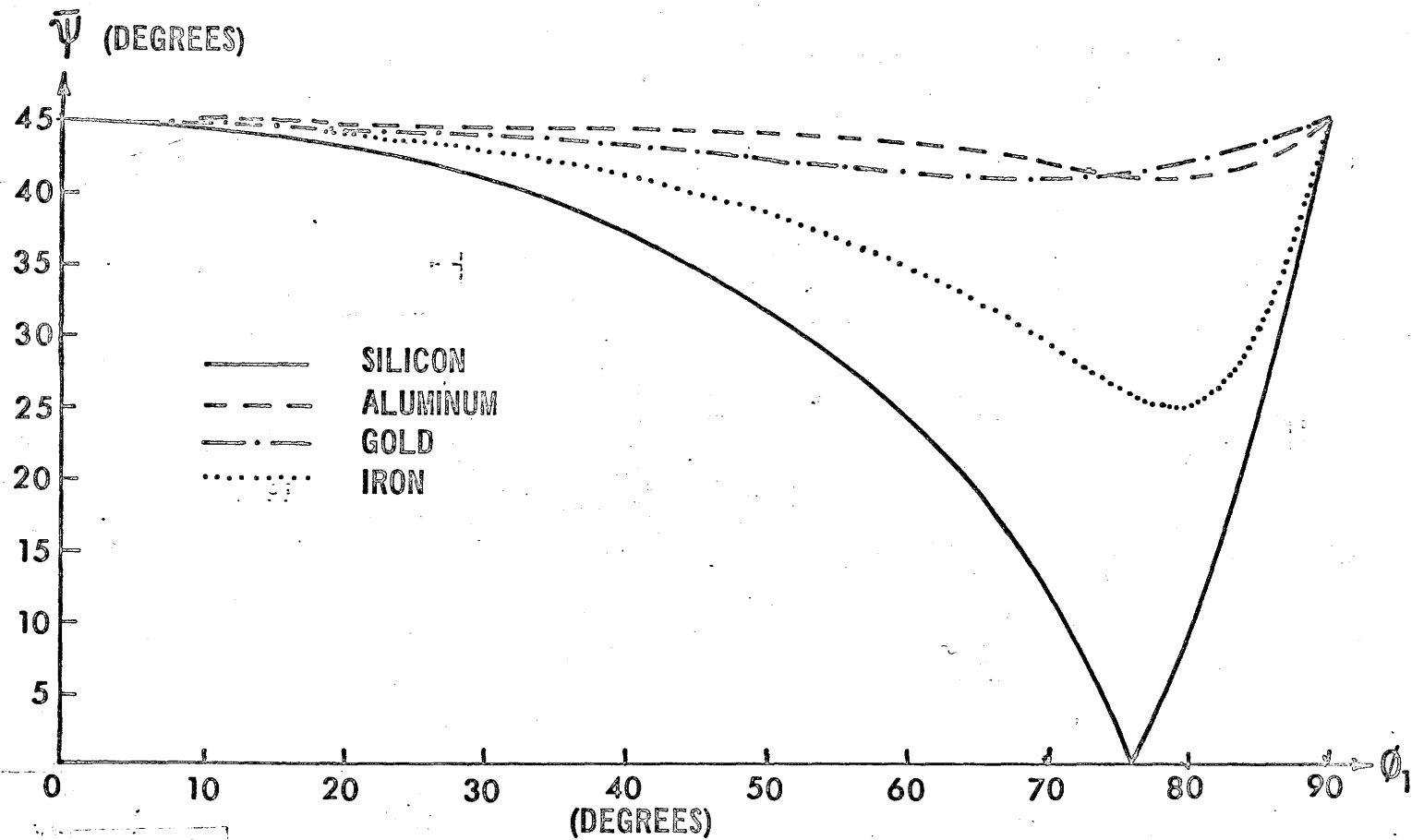


Figure 3-2

VARIATION OF FREE SURFACE ANGLE $\bar{\Psi}$ WITH ANGLE OF INCIDENCE ϕ_1

The Thin-Film Approximations

The next relations to be examined were the phase changes Δ from the free surface angle $\bar{\Delta}$ as a function of film thickness "d" for the exact equations of McCrackin and the approximate equations of Drude, Archer, Saxena, and those derived in Chapter II. The Drude, Archer, and Chapter II expansions are all of the form:

$$\Delta - \bar{\Delta} = -\alpha d$$

where the coefficient α contains successively more terms for each respective expansion. The expression of Saxena has been inverted to the form:

$$\Delta - \bar{\Delta} = -\tan^{-1}(\alpha d)$$

These plots are shown in figures 3-3, 3-4, 3-5, and 3-6 for several materials at an angle of incidence somewhat below the Brewster angle for the particular material involved. In all cases the expansion derived in Chapter II is within 10% of the exact expression for film thicknesses up to 100 angstroms, indicating that $\Delta - \bar{\Delta}$ does not deviate appreciably from a linear relation in film thickness "d" up to 100 angstroms. The difference between the Archer expression for α and that derived in Chapter II is simply the omission of the term $2n_1^2 a_3 \sin^2 \phi_1$ with respect to unity (see equation 2-58). For these calculations, the surrounding medium was assumed to have an index $n_1 = 1.0$, and the oxide was assumed to be non-absorbing (i.e. $k_2 = 0.0$). The more pronounced deviation in Archer's expansion from the exact expression is simply a reflection of his neglect of this term. This is most pronounced for gold ($n_3 = 0.382 - 2.295j$)¹⁸ where the quantity a_3 is approximately -0.175

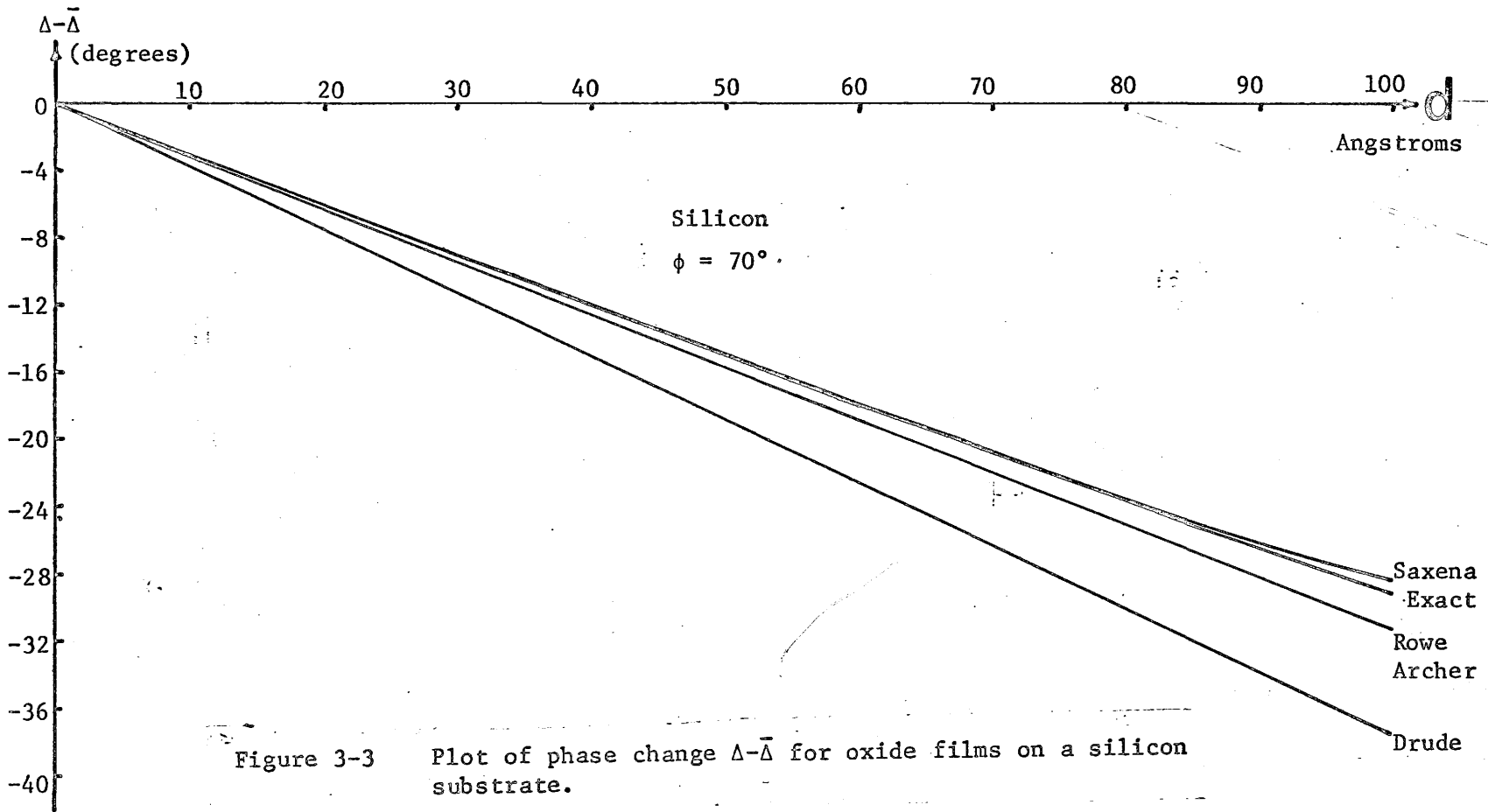
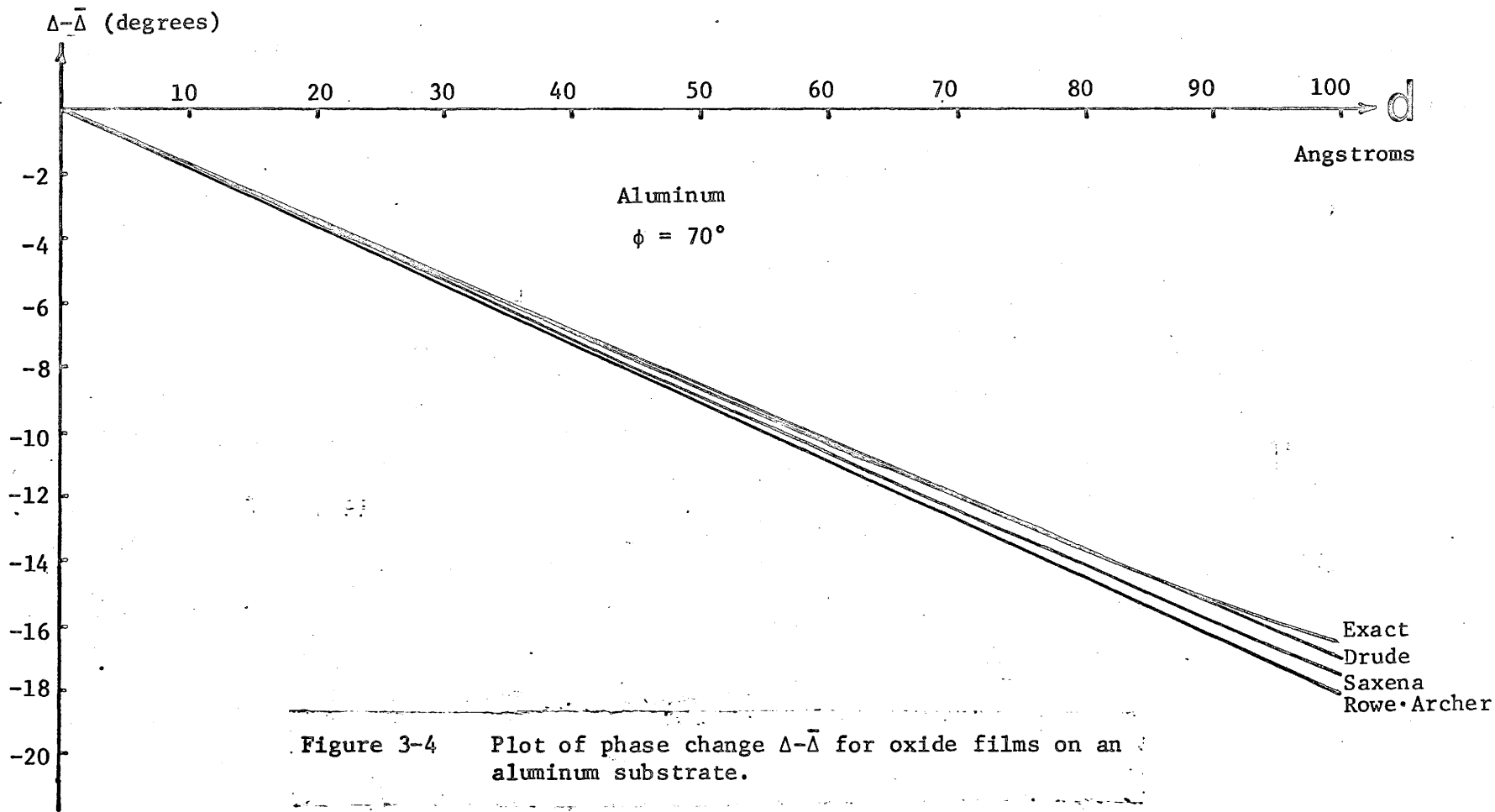


Figure 3-3 Plot of phase change $\Delta - \bar{\Delta}$ for oxide films on a silicon substrate.

Figure 3-3

Figure 3-4



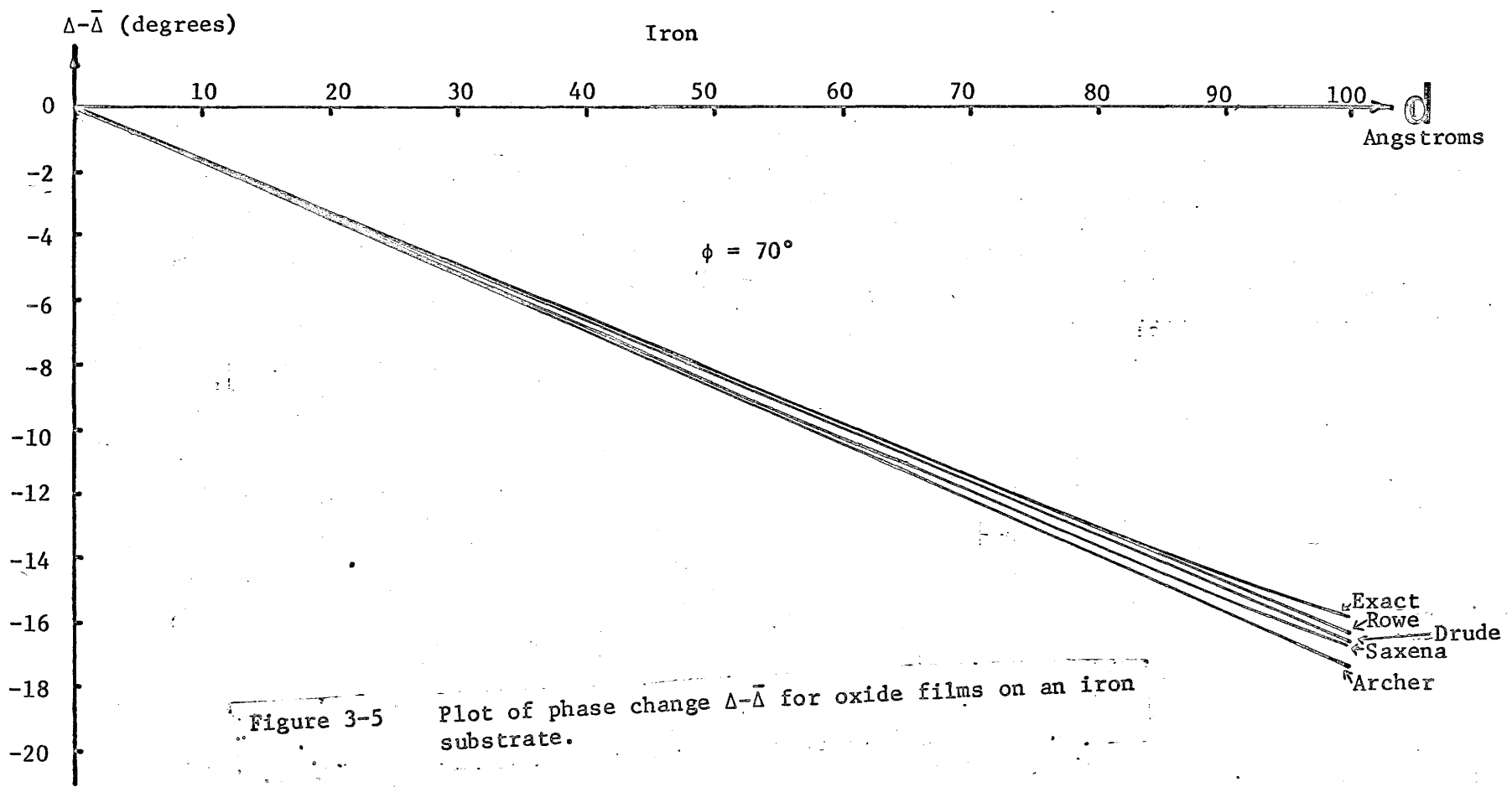


Figure 3-5

Figure 3-5

Plot of phase change $\Delta-\bar{\Delta}$ for oxide films on an iron substrate.

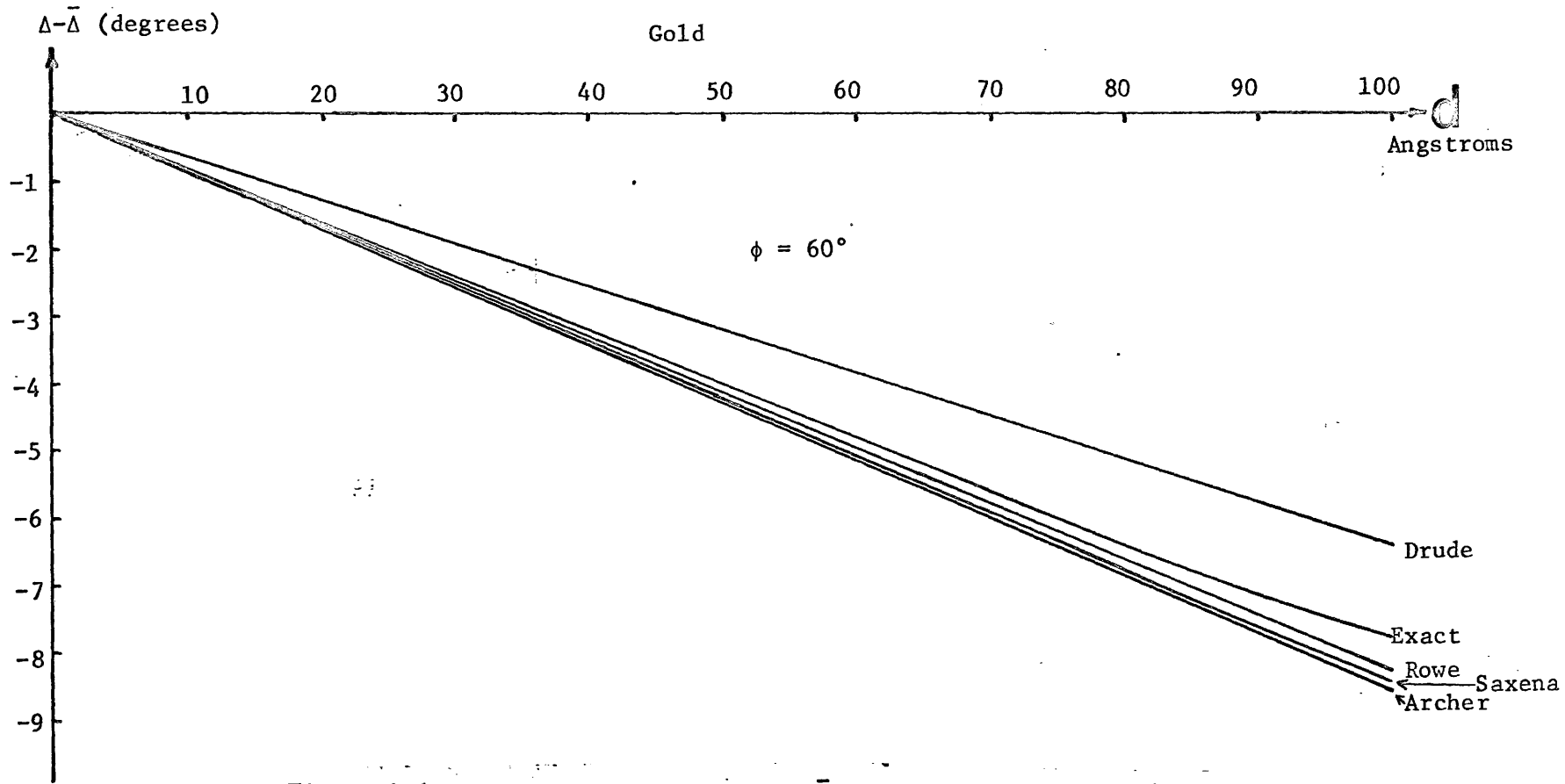


Figure 3-6 Plot of phase change $\Delta - \bar{\Delta}$ for oxide films on a gold substrate.

which is starting to become large with respect to unity (see fig. 3-6). For the other materials plotted the quantity a_3 is of order 10^{-2} or smaller and the term $2n_1^2 a_3 \sin^2 \phi_1$ is not so drastic.

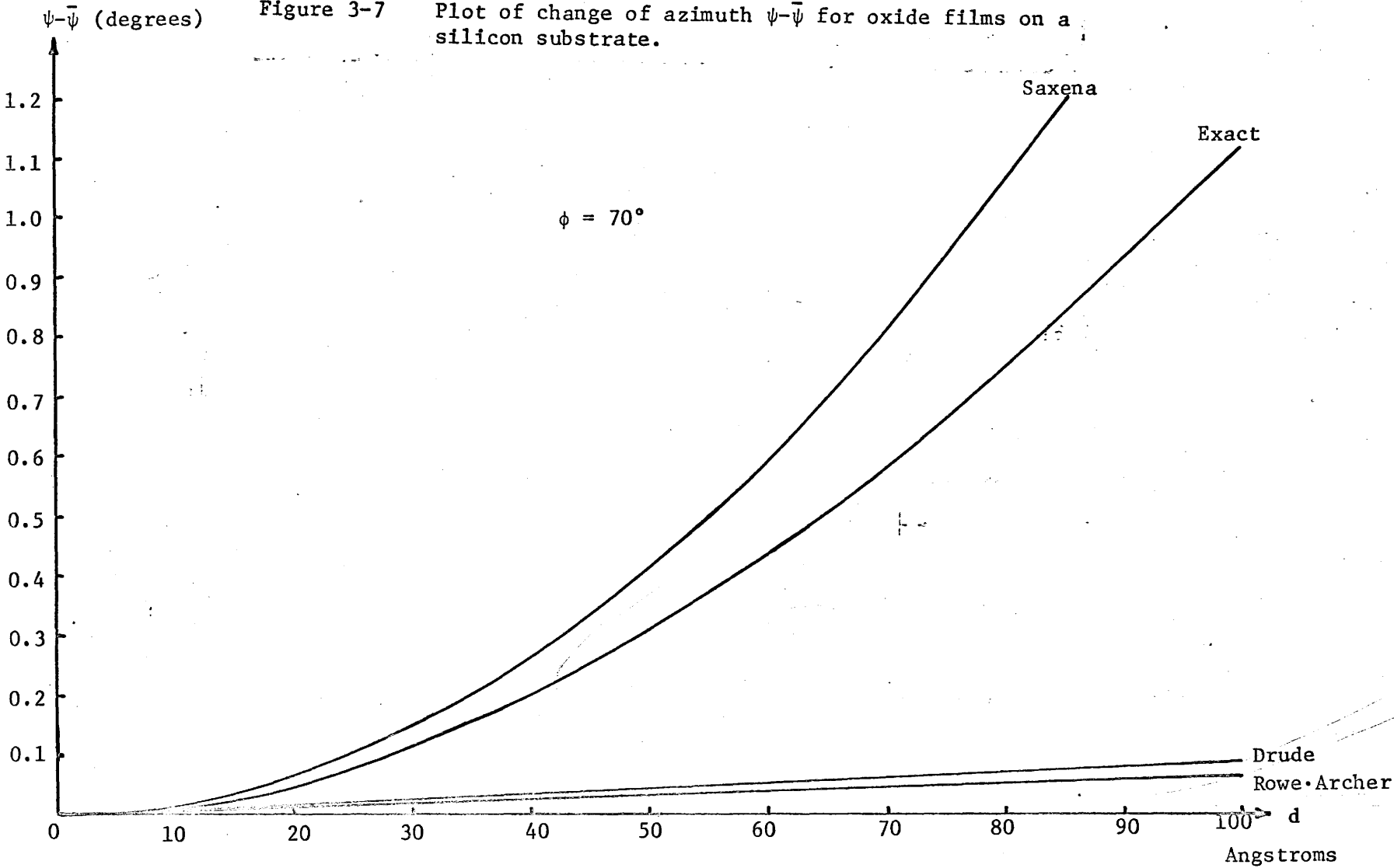
Analyzing the change in azimuth angle ψ from the free surface value $\bar{\psi}$ as a function of oxide film thickness "d" for both the exact and approximate relations showed one particularly interesting fact: If the substrate index n_3 is greater than the absorption coefficient k_3 , the plot of $\psi - \bar{\psi}$ versus film thickness "d" for the exact expression shows considerable curvature; if not, the plot of $\psi - \bar{\psi}$ versus film thickness "d" shows only a slight amount of curvature. As a result the parabolic expression of Saxena is a better fit to the exact curve provided the substrate index is greater than the substrate extinction coefficient than are any of the linear expansions. The converse for the substrate index less than the substrate extinction coefficient indicates that the linear expansion is better than the parabolic expression of Saxena. This effect is shown in figures 3-7 ($n_3 > k_3$); 3-8, 3-9, and 3-10 ($n_3 < k_3$).

The effect of an increasing oxide extinction coefficient appears to simply increase the slope of the plots of $\Delta - \bar{\Delta}$ versus film thickness. This is shown for silicon in figure 3-11 where the exact expansion using McCrakin's method has been used; in addition, the linear expansion derived in Chapter II has been plotted. Other expansions (Drude, Archer, and Saxena) neglect the effect of the film extinction coefficient and would not show any variation with increasing film extinction coefficient. The Chapter II expansion shows the same effect of increasing the slope of the curve and appears to be of the correct magnitude (the closeness of fit is always less than 5% even at

Figure 3-7

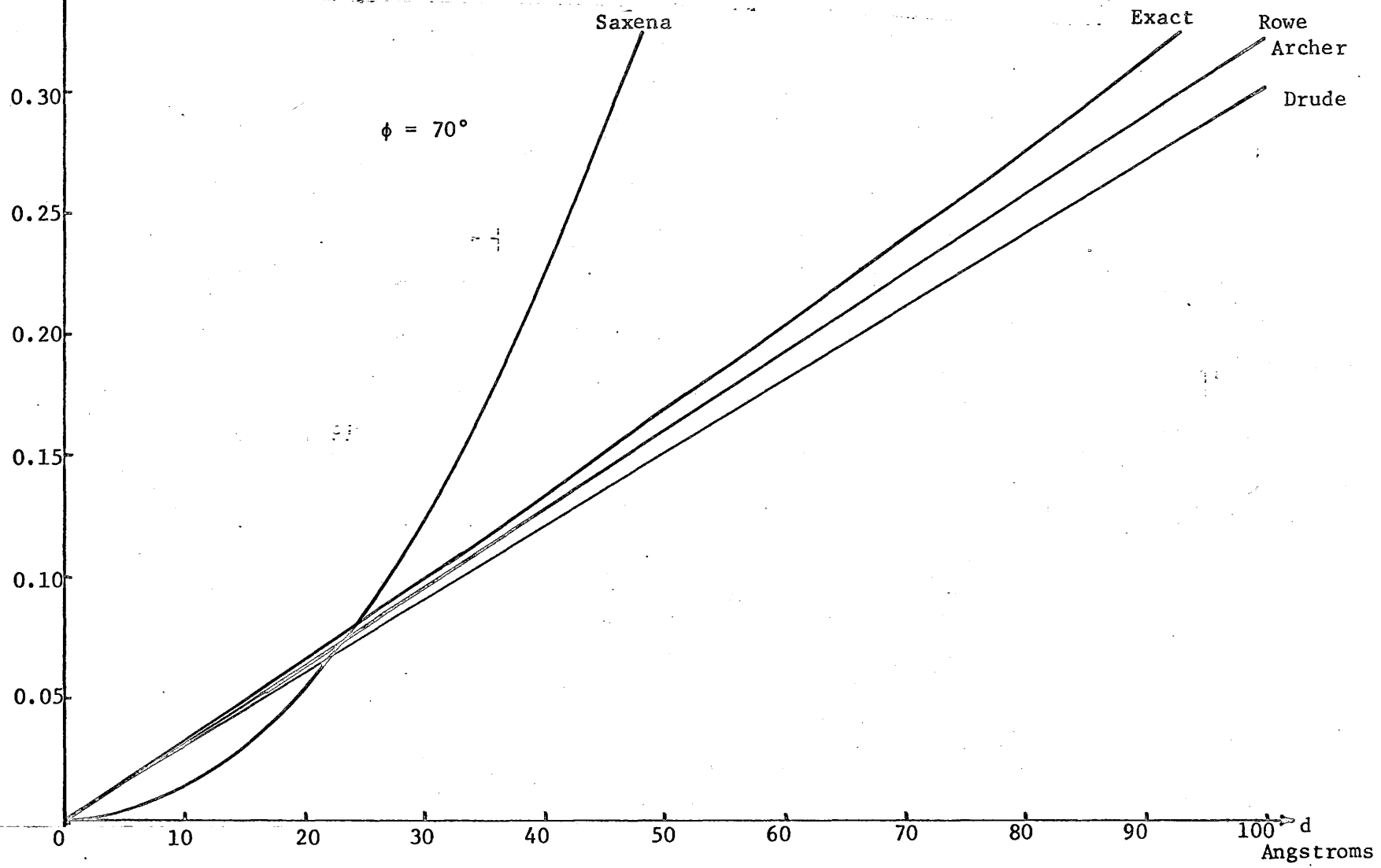
Plot of change of azimuth $\psi - \bar{\psi}$ for oxide films on a silicon substrate.

$\phi = 70^\circ$



$\psi - \bar{\psi}$ (degrees)

Figure 3-8 Plot of change of azimuth $\psi - \bar{\psi}$ for oxide films on an aluminum substrate.



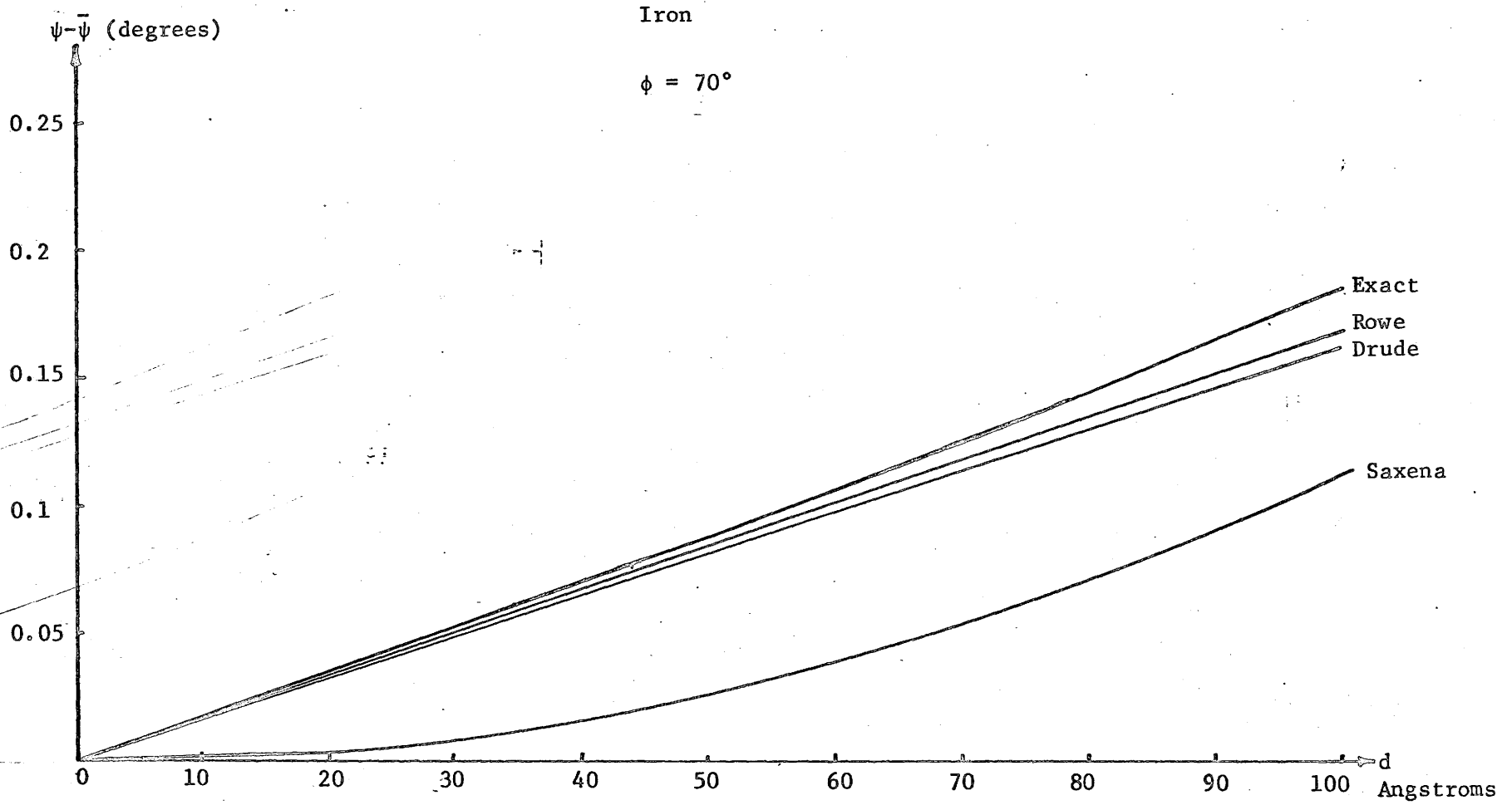
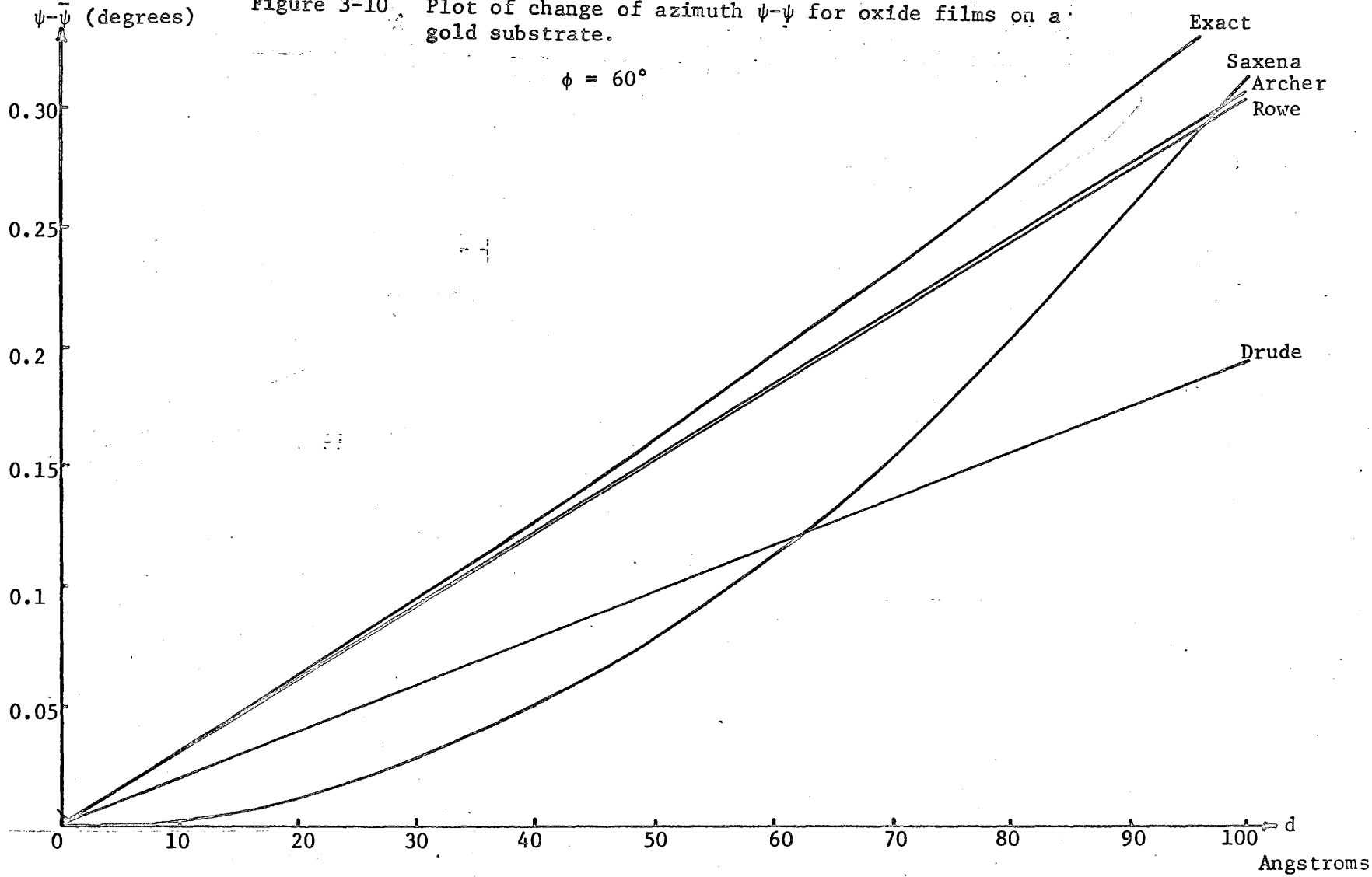


Figure 3-9 Plot of change of azimuth $\psi - \bar{\psi}$ for oxide films on an iron substrate.

Figure 3-10. Plot of change of azimuth $\psi - \bar{\psi}$ for oxide films on a gold substrate.

$\phi = 60^\circ$



a film thickness of 100 angstroms.). Consequently the expansions derived in Chapter II for the phase change $\Delta - \bar{\Delta}$ are better than any derived to date. Unfortunately, this expansion is not so good for the other materials studied (figures 3-12, 3-13, and 3-14), although it still shows the correct effect of increasing the slope.

The azimuth angle ψ shows a similar effect with increasing film extinction. The exact expressions show a decreasing slope with increasing film extinction coefficient (see figs. 3-15, 3-16, 3-17 and 3-18). Consequently for an absorbing oxide film on silicon, the parabolic expression would become progressively worse since the coefficient α is increasing with increasing oxide extinction coefficient k_2 , (Using the expression in Chapter II for α since Saxena's expression does not take into account absorptive effects in the oxide). The linear approximation derived in Chapter II contains the correct behaviour for very thin absorbing films (up to approximately 20 angstroms) but becomes progressively worse for thicker films once the curvature of the exact expression comes into play. This seems to indicate that the expansion for $\psi - \bar{\psi}$ should contain both a linear term and a parabolic term in film thickness; the linear term having a negative expansion coefficient which is very small when the extinction coefficient is very small (or zero) and becoming larger with increasing film extinction coefficient. Since in the method of determining optical constants in the computer program, the azimuth angles are not used for calculation of film thickness but only serve as a rough check that the correct solution has been chosen, further analysis of the azimuth angle has not been performed.

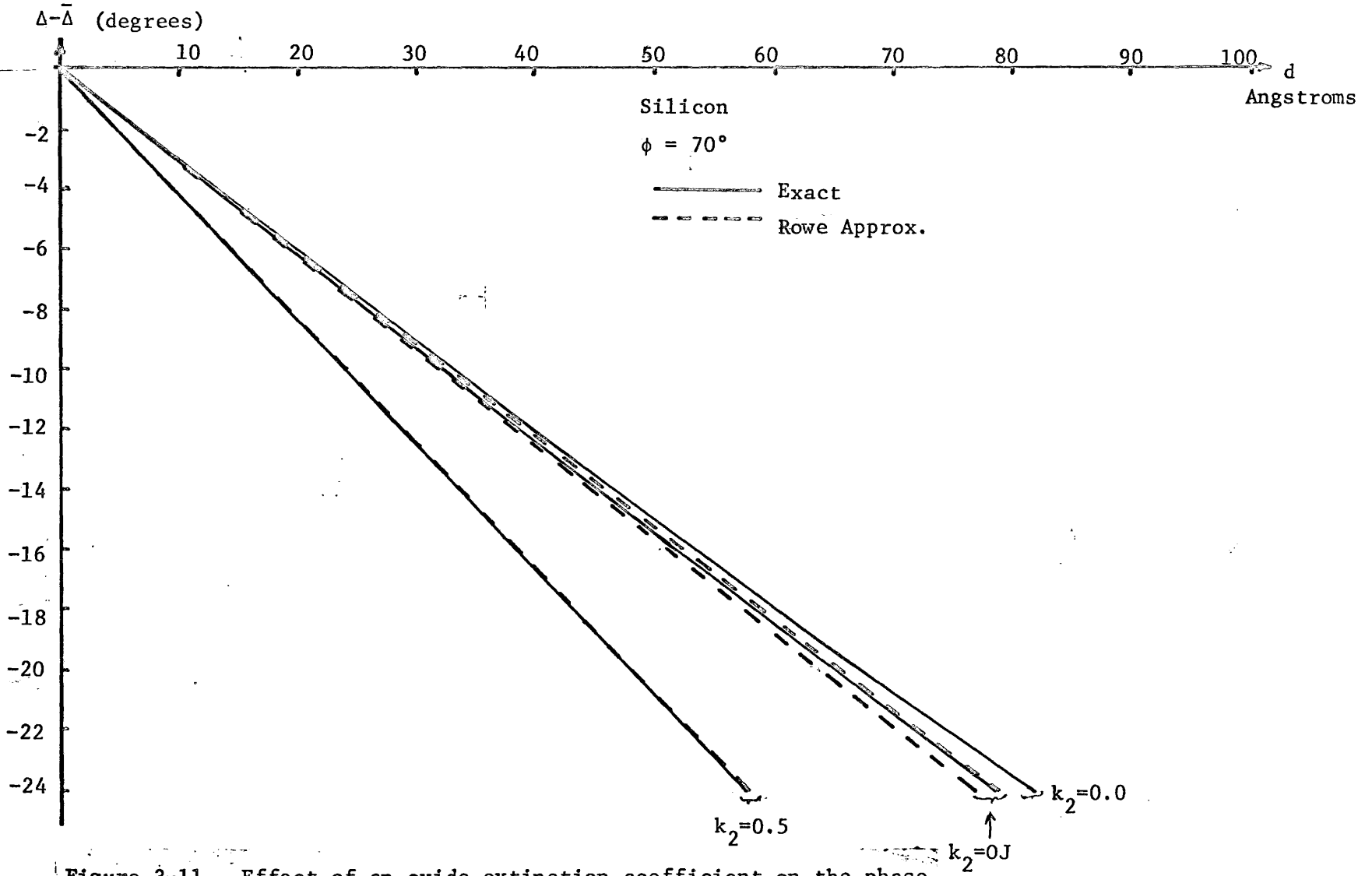


Figure 3-11 Effect of an oxide extinction coefficient on the phase charge $\Delta - \bar{\Delta}$ for oxide films on silicon.

Figure 3-11

- 45 -

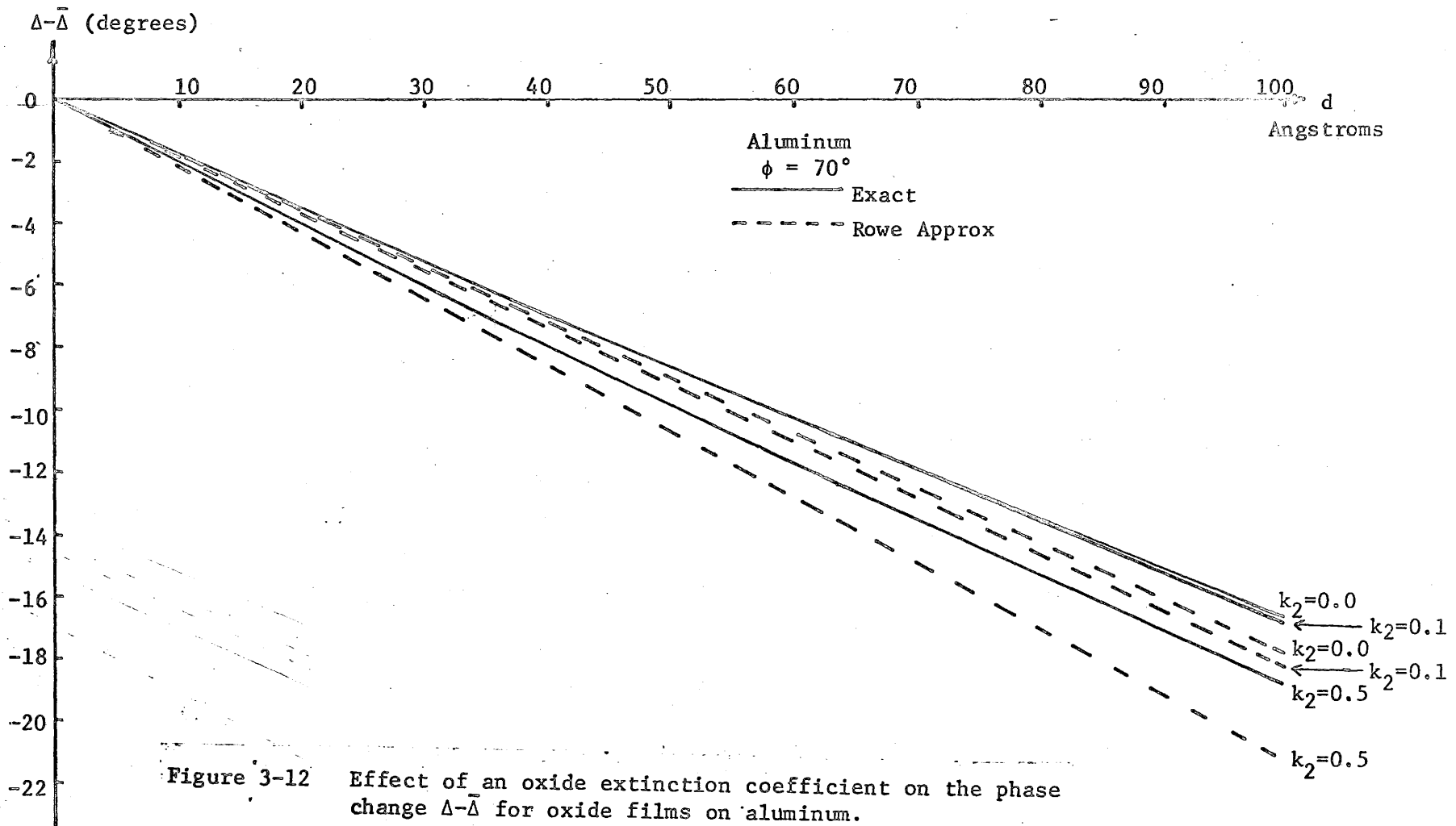


Figure 3-12

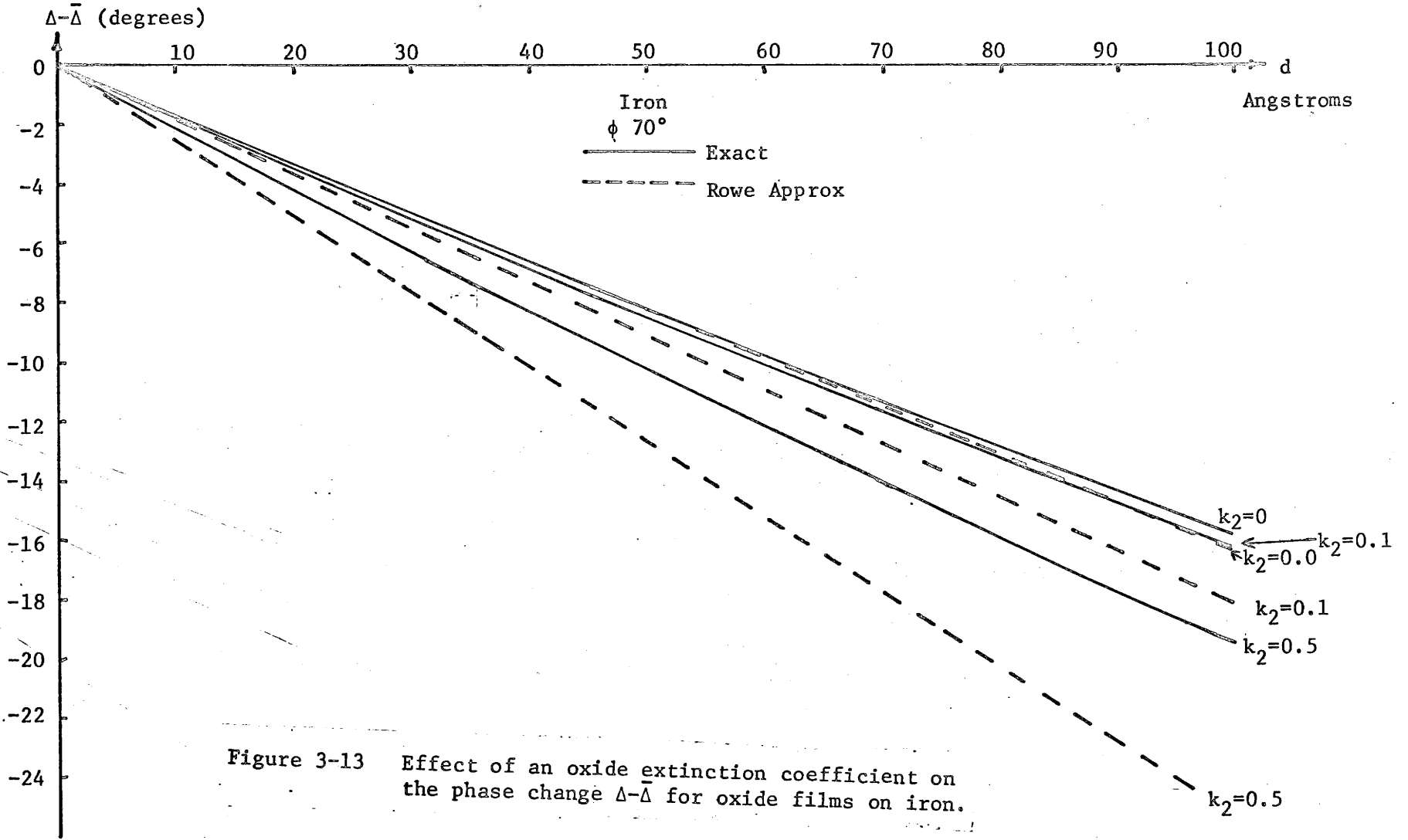


Figure 3-13 Effect of an oxide extinction coefficient on the phase change $\Delta-\bar{\Delta}$ for oxide films on iron.

Figure 3-13

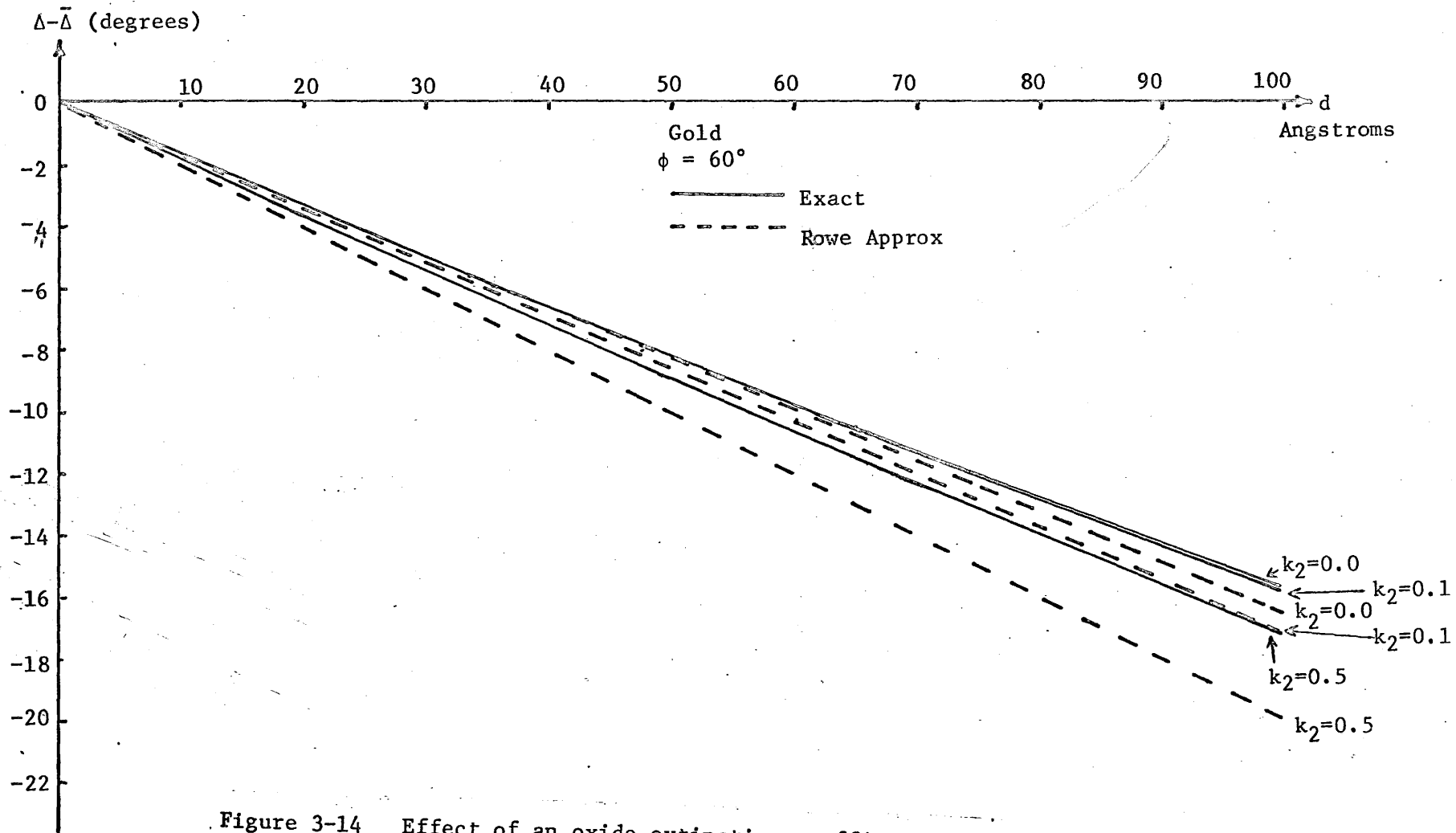


Figure 3-14 Effect of an oxide extinction coefficient on the phase change $\Delta - \bar{\Delta}$ for oxide films on gold.

Figure 3-15 Effect of an oxide extinction coefficient on the change in azimuth $\psi - \bar{\psi}$ for oxide films on silicon.

$\phi = 70^\circ$

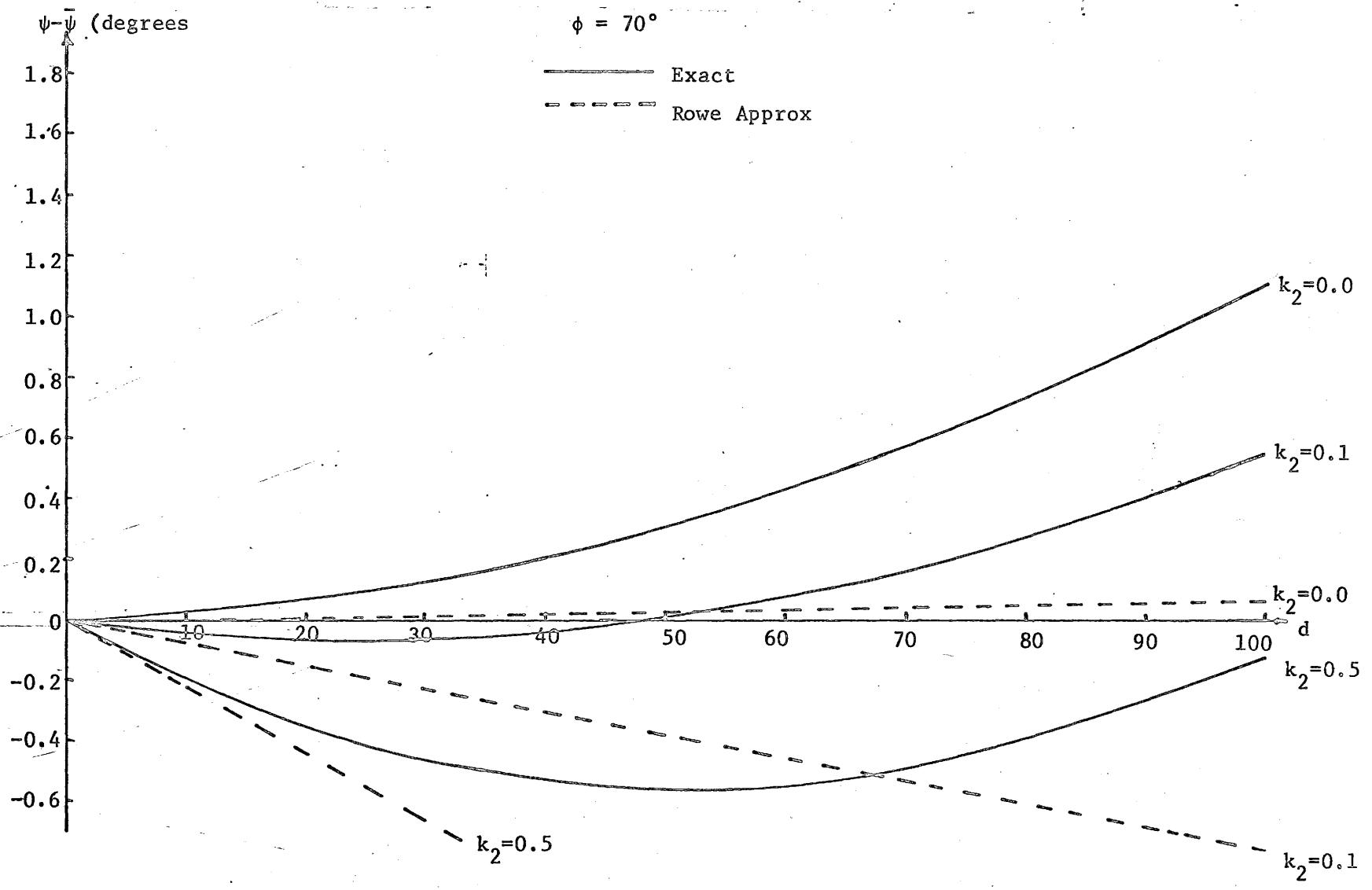


Figure 3-15

Figure 3-16 Effect of an oxide extinction coefficient on the change in azimuth $\psi - \bar{\psi}$ for oxide films on aluminum.

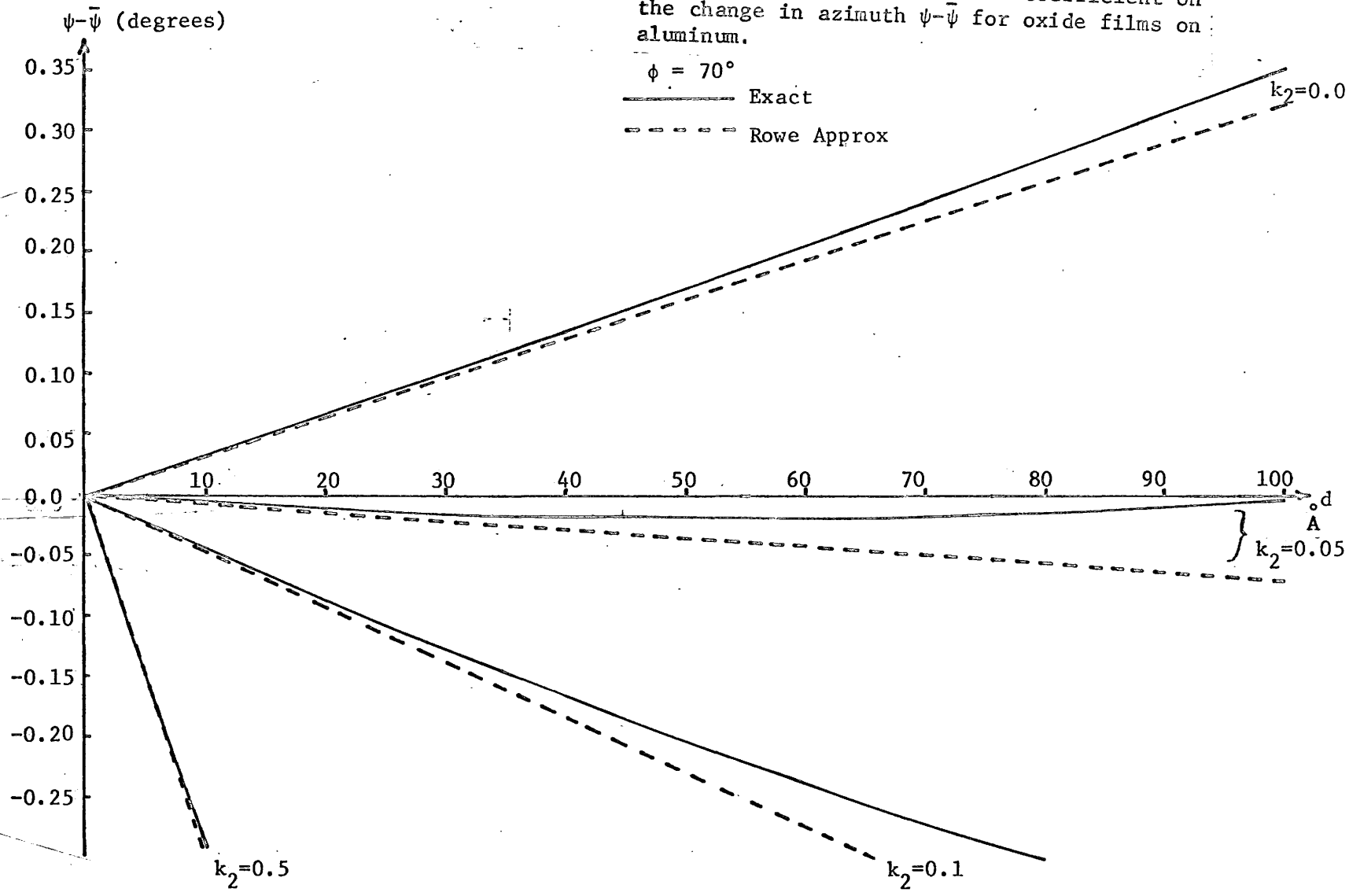


Figure 3-17 Effect of an oxide extinction coefficient on the change in azimuth $\psi - \bar{\psi}$ for oxide films on iron.

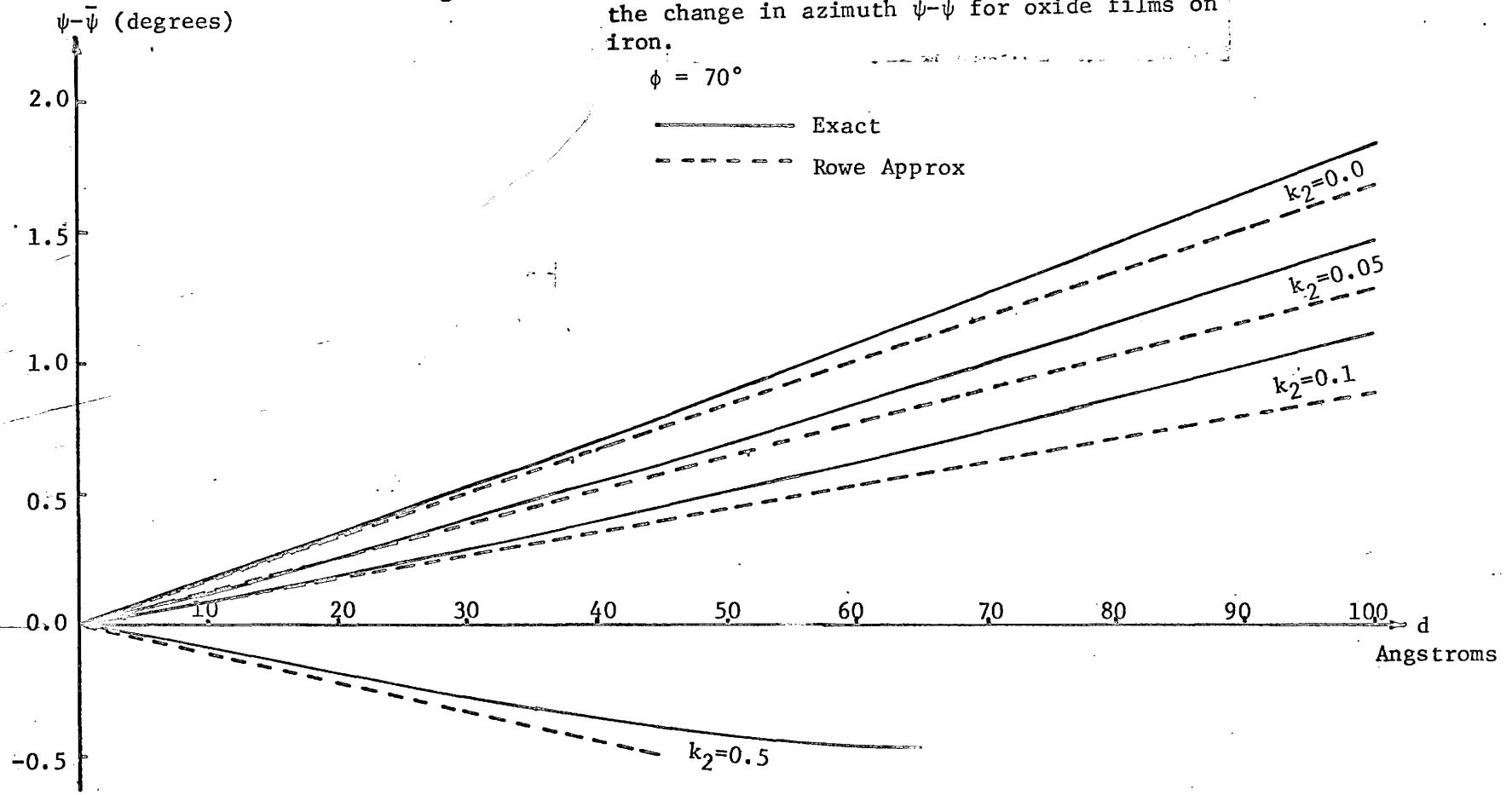


Figure 3-17

Figure 3-18 Effect of an oxide extinction coefficient on the change in azimuth $\psi - \bar{\psi}$ for oxide films on gold.

$\phi = 60^\circ$

— Exact
 - - - Rowe Approx

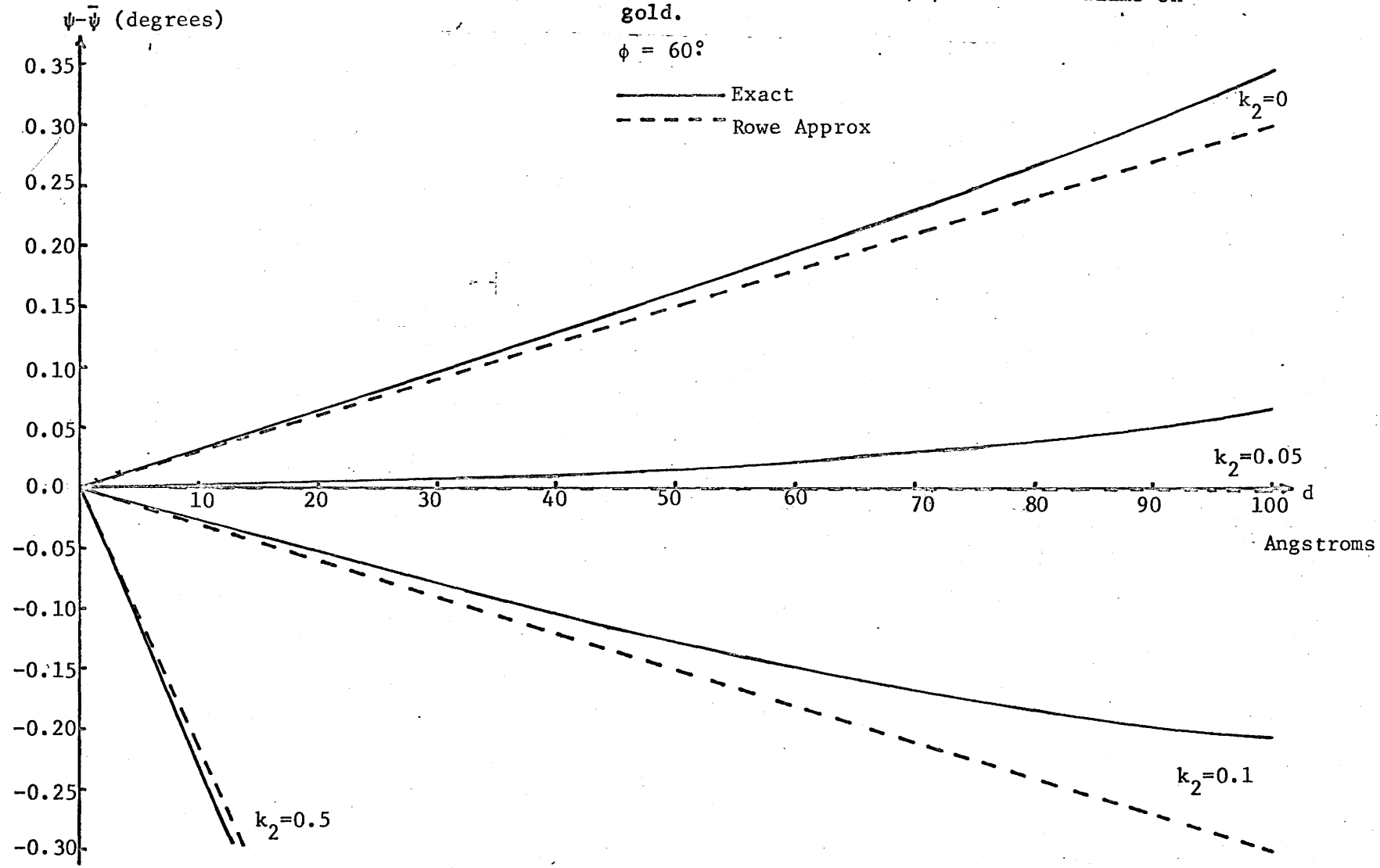


Figure 3-18

CHAPTER IV

EXPERIMENTAL

This chapter will primarily be concerned with methods of obtaining and measuring elliptically polarized light (both historical and recent); the relation of experimentally measured angles to the phase change Δ and the azimuth ψ ; and finally, the methods of sample fabrication.

Hauschild's Method

Hauschild's method of analyzing elliptically polarized light¹³ rests upon the fact that when elliptically polarized light passes through a quarter-wave plate, the emergent light is linearly polarized when suitably oriented. This can be extinguished with a Nicol prism (used as an analyzer) positioned at 90 degrees when the principal direction of the quarter-wave plate is oriented along the major axis of the ellipse. In such a case, the tangent of the angle between the linear vibrations and one of the principal directions of the quarter-wave plate measures the ellipticity (viz. the ratio of minor to major axis of the ellipse) of the original vibration. The orientation of the quarter-wave plate determines the position of the ellipse. If this can be correlated to the original major axis of the incident elliptically polarized light, this orientation is a measure of the phase change. This is indicated in figure 4-1.

Rothen's Early Ellipsometer

Rothen's ellipsometer is schematically indicated in figure 4-2. Referring to this diagram, monochromatic light passes through a polarizing

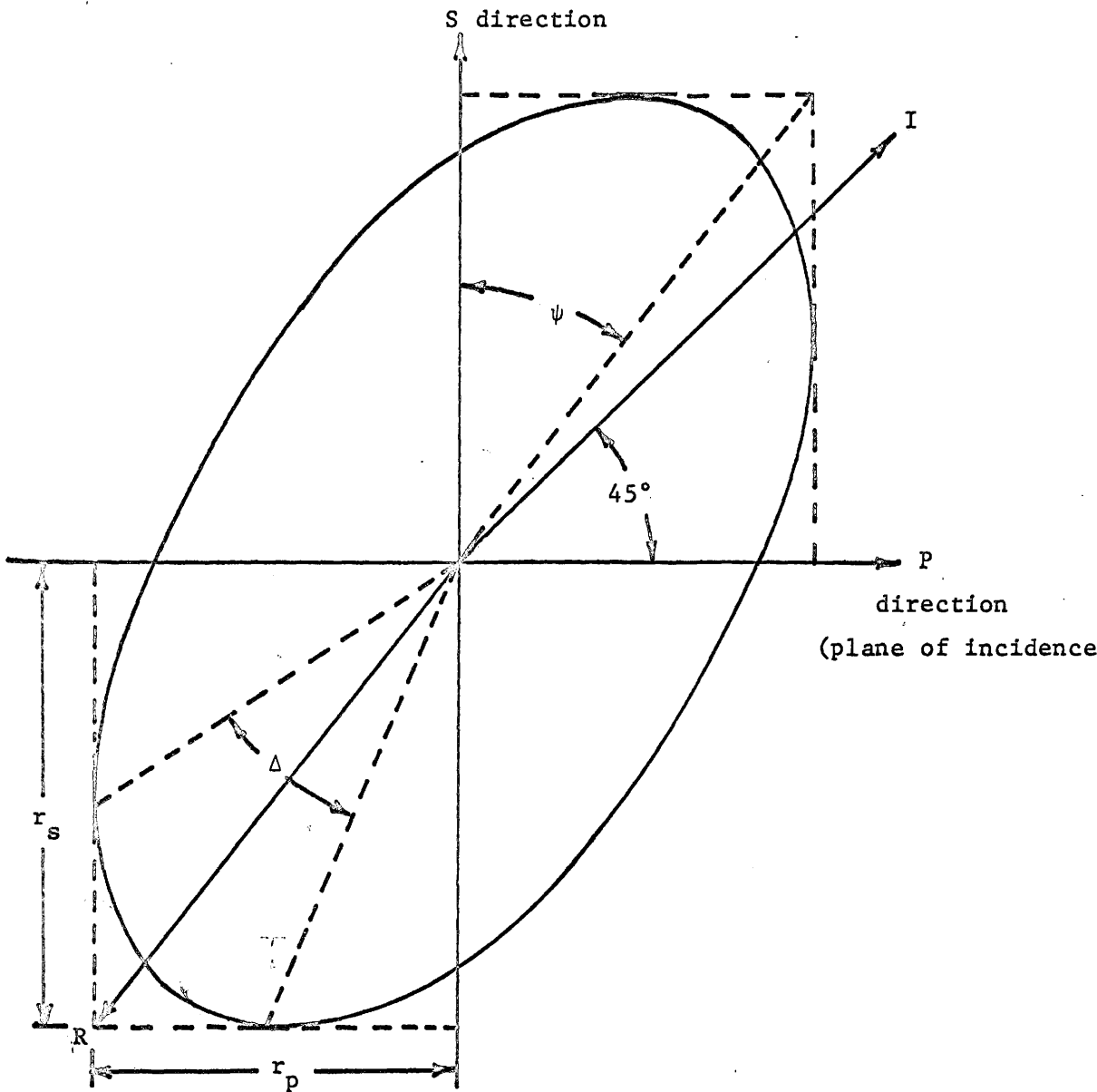


Figure 4-1 Graphical representation of the ellipsometer angles Δ and ψ for reflection greater than the principal angle.

Figure 4-2

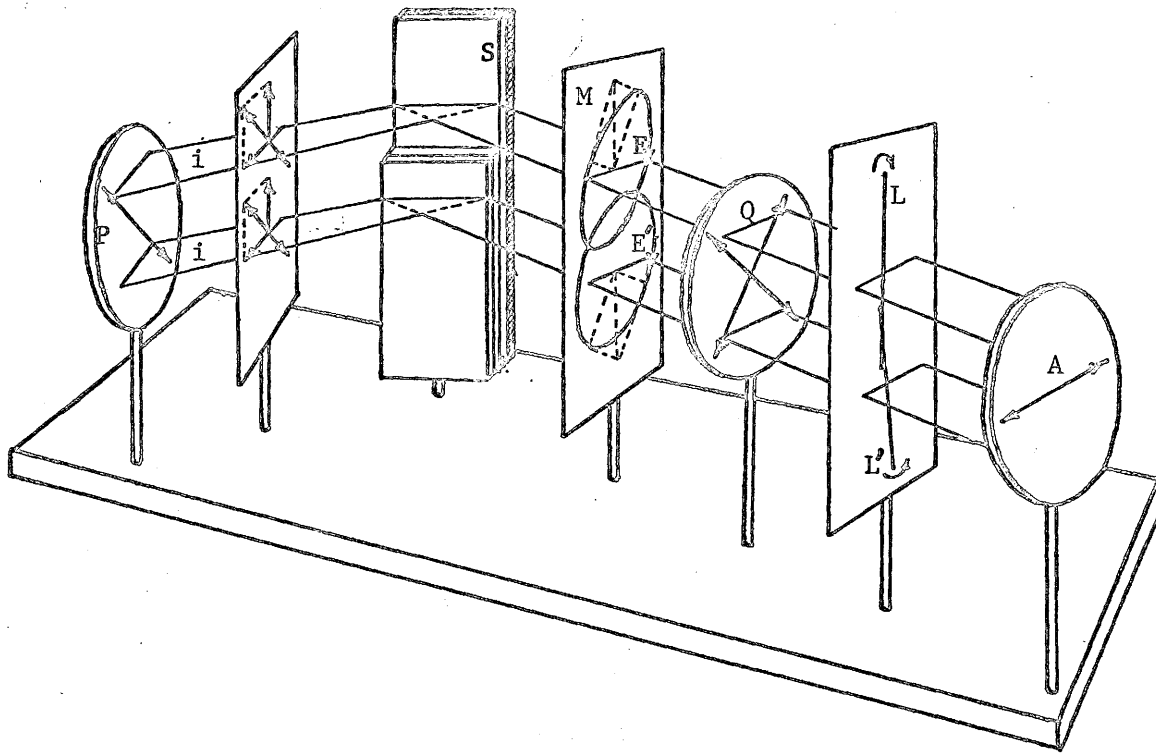


Figure 4-2 Representation of Rothen's early ellipsometer.

Nicol prism P with the transmitted vibration at 45 degrees to the plane of incidence i . This is indicated for two rays of light impinging upon the upper and lower parts of the sample S. The state of polarization of these two incident rays is indicated in the plane I. The upper and lower portions of the sample slide were coated with one and three monomolecular "reference" films of barium stearate respectively. Upon reflection from the slide S, the reflected light is elliptically polarized. Since the evaporated films in the upper and lower portions of the sample slide S differ in thickness, the corresponding ellipses E and E'; differ in ellipticity and orientation. The linear vibration of a ray can be considered as a resultant vector (shown in plane I) having a component in phase (OP) and a component perpendicular to it (OS). The change of phase of the components OP and OS upon reflection is greater than 90 degrees (if the angle of incidence is below the principal angle); the vector OP being in advance. With the original linear vibration in the direction indicated, the resulting ellipses rotate in a clockwise direction as shown in the plane M. Due to the difference in upper and lower film thicknesses, the ellipticity (ratio of minor to major axes) is greater in the lower ellipse. To an observer facing the light source, the lower ellipse has rotated counter-clockwise with respect to the upper one.

Now the two elliptical polarizations traverse a mica quarter-wave plate, Q, oriented with its "fast" axis parallel (or nearly so) to the bisector of the angle formed by the major axes of the two ellipses E and E'. Upon passing through the quarter-wave plate, the ellipses E and E' are transformed into elongated ellipses L and L' (i.e. near linear polarization).

Finally the beams pass through an analyzing Nicol prism A. As a consequence of the small ellipticity of the ellipses L and L', the angle made by the two major axes corresponds to the "half-shadow" angle of this polarimeter. The observation is made through an ocular focused on slide S. The angle read on the analyzer when both halves of the field appear of the same intensity gives the zero position of the apparatus. Now if a film of unknown thickness is added on the whole surface of the slide, the upper and lower parts become unequal in intensity since the ellipses E and E' have rotated counter-clockwise and their ellipticity is larger; the same applies to the ellipticity of ellipses L and L'. A counter-clockwise rotation of the analyzer returns the two halves of the field to equal intensity. The difference in position of the analyzer before and after deposition of the film is a measure of its thickness.

The Present Ellipsometer:

Light from a mercury vapour lamp first passes through a filter and collimating lens system producing a parallel beam of monochromatic light about 6 mm. in diameter (wavelength = 5460.74 Angstroms). Next it passes through a polarizing Nicol prism followed by a variable diaphragm which can vary the diameter of the beam from 1 mm. to 6 mm. When the electric vector or plane of polarization is set at an azimuth of 45 degrees to the plane of incidence, one of its component is propagating in the plane of incidence and the other perpendicular to it; each with equal intensity. The compensator or quarter-wave plate can be mounted in either of two locations;

- (1) between the polarizer and the sample (figures 4-3 and 4-4)

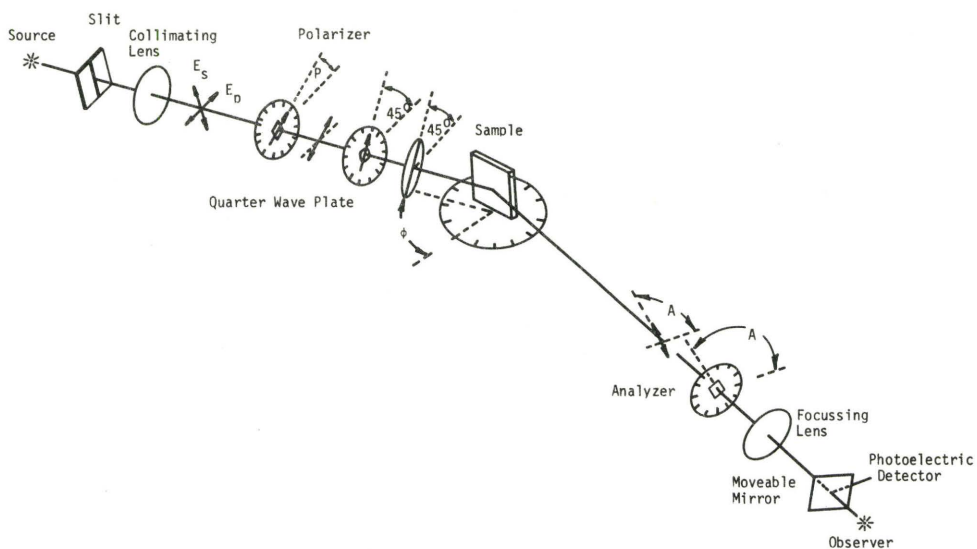


Figure 4-3 Symbolic representation of present ellipsometer for quarter-wave plate mounted before sample holder.

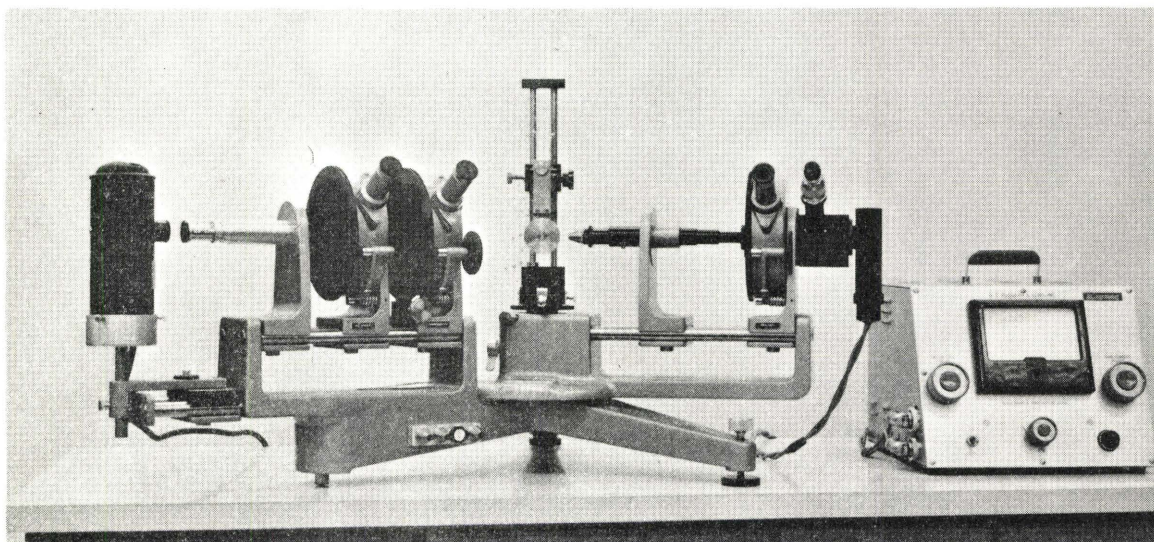


Figure 4-4 Photograph of present ellipsometer for quarter-wave plate mounted before sample holder.

(2) between the sample and the analyzer (figures 4-5 and 4-6)

Case (1)

When the compensator (quarter-wave plate) is mounted before the sample, the plane-polarized light upon passing through the compensator is elliptically polarized before striking the reflecting surface. Upon reflection, the light is linearly polarized and is analyzed with an analyzing Nicol prism connected to a photomultiplier tube and associated metering electronics.

Case (2)

When the compensator is mounted between the sample and the analyzer, the plane - polarized light striking the reflecting surface becomes elliptically polarized upon reflection. The elliptical polarization is converted to plane-polarized light after passing through the compensator. As in the other geometry, this is analyzed with another Nicol prism connected to a photomultiplier tube and associated metering electronics.

Correlation of Angles:

For the case of an exact quarter-wave plate, i.e. one whose fast and slow axes are exactly perpendicular to each other, the phase change Δ and the azimuth angle ψ are related to the polarizer P and analyzer A angles in a simple way:

$$\psi = A \quad (\text{eq. 4-1})$$

$$\Delta = 2P + 90 \quad (\text{eq. 4-2})$$

where Δ and ψ are in degrees.

The ellipsometric parametric parameters Δ and ψ characterizing the ellipse are shown in figure 4-7.

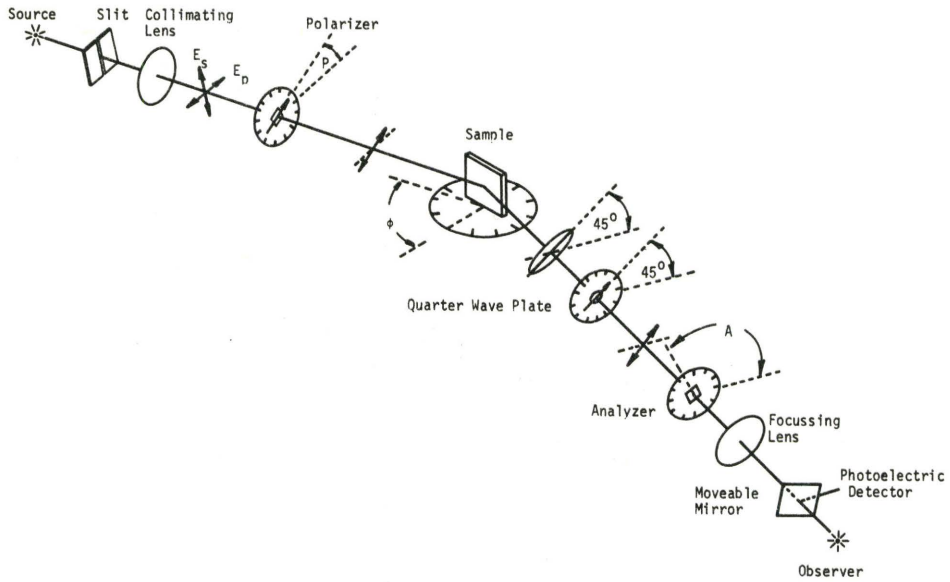


Figure 4-5 Symbolic representation of present ellipsometer for quarter-wave plate mounted after sample holder.

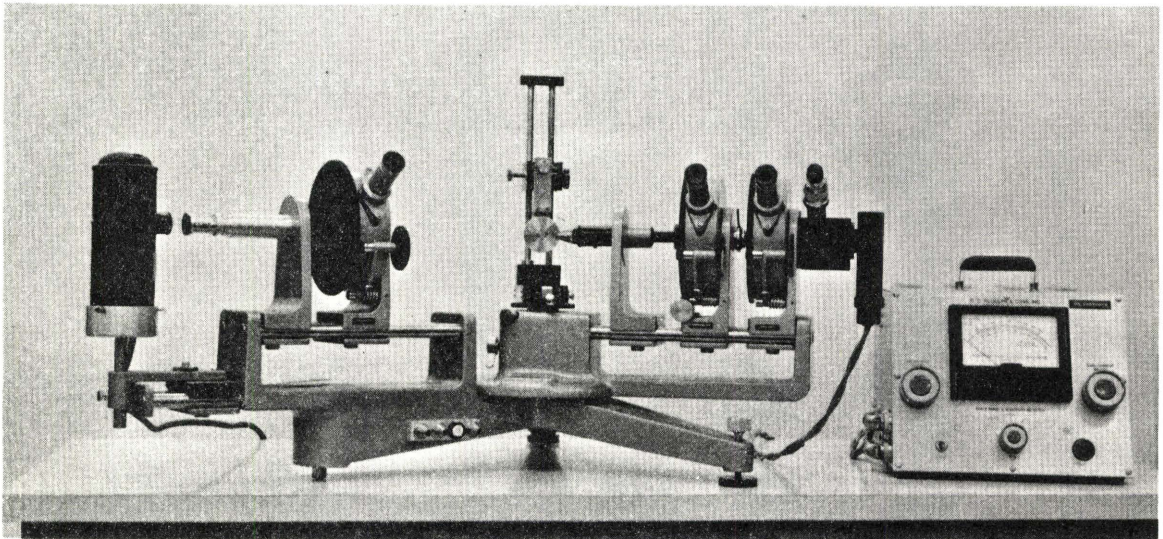
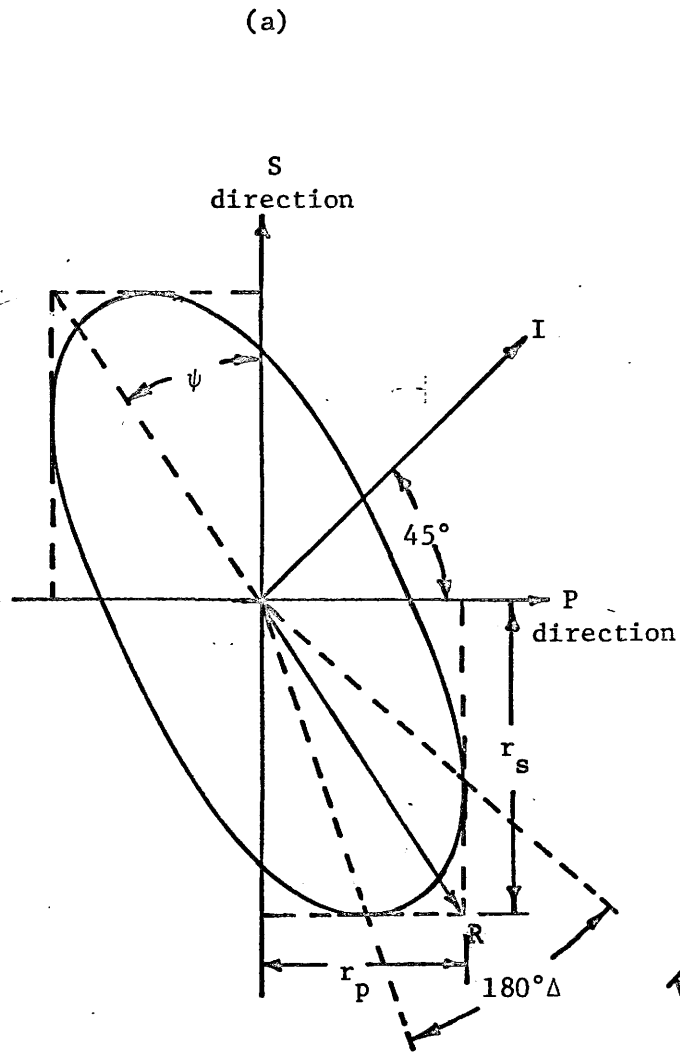
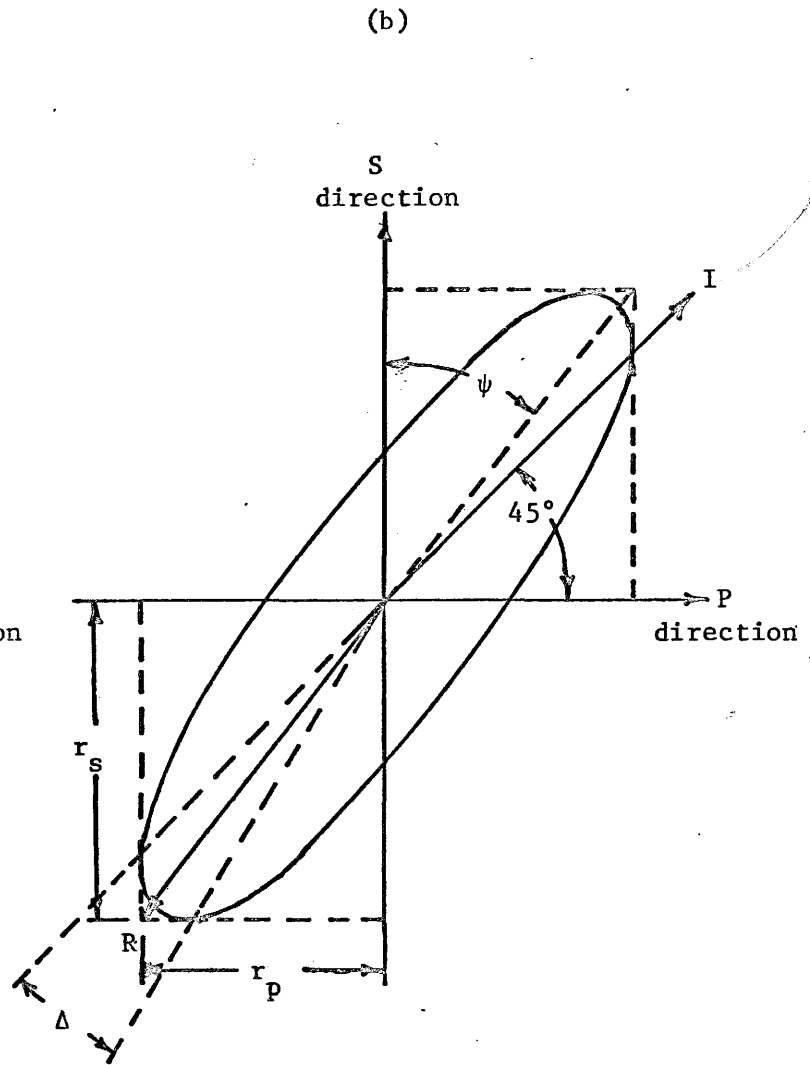


Figure 4-6 Photograph of present ellipsometer for quarter-wave plate mounted after sample holder.

Figure 4-7 Graphical representation of ellipsometric parameters.



Réflexion below principal angle



Réflexion above principal angle

For the case of a non-exact quarter-wave plate, Archer¹⁴ has shown the retardation can be corrected for by performing measurements with the quarter-wave plate oriented at +45 degrees and -45 degrees to the plane of incidence. This results in two analyzer readings denoted a_p and a_s measured in the -45 and +45 degree orientations respectively (taking only the first two zones into account). The zone scheme of measuring will be discussed later when referring to the computer program. The ellipticity can be obtained from the relation:

$$\tan^2 \psi = \tan a_p \tan a_s \quad (\text{eq. 4-3})$$

The retardation of the quarter-wave plate δ can be calculated using the expressions:

$$\tan \psi = \tan L \tan a_p = \cot L \tan a_s \quad (\text{eq. 4-4})$$

$$\cos 2L = -\cos \delta \cos 2P \quad (\text{eq. 4-5})$$

From this the phase change Δ is obtained simply:

$$\tan \Delta = \sin \delta \cot 2P \quad (\text{eq. 4-6})$$

It is obvious that for a perfect quarter-wave plate i.e. $\delta=90^\circ$, $L = 45^\circ$ and equation 4-6 reduces to equation 4-2.

Sample Preparation

Aluminum

Aluminum films were prepared by evaporating 99.999 percent aluminum wire from a tungsten filament onto microscope glass slides. Both the slides and the aluminum wire were etched and degreased before mounting into the vacuum system, an NRC model 720 with liquid nitrogen cold trap. The aluminum films were evaporated at a base pressure of 2×10^{-7} torr and a Sloan Deposit

Control Master model Omni II was used to monitor the evaporation rate and film thickness during deposition. The aluminum films obtained in this way were approximately 3000 Angstroms thick. The bell jar was returned to atmospheric pressure by back-filling with nitrogen gas. The aluminum was then allowed to oxidize in room air. For thicker oxide films, the glass slides were heated in air on a small hot plate.

Molybdenum

Molybdenum metal 99.99 percent pure was anodically oxidized in acetic acid, 1 mole of distilled water, and 0.02 moles of sodium borate ($\text{Na}_2\text{B}_4\text{O}_7 \cdot 10 \text{H}_2\text{O}$). The cathodic material used in the reaction was platinum. One sample was oxidized naturally and the other three were oxidized at potentials of 3 volts, 4 volts, and 6 volts.

Silicon

Polished 10 ohm-cm. silicon wafers were rinsed for approximately ten minutes in a mixture of sulphuric acid and doubly-distilled de-ionized water mixed in equal parts. This rinsing was performed to remove any surface grease. Following the rinse, the mixture was decanted with de-ionized water and cleaned in a mixture of one part hydrogen peroxide, one part hydrochloric acid, and four parts doubly-distilled de-ionized water to remove any surface metal ions. The mixture was heated to boiling and the sample decanted with the distilled de-ionized water. One drop of hydrofluoric acid was added to the sample in a distilled water solution and the solution heated to boiling in order to remove the remaining surface oxide. The sample was then decanted into doubly-distilled de-ionized water until ready to oxidize. For very thin

oxides, the oxidation process simply involves allowing the sample to come into contact with room air; for thicker ones, the sample was oxidized in a furnace at 900 degrees Centigrade in a wet air mixture for appropriate times up to 5 minutes. This procedure was developed in order to correlate oxide film thickness measurements by ellipsometry with MOS tunneling measurements.

CHAPTER V

COMPUTER PROGRAM

The computer program used to solve for substrate optical constants consists of three major parts:

- 1). Reduction of input polarizer and analyzer angles to phase change Δ and ellipticity ψ .
- 2). Solution of the exact ellipsometry equations for the substrate optical constants n_3 and k_3 .
- 3). Solution of the exact ellipsometry equations for the oxide film optical constants n_2 and k_2 .

Figure 5-1 shows a simplified flow chart indicating the basic outline of the computer program.

1). Reduction of input data

Here we simply calculate the phase change Δ and azimuth ψ from the experimental polarizer and analyzer readings P and A. These can be calculated either by assuming that the quarter-wave plate is exact or by calculating the retardation of the quarter-wave plate. In the exact assumed case, the polarizer and analyzer angles are related to the phase change Δ and azimuth ψ simply

$$\Delta = 2 P + 90 \quad , \quad (\text{eq. 5-1})$$

and $\psi = A \quad . \quad (\text{eq. 5-2})$

The added complication of performing measurements in all four zones and calculating the retardation of the quarter-wave plate, as done by McCrackin⁸, does not improve the convergence to any noticeable extent. These "improved"

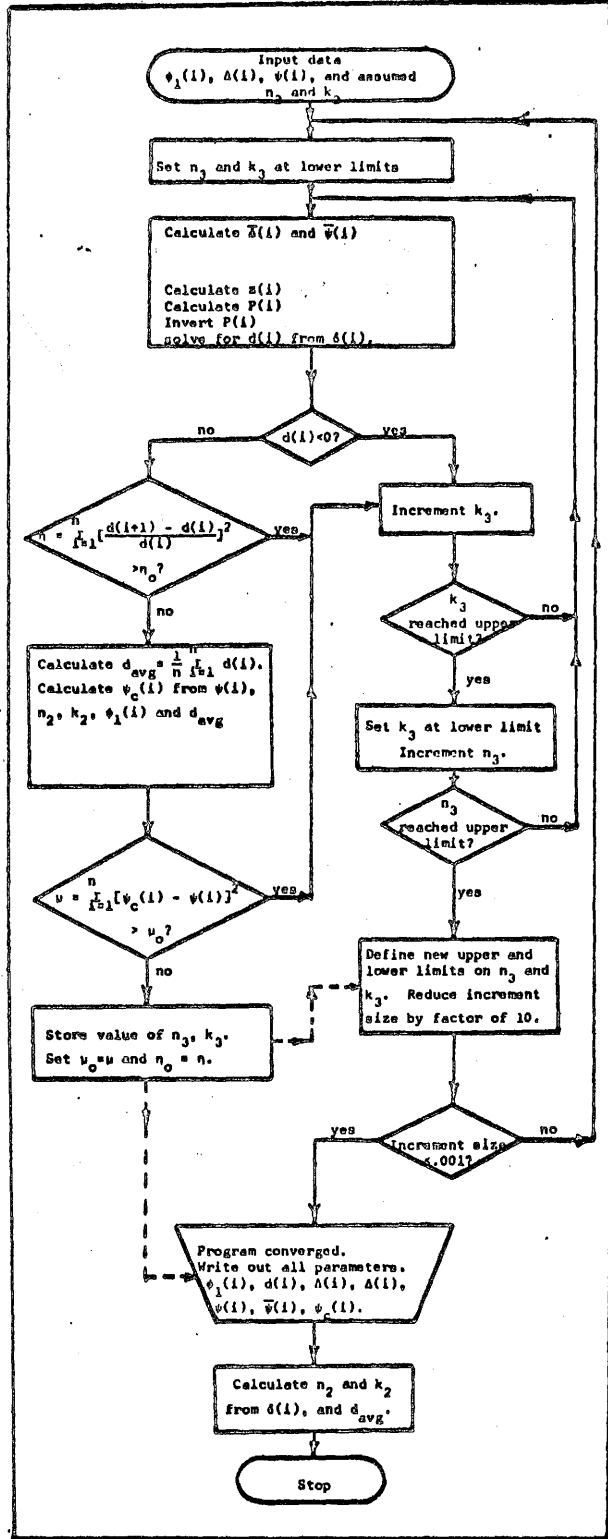


Figure 5-1 · Flow chart of Computer program used to determine substrate optical constants n_3 and k_3 .

angles are still typically in error several hundredths of a degree. However, for completeness, the meanings of the angles a_p , a_s , and p , mentioned in chapter IV, will be expounded here.

McCrackin's Zone Scheme⁸

Since the experimentally measured angles are only measurable to 0.01 degrees (even if there is no error in quarter-wave plate retardation), an averaging process is performed over all four zones. The meanings of p , a_p , and a_s in the four zones are as follows:

zone 1:

The fast axis of the quarter-wave plate is at -45° . The polarizer makes an angle of $+p$ with the plane of incidence; the analyzer makes an angle of $+a_p$ with the plane of incidence.

zone 2:

The fast axis of the quarter-wave plate is at $+45^\circ$. The polarizer makes an angle of $-p$ with the surface or 90° with the plane of incidence; the analyzer makes an angle of $+a_s$ with the plane of incidence.

zone 3:

The fast axis of the quarter-wave plate is at -45° . The polarizer makes an angle of $+p$ with the surface or 90° with the plane of incidence; the analyzer makes an angle of $-a_s$ with the plane of incidence.

zone 4:

The fast axis of the quarter-wave plate is at $+45^\circ$. The polarizer makes an angle of $-p$ with the plane of incidence; the analyzer makes an angle of $-a_p$ with the plane of incidence.

ZONE	QUARTER WAVE PLATE	POLARIZER	ANALYZER
1	-45°	$P_1 = p_1 + \delta p$	$A_1 = a_{p1} - \delta a$ <hr/> $a_{s1} = 0$
2	$+45^\circ$	$P_2 = 90^\circ - (p_2 + \delta p)$	$A_2 = a_{s2} - \delta a$ <hr/> $a_{p2} = 0$
3	-45°	$P_3 = 90^\circ + (p_3 + \delta p)$	$A_3 = 180^\circ - (a_{s3} + \delta a)$ <hr/> $a_{p3} = 0$
4	$+45^\circ$	$P_4 = 180^\circ - (p_4 - \delta p)$	$A_4 = 180^\circ - (a_{p4} + \delta a)$ <hr/> $a_{s4} = 0$

Table 5-1 McCrackin's Zone Scheme.

With this zone scheme, the measured polarizer angle P and the measured analyzer angle A are related to the angles p , a_p , and a_s in the way shown in table 5-1. The sum of the four polarizer readings should total 360 degrees; if not, the difference $(360 - \sum_{i=1}^4 P_i)$ is four times the polarizer zero correction factor¹⁵. Each polarizer reading in each zone is corrected by the zero correction factor and the angles a_p , a_s , and p are calculated in the following manner:

$$p = 1/4 \sum_{i=1}^4 p_i \text{ (corrected),} \quad (\text{eq. 5-2})$$

$$a_p = 1/2 \sum_{i=1}^4 a_{pi} \text{ ,} \quad (\text{eq. 5-3})$$

$$a_s = 1/2 \sum_{i=1}^4 a_{si} \text{ .} \quad (\text{eq. 5-4})$$

With these values p , a_p , and a_s , the angles Δ and ψ are determined using the relations eq. 4-3 through 4-6.

2). Solution to substrate optical constants

The computer program basically consists in solving the exact equation 2-50 at several angles of incidence for a consistent film thickness, d . With the calculated angles Δ and ψ from the experimental polarizer and analyzer angles, and an assumed oxide index (either the reported bulk value for the oxide material or a typical dielectric value of 1.5), the exact equation is solved for the substrate optical constants n_3 and k_3 , subject to the constraint that the percent deviation in oxide film thickness be minimized. The method

involved is to increment n_3 and k_3 (initially in steps of 1.0) and calculate at each angle of incidence the free surface angles $\bar{\Delta}$ and $\bar{\psi}$. This is done using the inversion expressions in appendix II. Armed with these parameters and the angles Δ and ψ , the phase term P in eq. 2-50 is calculated. This phase term is then inverted giving the oxide phase angle δ by application of eq. 2-42. From this parameter, it is a relatively simple matter to solve for film thickness d .

The rejection of a trial n_3, k_3 pair is performed by the following convergence requirements;

1. Negative thicknesses are rejected immediately.
2. A percent deviation in oxide film thickness is calculated. If greater than the previous value (or a large initial value), the n_3, k_3 trial pair are rejected. The reason for using a percent deviation for convergence rather than an absolute difference was that the thickness tended to converge towards zero on an absolute difference calculation.
3. For non-absorbing oxides, i.e. the oxide extinction coefficient k_2 equal to zero, the azimuth angle ψ is tested to make sure that it is greater than its free surface counterpart $\bar{\psi}$. This check is deleted for absorbing oxides.
4. From the average thickness and the trial optical constants, a calculated value of the azimuth angle ψ_{calc} is generated. This value is compared with the measured value of ψ and the sum of the squares of the difference is calculated. If greater than an

an initial large value or the previous value, the trial n_3, k_3 pair is rejected.

After having chosen the best fit by the previous convergence technique in this coarse increment range, the increment size is reduced by a factor of ten. Only solutions near to the coarse best fit are tested. The increment size is made smaller sequentially at the end of each range, until the increment size on n_3 and k_3 is smaller than 0.001.

3). Solution to Oxide optical constants

Once the substrate optical constants, n_3 and k_3 , have been determined, the oxide phase angle δ is known quite accurately. In general, this quantity is a complex number (except in the case of non-absorbing oxide). From this phase change, the average oxide thickness, and the wavelength, the product $\tilde{n}_2 \cos^* \phi_2$ can be calculated. Knowing these quantities for each angle of incidence and the refractive index for the immersion medium, and applying Snell's law, the only unknown quantity is the complex refractive index for the oxide $\tilde{n}_2 = n_2 - j k_2$. As a result, it may be solved exactly. Fortunately the coefficients a, b, c and e, in eq. 2-50 needed to solve for the phase term P are not too sensitive to the oxide index and the oxide extinction coefficient. This means that if the initial assumed oxide index was reasonably close to the calculated value, it is not necessary to correct the phase term P each time the oxide index is slightly altered; then the resulting oxide optical constants are reasonably valid.

CHAPTER VI
DISCUSSION

Aluminum

For evaporated films of aluminum, the calculated substrate optical constants were found to lie within the reported values found in the literature^{10,17,24}. The literature shows a scatter in the reported values of the substrate index n_3 between 0.786 and 1.140. By this self-consistent ellipsometric technique, the substrate index n_3 was found to lie between 0.700 and 1.200 showing reasonable agreement. Table 6-1 shows the calculated values for both naturally occurring and thermally grown oxides on aluminum. A statistical analysis of the twelve data points shows the average refractive index to be $n_3 = 0.989$ with a standard deviation of 0.140. Figure 6-1 shows a plot of the refractive index of the aluminum substrate as a function of the aluminum oxide film thickness.

The scatter in the reported values of the substrate extinction coefficient is also reasonably large, with values lying between 5.45 and 6.77. By the technique reported here, the extinction coefficient for the aluminum substrate was found to lie between 5.201 and 6.701. A similar statistical average of the twelve data points shows the average extinction coefficient for aluminum to be 6.036 with a standard deviation of 0.312. Both the aluminum refractive index and extinction coefficient are in reasonable agreement with that reported by Hass and Waylonis¹⁷ ($n_3 = 0.82$ and $k_3 = 5.99$ at the 5461 Angstrom wavelength) who determined these values from reflectance and transmittance measurements on semitransparent aluminum films.

The oxide index for aluminum was found to be 1.66 ± 0.01 . However,

TABLE 6-1.

Experimentally determined optical constants for evaporated aluminum films containing an adhering oxide film.

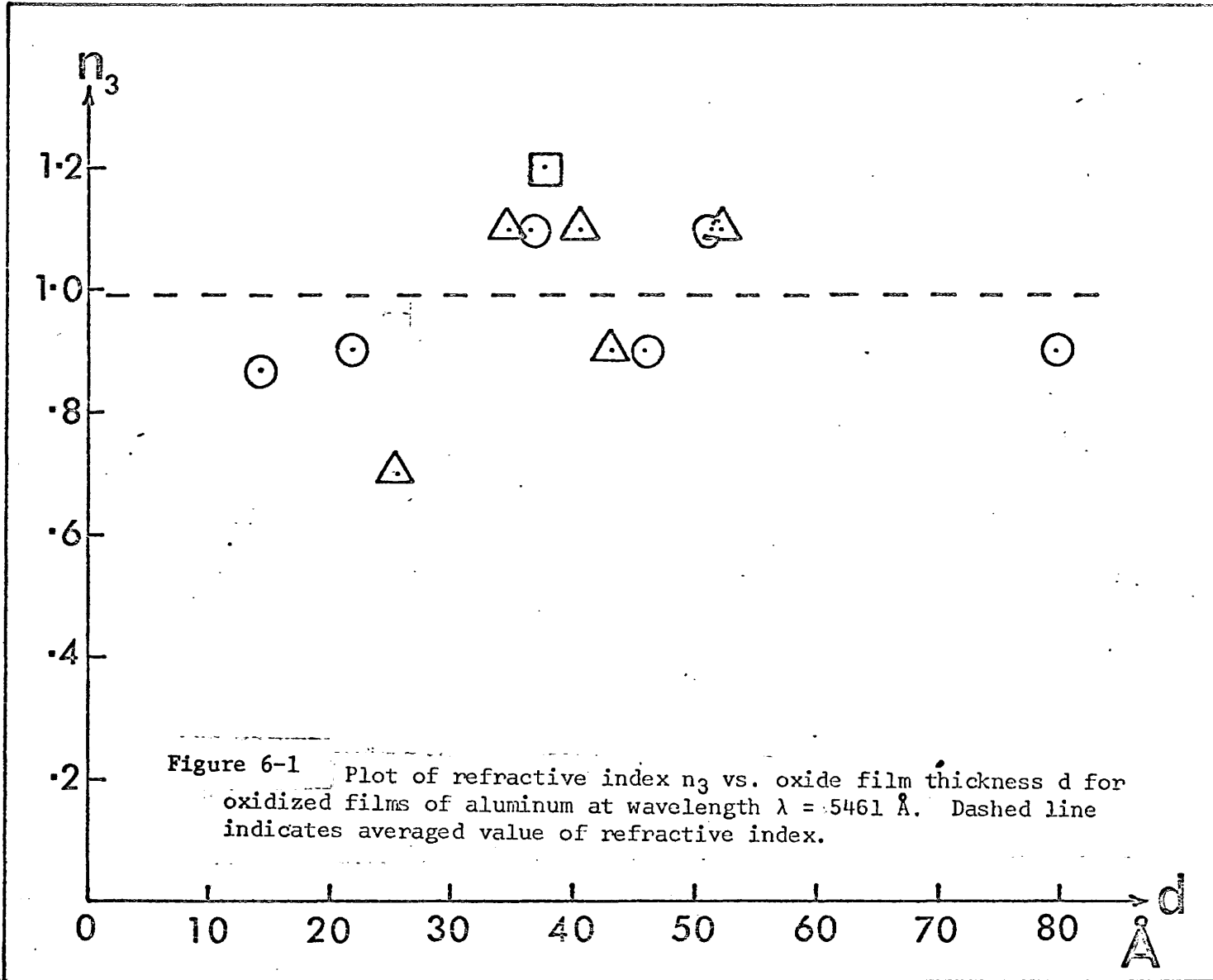
Sample Group	Refractive Index n_3	Extinction Coefficient k_3	Oxide film Thickness d (Å)
0	0.870	6.121	14.186
0	0.900	6.101	21.857
Δ	0.700	5.201	26.109
Δ	1.100	6.001	35.300
0	1.100	6.001	36.206
□	1.200	6.701	37.685
Δ	1.100	6.001	40.503
Δ	0.900	6.101	43.012
0	0.900	6.101	45.765
0	1.100	6.001	51.110
Δ	1.100	6.001	51.361
0	0.900	6.101	79.603

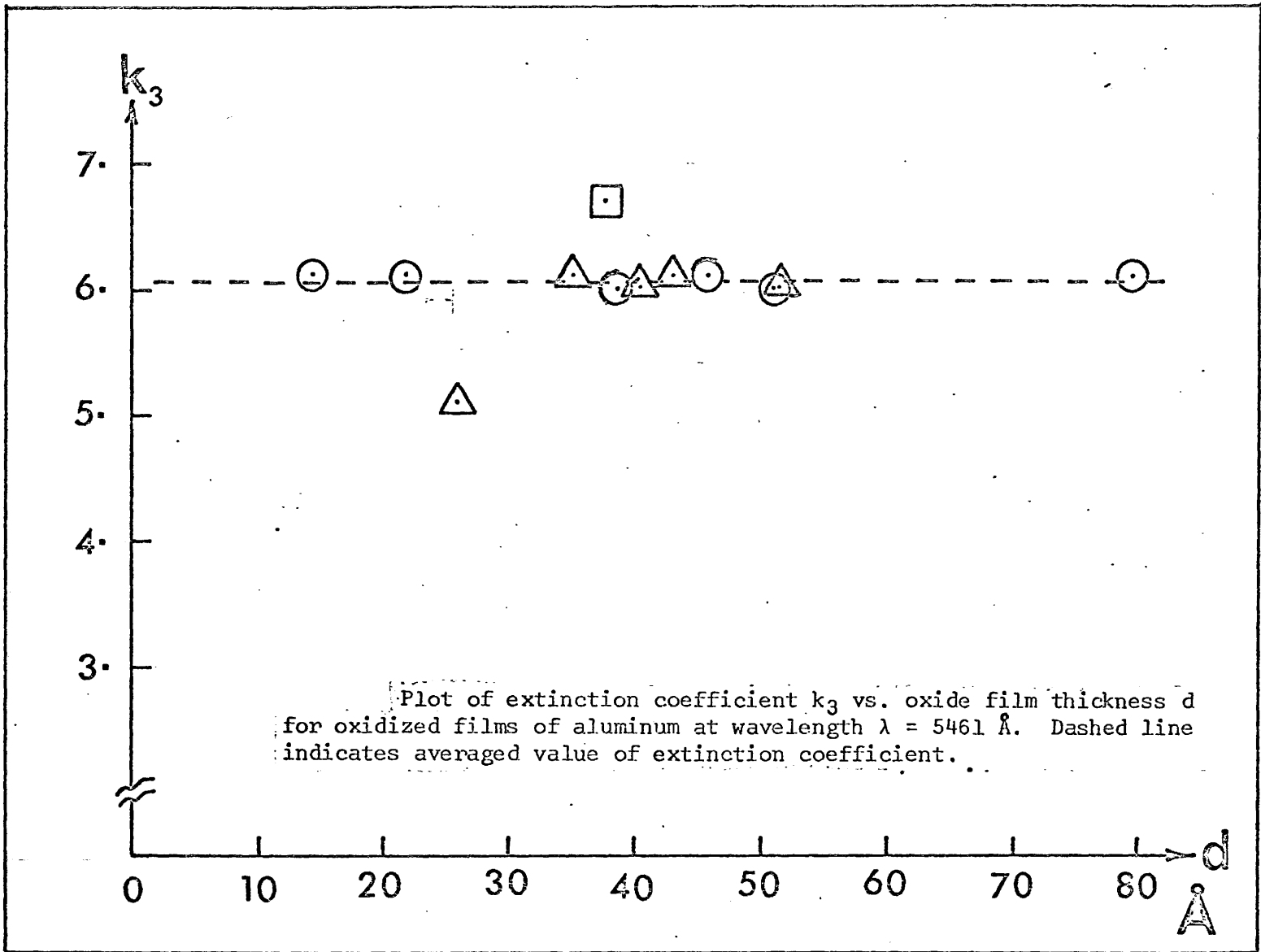
Average n_3 = 0.989

Standard deviation = 0.140

Average k_3 = 6.036

Standard deviation = 0.312





since the reported value of 1.66 was initially assumed for the thickness calculation, it is not unreasonable to expect the program to converge to a value close to this assumed number once the substrate optical constants have been determined.

The extinction coefficient for the oxide film on the evaporated aluminum was found to lie between 0.023 for a thin oxide film and 0.0024 for thicker ones (68 Angstroms). Figure 6-3 shows the oxide extinction coefficient plotted versus oxide film thickness. The decrease in oxide extinction coefficient with increase in oxide film thickness seems to support the work of Bashara and Peterson²⁵ who propose the absorption should decrease exponentially with increasing oxide film thickness. Since the thinner films show larger scatter in the oxide extinction coefficient with angle of incidence (shown by error bars in fig. 6-3), it was not possible to determine such an empirical exponential fit. This effect of the larger scatter in extinction coefficient with angle of incidence might be evidence to the fact that we are really seeing the random film nucleation as the oxide grows. The fact that the initial oxidation of aluminum is rather amorphous in nature implies validity of the plane parallel model used in the calculation as will be shown later in this chapter.

Molybdenum

The results of the ellipsometer measurements on molybdenum are presented in Table 6-2. In this case there was found to be a larger scatter in the calculated optical constants presumably attributed to two factors;

- (1) instability of the oxide material³⁰,
- and (2) a rougher oxide-air surface.

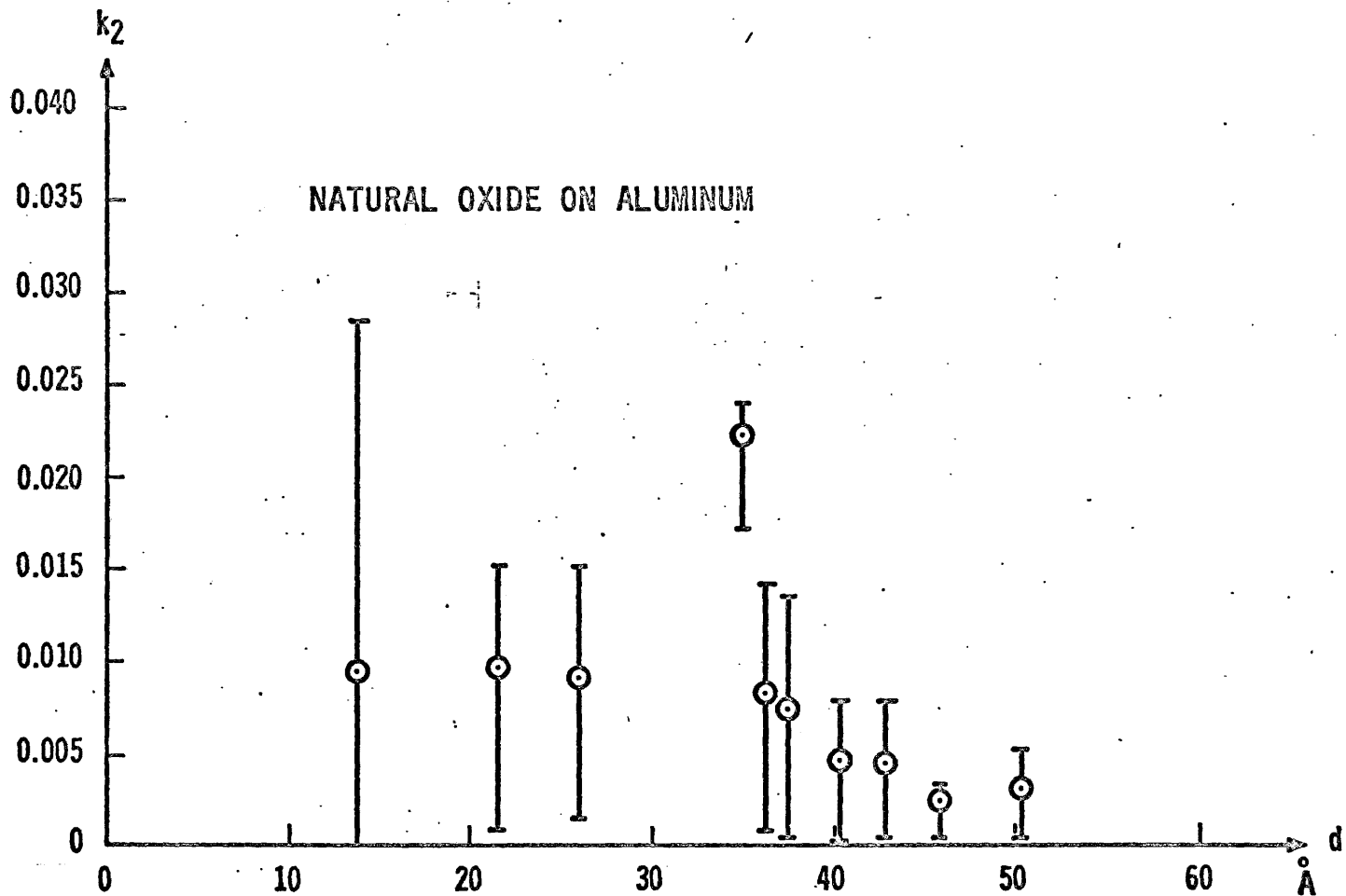


Figure 6-3 Plot of oxide extinction coefficient versus oxide film thickness for aluminum substrate.

SAMPLE	REFRACTIVE INDEX n_3	EXTINCTION COEFFICIENT k_3
NATURAL OXIDE	3.146	3.601
3 VOLT OXIDE	3.237	3.555
4 VOLT OXIDE	2.760	3.500
6 VOLT OXIDE	2.672	3.480

AVERAGE $n_3 = 2.954$; STANDARD DEVIATION = 0.242

AVERAGE $k_3 = 3.534$; STANDARD DEVIATION = 0.047

TABLE 6-2 Experimentally determined optical constants for anodically oxidized Molybdenum metal.

A similar statistical analysis on the four molybdenum samples gives an average refractive index $n_3 = 2.954$ with a standard deviation of 0.242 and an average extinction coefficient $k_3 = 3.534$ with a standard deviation of 0.047. Upon re-calculating the film thickness with these average substrate optical constants, the natural oxide thickness is found to be a negative number; clearly a non-physical solution. However if we use the upper statistical limits for the substrate constants i.e., $n_3 = 2.954 + 0.242 = 3.196$, and $k_3 = 3.534 + 0.047 = 3.581$, the re-calculated natural oxide thickness is 5.605 angstroms, a more realistic number physically. Waldron and Juenker²⁶ report the optical constants of unpolished molybdenum as $n_3 = 3.61$ and $k_3 = 3.67$ at the 5461 angstrom wavelength. Here they estimate the optical constants from reflectance versus angle of incidence data. Summers²⁷ has also reported the optical constants of polished bulk molybdenum as $n_3 = 3.59$ and $k_3 = 3.40$.

Silicon

Initially the program tended to converge toward $k_3 = 0.0$ since the extinction coefficient is so small for silicon. However by solving the equations involving the free-surface angles $\bar{\Delta}$ and $\bar{\psi}$ (Eqs. 2-26 and 2-27) in a self consistent manner knowing that the converged substrate refractive index n_3 is close to the true value, it is possible to determine the substrate extinction coefficient k_3 . The results of the ellipsometer measurements on silicon are presented in table 6-3. A statistical analysis of the refractive index for silicon gives an average value of $n_3 = 4.044$ with a standard deviation of 0.0144. Figure 6-4 shows a plot of substrate refractive

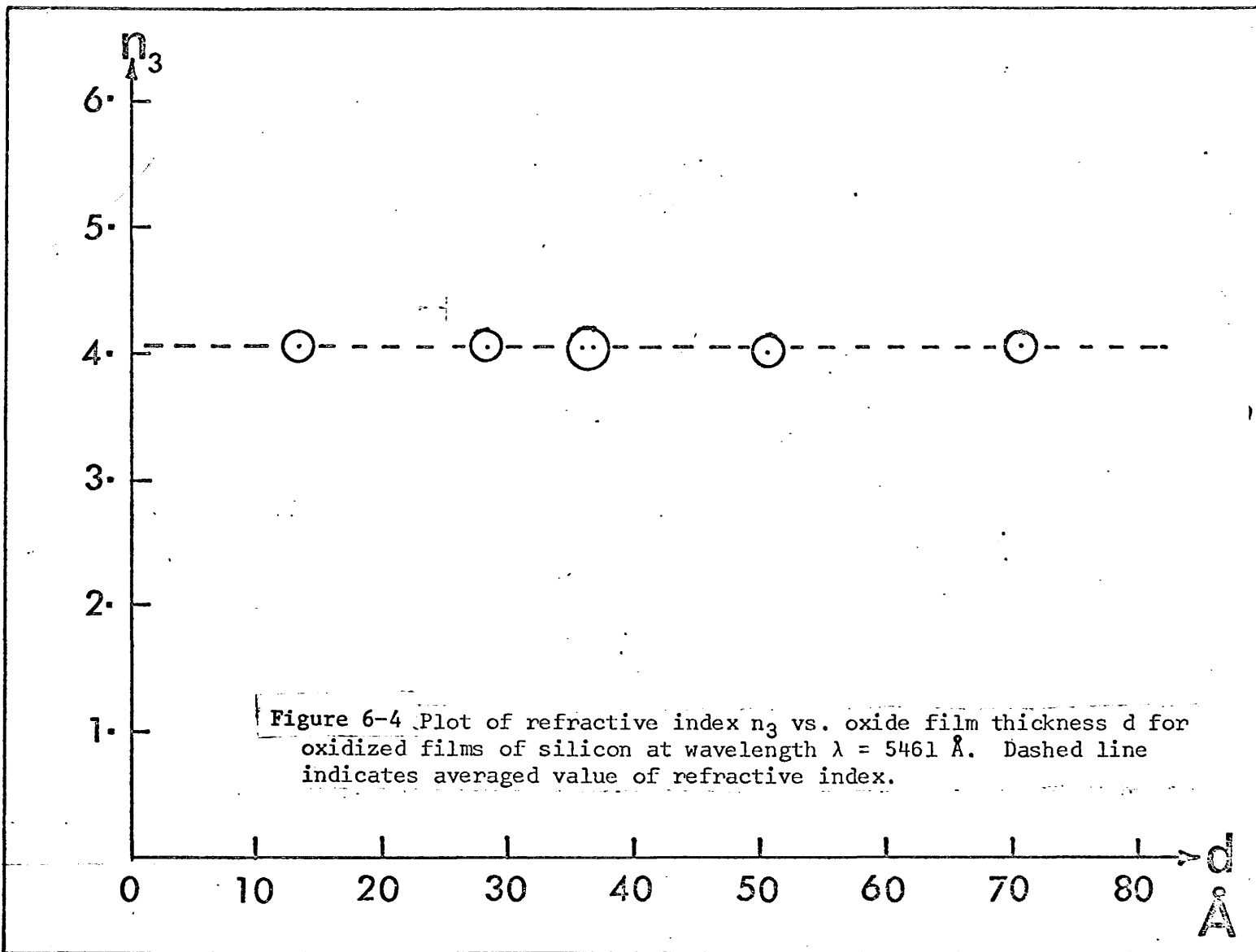
TABLE 6-3

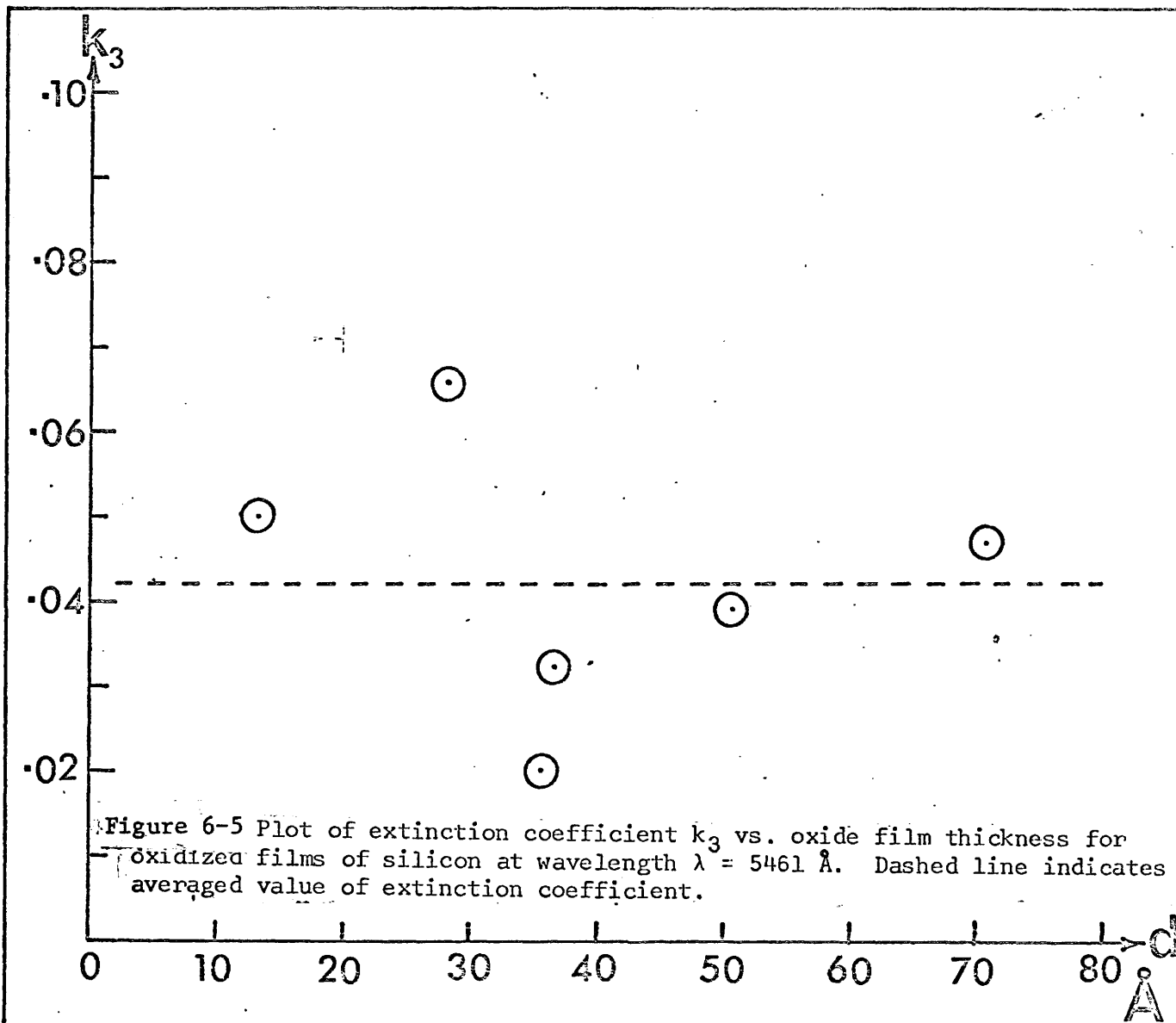
Experimentally determined optical constants for steam grown oxides on silicon.

Refractive index n_3	Extinction Coefficient k_3	Oxide-film thickness d (\AA)
4.050	0.050	13.13
4.050	0.066	28.31
4.050	0.020	35.82
4.050	0.032	36.62
4.011	0.039	50.65
4.050	0.047	70.59

Average $n_3 = 4.0445$; Standard deviation = 0.0144

Average $k_3 = 0.042$; Standard deviation = 0.0284





index versus oxide film thickness for/silicon.

An identical statistical analysis of the substrate extinction coefficient for silicon gives an average value of $k_3 = 0.042$ with a standard deviation of 0.0284. Archer¹⁴ reports the optical constants of silicon as $n_3 = 4.050$ and $k_3 = 0.028$. However he has to rely upon other well-known optical absorption techniques in order to establish the extinction coefficient for silicon. Vedam's constant reflectivity technique²⁸ suffers from the fact that a small change in n_3 causes a significant change in k_3 . He reports that a change from 4.0517 to 4.0518 in the refractive index causes a change from 0.029 to 0.022 in the value of the extinction coefficient.

Validity of the plane-parallel assumption

For the materials studied here, namely aluminum, molybdenum, and silicon, the initial oxidation is known to produce an amorphous oxide relatively free of any definite crystallographic structure. In addition, since the oxide films are very thin, the oxide-immersion medium surface is essentially an exact replica of the substrate-oxide interface. The validity of the plane parallel boundaries then relies upon the substrate surface being optically flat. For evaporated films of aluminum, the grain size is small and the surface fulfills the optically flat criterion. The silicon wafers are mechanically polished and also fulfill this same criterion. The molybdenum samples are also purported to be the best attainable surface. Some of the samples were analyzed with an interference microscope and no discontinuities in the fringe structure were observed.

Walk-off error

A simplified calculation using the normal reflectivities of the substrate-oxide and the substrate-immersion medium interfaces shows that approximately four reflections of significance take place in the oxide. This implies that the reflected beam displacement is of order 10^{-4} cm. The initial beam aperture is of order 1 mm. so this "walk-off" error is negligible.

Conclusions

We have been able to show that it is possible to determine substrate optical constants by analyzing the ellipsometry parameters Δ and ψ with angle of incidence - previously reported in the literature to be impossible¹⁰. A recent paper by Vedam et al²⁸ reports a method of determining substrate optical constants making use of the fact that the normal reflectivity is almost constant (within 0.1%) for oxide films up to 230 Angstroms on silicon. However, they fail to mention strongly that this constancy in normal reflectivity is very dependent upon the extinction coefficient of the substrate material, i.e. their method is very much dependent upon the material being studied. Table 6-4 shows the variation in normal reflectivity with oxide film thickness for oxide films on silicon. Similar tables for aluminum and tungsten (Tables 6-5 and 6-6) show progressively larger deviation in normal reflectivity with oxide film thickness. Table 6-7 shows a list of several materials and an upper limit to oxide film thickness calculated from a 0.1% deviation in film free normal reflectivity. It can be seen quite readily that very few of these materials support the constant

TABLE 6-4. Calculated values of Δ and ψ for various thicknesses d of a film of refractive index $n_2 = 1.460$ on a substrate of refractive index $n_3 = 4.050$ and extinction coefficient $k_3 = 0.028$. The wavelength λ is 5461 Angstroms and angle of incidence ϕ_1 is 70 degrees. The "pseudo optical constants" \bar{n}_3 and \bar{k}_3 and normal reflectivity R calculated from these angles Δ and ψ are also given in the table.

(Reproduced in part from Vedam et al¹.)

d (Å)	Δ (degrees)	ψ (degrees)	\bar{n}_3	\bar{k}_3	R
0.00	179.038	11.763	4.05000	0.02800	0.36479
5.00	177.488	11.769	4.04877	0.07313	0.36478
10.00	175.941	11.781	4.04647	0.11819	0.36478
15.00	174.396	11.798	4.04311	0.16315	0.36478
20.00	172.857	11.821	4.03869	0.20799	0.36478
25.00	171.323	11.850	4.03322	0.25264	0.36478
35.00	168.279	11.923	4.01917	0.34131	0.36477
50.00	163.788	12.073	3.99048	0.47214	0.36477
75.00	156.569	12.424	3.92346	0.68230	0.36478
100.00	149.763	12.889	3.83471	0.87954	0.36480
125.00	143.427	13.453	3.72738	1.06106	0.36485
150.00	137.578	14.099	3.60498	1.22495	0.36494
200.00	127.295	15.580	3.32920	1.49648	0.36531
250.00	118.690	17.226	3.03376	1.69749	0.36641
300.00	111.466	18.961	2.73850	1.82797	0.36747
400.00	100.173	22.516	2.19513	1.95168	0.37362
500.00	91.992	26.063	1.73662	1.96530	0.38806

TABLE 6-5. Calculated values of Δ and ψ for various thicknesses of a film of refractive index $n_2 = 1.66$ on a substrate of refractive index $n_3 = 0.820$ and extinction coefficient $k_3 = 5.990$. The wavelength λ is 5461 Angstroms and angle of incidence ϕ_1 is 70 degrees. The "pseudo optical constants" \bar{n}_3 and \bar{k}_3 and normal reflectivity R calculated from these angles Δ and ψ are also given in the table.

d (Å)	Δ (degrees)	ψ (degrees)	\bar{n}_3	\bar{k}_3	R
0.00	134.480	42.276	0.82000	5.99000	0.91631
5.00	133.539	42.292	0.78514	5.85590	0.91620
10.00	132.605	42.309	0.75249	5.72735	0.91610
15.00	131.678	42.326	0.72187	5.60402	0.91599
20.00	130.757	42.343	0.69312	5.48560	0.91588
25.00	129.843	42.360	0.66609	5.37182	0.91577
35.00	128.035	42.395	0.61665	5.15712	0.91555
50.00	125.376	42.448	0.55241	4.86383	0.91523
75.00	121.087	42.540	0.46607	4.43937	0.91471
100.00	116.985	42.634	0.39892	4.07976	0.91422
125.00	113.073	42.730	0.34562	3.77155	0.91378
150.00	109.357	42.826	0.30255	3.50490	0.91344
200.00	102.524	43.022	0.23768	3.06851	0.91316
250.00	96.509	43.218	0.19133	2.73027	0.91375
300.00	91.341	43.417	0.15623	2.46645	0.91578
400.00	83.764	44.840	0.10320	2.11429	0.92742
500.00	80.661	44.367	0.05434	1.97987	0.95680

TABLE 6-6. Calculated values of Δ and ψ for various thicknesses d of a film of refractive index $n_2 = 2.50$ on a substrate of refractive index $n_3 = 3.460$ and extinction coefficient $k_3 = 3.250$. The wavelength λ is 5461 Angstroms and the angle of incidence ϕ_1 is 70 degrees. The "pseudo optical constants" \bar{n}_3 and \bar{k}_3 and normal reflectivity R calculated from these angles Δ and ψ are also given in the table.

d (Å)	Δ (degrees)	ψ (degrees)	\bar{n}_3	\bar{k}_3	R
0.00	132.769	26.538	3.46000	3.25000	0.54555
5.00	131.365	26.595	3.35270	3.22787	0.54331
10.00	129.967	26.653	3.24943	3.20313	0.54100
15.00	128.574	26.713	3.15007	3.17606	0.53863
20.00	127.187	26.775	3.05453	3.14696	0.53618
25.00	125.806	26.839	2.96269	3.11607	0.53367
35.00	123.062	26.972	2.78962	3.04983	0.52844
50.00	118.993	27.184	2.55468	2.94216	0.52007
75.00	112.342	27.576	2.22058	2.75025	0.50478
100.00	105.865	28.020	1.94576	2.55345	0.48788
125.00	99.571	28.522	1.71755	2.35921	0.46952
150.00	93.469	29.094	1.52535	2.17144	0.44995
200.00	81.848	30.526	1.21475	1.82070	0.40888
250.00	70.948	32.569	0.95474	1.49841	0.37046
300.00	60.385	35.734	0.68928	1.17470	0.34875
400.00	30.420	48.905	-0.68434	0.19310	20.99105
500.00	-39.842	49.576	0.50745	0.42754	0.17326

MATE- RIAL	RE- FRACTIVE INDEX n_3	EXTINCTION COEFFICIENT k_3	RATIO (k_3/n_3)	OXIDE INDEX n_2	MAXIMUM THICKNESS d (Å)	FILM-FREE NORMAL REFLECTIVITY
Si	4.050	0.028	0.00691	1.460	235	0.36479
GaAs	3.923	0.304	0.07749	1.930	25	0.35499
Ge	5.010	1.030	0.38703	1.900	11	0.49749
InSb	4.104	2.058	0.50146	1.90 (?)	10	0.45797
Ta	3.500	2.440	0.69714	2.260	5	0.46572
W	3.460	3.250	0.93931	2.500	3	0.54555
Mo	3.610	3.670	1.01662	1.548 (?)	25	0.58411
Fe	3.350	3.840	1.14627	2.130	4	0.60200
Au	0.382	2.295	6.00785	1.330	85	0.78710
Al	0.820	5.990	7.30488	1.660	50	0.91631
Ag	0.055	3.320	60.36363	1.50 (?)	275	0.98187

TABLE 6-7. Calculated maximum thickness for which constant reflectivity method of determining substrate optical constants n_3 and k_3 is valid. Thickness is determined by 0.1 percent deviation in normal reflectivity from the film-free surface value of normal reflectivity.

reflectivity for oxides of order of several hundreds of Angstroms in thickness.

Our method does not suffer from this fault. In addition, we need only study one film thickness in order to make an estimate of the optical constants of the substrate. We need not assume that the optical properties of two films of different oxide film thickness be the same. For example, we have seen the variation in oxide extinction coefficient with oxide film thickness that Vedam et al would, of necessity, omit. Finally, our method does not lead to a direct error in k_3 from an error in n_3 as the constant reflectivity does.

APPENDIX I

Derivation of the Wave Equations

The fundamental equations governing the propagation of electromagnetic waves in a medium are the Maxwell equations²². These can be summarized as follows:

Coulomb's law

$$\nabla \cdot \vec{D} = 4\pi\rho \quad . \quad (\text{eq. I-1})$$

This describes the production of a displacement current density \vec{D} from a free charge ρ .

Ampere's law

$$\nabla \times \vec{H} = \frac{4\pi}{c} \vec{J} + \frac{1}{c} \frac{\partial \vec{D}}{\partial t} \quad . \quad (\text{eq. I-2})$$

This describes the production of a magnetic field \vec{H} from a current density \vec{J} and a displacement current density \vec{D} .

Faraday's law

$$\nabla \times \vec{E} = -\frac{1}{c} \frac{\partial \vec{B}}{\partial t} \quad . \quad (\text{eq. I-3})$$

This describes the production of an electric field \vec{E} from a magnetic induction \vec{B} .

Absence of free magnetic poles

$$\nabla \cdot \vec{B} = 0 \quad . \quad (\text{eq. I-4})$$

For isotropic, homogeneous, linear dielectric media, the displacement current density, \vec{D} , current density, \vec{J} , and magnetic induction, \vec{B} , are related to the electric field, \vec{E} , and magnetic field, \vec{H} , by the following relations:

$$\vec{D} = \epsilon \vec{E} \quad , \quad (\text{eq. I-5})$$

$$\vec{J} = \sigma \vec{E} \quad (\text{eq. I-6})$$

and
$$\vec{B} = \mu \vec{H} \quad (\text{eq. I-7})$$

In the absence of free charge, the equations describing the wave propagation in the isotropic, homogeneous dielectric medium simplify. These simplified Maxwell equations are:

$$\nabla \cdot \vec{E} = 0 \quad , \quad (\text{eq. I-8})$$

$$\nabla \times \vec{B} = \frac{\mu\epsilon}{c} \frac{\partial \vec{E}}{\partial t} + \frac{4\pi\mu\sigma}{c} \vec{E} \quad , \quad (\text{eq. I-9})$$

$$\nabla \times \vec{E} = -\frac{1}{c} \frac{\partial \vec{B}}{\partial t} \quad , \quad (\text{eq. I-10})$$

and
$$\nabla \cdot \vec{B} = 0 \quad . \quad (\text{eq. I-11})$$

Taking the curl of both sides of eq. I-10 gives

$$\begin{aligned} \nabla \times (\nabla \times \vec{E}) &= \frac{-1}{c} \nabla \times \frac{\partial \vec{B}}{\partial t} \\ &= \frac{-1}{c} \frac{\partial}{\partial t} (\nabla \times \vec{B}) \\ &= \nabla (\nabla \cdot \vec{E}) - \nabla \cdot (\nabla \vec{E}) \quad . \end{aligned}$$

Applying eqs. I-8 and I-9 for time independent permittivity and conductivity gives the result

$$\nabla^2 \vec{E} = \frac{\mu\epsilon}{c^2} \frac{\partial^2 \vec{E}}{\partial t^2} - \frac{4\pi\mu\sigma}{c^2} \frac{\partial \vec{E}}{\partial t} . \quad (\text{eq. I-12})$$

In a similar way, the wave equation for the magnetic induction can be obtained by taking the curl of eq. I-9 and substituting eqs. I-10 and I-11 into the resulting expression.

APPENDIX II
INVERSION OF THE TRANSCENDENTAL ELLIPSOMETRY
EQUATIONS

Referring to chapter II, we start with equation 2-16 and definition equation I-12:

$$\begin{aligned} \frac{w}{n_1 \cdot \sin \phi_1 \cdot \tan \phi_1} &= \frac{\cos 2\bar{\psi} - j \sin 2\bar{\psi} \sin \bar{\Delta}}{1 + \sin 2\bar{\psi} \cos \bar{\Delta}} \\ &= \frac{n_3^2 - k_3^2 - n_1^2 \cdot \sin^2 \phi_1 - 2j \cdot n_3 \cdot k_3}{n_1 \cdot \sin \phi_1 \cdot \tan \phi_1} \end{aligned} \quad (\text{eq. II-1})$$

The complex expression under the square-root sign is written in Euler form as $t \cdot \exp -2jQ$, so that:

$$\begin{aligned} n_3^2 - k_3^2 - n_1^2 \cdot \sin^2 \phi_1 - 2j \cdot n_3 \cdot k_3 &= t \cdot \exp -2jQ \\ &= t \cdot (\cos 2Q - j \sin 2Q) \end{aligned} \quad (\text{eq. II-2})$$

This requires that:

$$\begin{aligned} t &= \sqrt{(n_3^2 - k_3^2 - n_1^2 \cdot \sin^2 \phi_1)^2 + (2 \cdot n_3 \cdot k_3)^2} \\ &= \sqrt{n_3^4 + k_3^4 + n_1^4 \cdot \sin^4 \phi_1 + 2n_3^2 \cdot k_3^2 - 2 \cdot (n_3^2 - k_3^2) \cdot n_1^2 \cdot \sin^2 \phi_1} \end{aligned} \quad (\text{eq. II-3})$$

Also:

$$\tan 2Q = \frac{2 \cdot n_3 \cdot k_3}{n_3^2 - k_3^2 - n_1^2 \cdot \sin^2 \phi_1} \quad (\text{eq. II-4})$$

$$\begin{aligned} \text{Now } \sqrt{t \cdot \exp -2jQ} &= \sqrt{t} \cdot \exp -jQ \\ &= \sqrt{t} \cdot (\cos Q - j \sin Q) \end{aligned} \quad (\text{eq. II-5})$$

Applying this result to equation II-1:

$$\frac{\sqrt{t} \cdot (\cos Q - j \sin Q)}{n_1 \cdot \sin \phi_1 \cdot \tan \phi_1} = \frac{\cos 2\bar{\psi} - j \sin 2\bar{\psi} \cos \bar{\Delta}}{1 + \sin 2\bar{\psi} \cos \bar{\Delta}} \quad (\text{eq. II-6})$$

Separating into real and complex parts yields:

A. Real part:

$$\frac{\sqrt{t} \cdot \cos Q}{n_1 \cdot \sin \phi_1 \cdot \tan \phi_1} = \frac{\cos 2\bar{\psi}}{1 + \sin 2\bar{\psi} \cos \bar{\Delta}} \quad (\text{eq. II-7})$$

B. Complex part:

$$\frac{\sqrt{t} \cdot \sin Q}{n_1 \cdot \sin \phi_1 \cdot \tan \phi_1} = \frac{\sin 2\bar{\psi} \cos \bar{\Delta}}{1 + \sin 2\bar{\psi} \cos \bar{\Delta}} \quad (\text{eq. II-8})$$

For simplicity we now define:

$$\tan P = \frac{\sqrt{t}}{n_1 \cdot \sin \phi_1 \cdot \tan \phi_1}$$

$$= \frac{\sqrt[4]{n_3^4 + k_3^4 + n_1^4 \cdot \sin^4 \phi_1 + 2 \cdot n_3^2 \cdot k_3^2 - 2 \cdot (n_3^2 - k_3^2) \cdot n_1^2 \cdot \sin^2 \phi_1}}{n_1 \cdot \sin \phi_1 \cdot \tan \phi_1}$$

(eq. II-9)

so that equations II-7 and II-8 reduce to:

$$\tan P \cos Q = \frac{\cos 2\bar{\psi}}{1 + \sin 2\bar{\psi} \cos \bar{\Delta}} \quad (\text{eq. II -10})$$

$$\tan P \sin Q = \frac{\sin 2\bar{\psi} \sin \bar{\Delta}}{1 + \sin 2\bar{\psi} \cos \bar{\Delta}} \quad (\text{eq. II-11})$$

Squaring these last two equations and adding gives:

$$\tan^2 P = \frac{\cos^2 2\bar{\psi} + \sin^2 2\bar{\psi} \sin^2 \bar{\Delta}}{(1 + \sin 2\bar{\psi} \cos \bar{\Delta})^2} \quad (\text{eq. II-12})$$

$$\begin{aligned} \text{Hence } 1 - \tan^2 P &= \frac{(1 + \sin 2\bar{\psi} \cos \bar{\Delta})^2 - \cos^2 2\bar{\psi} + \sin^2 2\bar{\psi} \sin^2 \bar{\Delta}}{(1 + \sin 2\bar{\psi} \cos \bar{\Delta})^2} \\ &= \frac{1 + 2\sin 2\bar{\psi} \cos \bar{\Delta} + \sin^2 2\bar{\psi} (\cos^2 \bar{\Delta} - \sin^2 \bar{\Delta}) - \cos^2 2\bar{\psi}}{(1 + \sin 2\bar{\psi} \cos \bar{\Delta})^2} \end{aligned}$$

Combining the first and last term in the numerator, since

$$1 - \cos^2 2\bar{\psi} = \sin^2 2\bar{\psi}, \text{ yields:}$$

$$\begin{aligned} 1 - \tan^2 P &= \frac{2 \sin 2\bar{\psi} \cos \bar{\Delta} + \sin^2 2\bar{\psi} \cdot (1 + \cos^2 \bar{\Delta} - \sin^2 \bar{\Delta})}{(1 + \sin 2\bar{\psi} \cos \bar{\Delta})^2} \\ &= \frac{2 \sin 2\bar{\psi} \cos \bar{\Delta} \cdot (1 + \sin 2\bar{\psi} \cos \bar{\Delta})}{(1 + \sin 2\bar{\psi} \cos \bar{\Delta})^2} \end{aligned}$$

$$1 - \tan^2 P = \frac{2 \sin 2\bar{\psi} \cos \bar{\Delta}}{(1 + \sin 2\bar{\psi} \cos \bar{\Delta})} \quad (\text{eq. II-13})$$

Dividing equation II-11 by II-13 gives:

$$\frac{\tan P \sin Q}{1 - \tan^2 P} = \frac{\sin 2\bar{\psi} \sin \bar{\Delta}}{2 \sin 2\bar{\psi} \cos \bar{\Delta}} = 1/2 \tan \bar{\Delta}$$

$$\text{Or: } \tan \bar{\Delta} = \frac{2 \tan P}{1 - \tan^2 P} \cdot \sin Q = \sin Q \tan 2P \quad (\text{eq. II-14})$$

This is the inverted equation for the phase change $\bar{\Delta}$ where the angles P and Q are defined by equations II-9 and II-4 respectively. The azimuth can be solved by starting with equation II-10 in the form:

$$\begin{aligned} \cos 2\bar{\psi} &= \tan P \cos Q \cdot (1 + \sin 2\bar{\psi} \cos \bar{\Delta}) \\ &= \frac{2 \cdot \tan P \cos Q \cdot (1 + \sin 2\bar{\psi} \cos \bar{\Delta})^2}{2 + 2 \sin 2\bar{\psi} \cos \bar{\Delta}} \\ &= \frac{2 \tan P \cos Q \cdot (1 + \sin 2\bar{\psi} \cos \bar{\Delta})^2}{1 + (\cos^2 2\bar{\psi} + \sin^2 2\bar{\psi}) + 2 \sin 2\bar{\psi} \cos \bar{\Delta}} \\ &= \frac{2 \tan P \cos Q \cdot (1 + \sin 2\bar{\psi} \cos \bar{\Delta})^2}{\cos^2 2\bar{\psi} + \sin^2 2\bar{\psi} \cdot (\sin^2 \bar{\Delta} + \cos^2 \bar{\Delta}) + 1 + 2 \sin 2\bar{\psi} \cos \bar{\Delta}} \\ &= \frac{2 \tan P \cos Q \cdot (1 + \sin 2\bar{\psi} \cos \bar{\Delta})^2}{\cos^2 2\bar{\psi} + \sin^2 2\bar{\psi} \sin^2 \bar{\Delta} + 1 + 2 \sin 2\bar{\psi} \cos \bar{\Delta} + \sin^2 2\bar{\psi} \cos^2 \bar{\Delta}} \\ &= \frac{2 \tan P \cos Q}{(\cos^2 2\bar{\psi} + \sin^2 2\bar{\psi} \sin^2 \bar{\Delta}) + 1} \cdot \frac{1}{(1 + \sin 2\bar{\psi} \cos \bar{\Delta})^2} \quad (\text{eq. II - 15}) \end{aligned}$$

However the first term in the denominator of equation II-15 is exactly $\tan^2 P$ --- see expression II-12. Making this substitution in II-15:

$$\begin{aligned} \cos 2\bar{\psi} &= \frac{2 \tan P \cos Q}{\tan^2 P + 1} = \frac{2 \tan P \cos Q}{\sec^2 P} \\ &= 2 \sin P \cos P \cos Q \\ &= \sin 2P \cos Q \end{aligned} \quad (\text{eq. II-16})$$

to summarize, the inverted equations are:

$$\tan \bar{\Delta} = \sin Q \tan 2P \quad (\text{eq. II-14})$$

$$\cos 2\bar{\psi} = \cos Q \sin 2P \quad (\text{eq. II-16})$$

where:

$$\tan P = \frac{\sqrt{n_3^4 + k_3^4 + n_1^4 \sin^4 \phi_1 + 2 \cdot n_3^2 \cdot k_3^2 - 2 \cdot (n_3^2 - k_3^2) \cdot n_1^2 \cdot \sin^2 \phi_1}}{n_1 \cdot \sin \phi_1 \cdot \tan \phi_1} \quad (\text{eq. II-3})$$

and

$$\tan 2Q = \frac{2 \cdot n_3 \cdot k_3}{n_3^2 - k_3^2 - n_1^2 \cdot \sin^2 \phi_1} \quad (\text{eq. II-4})$$

BIBLIOGRAPHY

1. Lord Rayleigh, Phil. Mag. 33, 1 (1892).
2. P. Drude, Ann. Physik Chemie 39, 481 (1890).
3. P. Drude, Weid. Ann. Phys. 36, 884 (1889).
4. L. Tronstad, Trans. Faraday Soc. 31, 1151 (1935).
5. A. Rothen, Rev. Sci. Instr. 16, 26 (1945).
6. A. Vasicek, J. Opt. Soc. Am. 37, 145 (1947).
7. R. J. Archer, J. Electrochem. Soc. 104, 619 (1957).
8. F. L. McCrackin, E. Passaglia, R. R. Stromberg, and H. L. Steinberg, J. Res. Nat. Bur. Std. 67A, 363 (1963).
9. F. L. McCrackin and J. P. Coulson, Nat. Bur. Std. Technical Note 242, Washington, 1964.
10. D. K. Burge and H. E. Bennett, J. Opt. Soc. Am. 54, 1428 (1964).
11. A. N. Saxena, J. Opt. Soc. Am. 55, 1061 (1965).
12. C. E. Leberknight and B. Lustman, J. Opt. Soc. Am. 29, 59 (1939).
13. H. Hauschild, Ann. Physik Chemie 63, 816 (1920).
14. R. J. Archer, J. Opt. Soc. Am. 52, 970 (1962).
15. A. B. Winterbottom, Optical Studies of Metal Surfaces, p.59, I. Kommissjon Hos. F. Bruns Bokhandel, Trondheim, 1955.
16. R. J. Archer, Phys. Rev. 110, 354 (1958).
17. G. Hass and J. E. Waylonis, J. Opt. Soc. Am. 51, 719 (1961).
18. H. T. Yolken and J. Kruger, J. Opt. Soc. Am. 55, 842 (1965).
19. A. C. Hall, J. Opt. Soc. Am. 55, 913 (1965).
20. M. Born and E. Wolf, Principles of Optics, p. 39, Pergamon Press, New York, 1959.

21. R. W. Ditchburn, *Light*, p.535, Interscience Publishers, New York, 1963.
22. J. D. Jackson, *Classical Electrodynamics*, p.178, J. Wiley and Sons, New York, 1962.
23. E. C. Rowe and J. Shewchun, *J. Opt. Soc. Am.* 59, 1385 (1969).
24. A. B. Winterbottom, *Op. Cit.*, p.122.
25. N. M. Bashara and D. W. Peterson, *J. Opt. Soc. Am.* 56, 1320 (1966).
26. J. P. Waldron and D. W. Juenker, *J. Opt. Soc. Am.* 54, 204 (1964).
27. R. D. Summers, *J. Opt. Soc. Am.* 24, 261 (1934).
28. K. Vedam, W. Knausenberger, and F. Lukes, *J. Opt. Soc. Am.* 59, 64 (1969).
29. E. C. Rowe and J. Shewchun, (to be published).
30. R. G. Keil and R. E. Saloman, *J. Electrochem. Soc.* 115, 628 (1968).